IMAGE: A MAP OF THE STARS OF THE ORION CONSTELLATION

JournalPreview

London Journal of Research in Science: Natural & Formal

Volume 24 | Issue 14 | Compilation 1.0

Great Britain Journals Press

WWW.JOURNALSPRESS.COM

Journal Content
In this Issue

Great Britain Journals Press

Design and Good Living

Doutoranda Evânia de Paula Muniz & Doutor Carlos Eduardo Félix da Costa

ABSTRACT

Design and Good Living are interconnected concepts that promote quality of life, especially invulnerable territories. Design acts as a tool for social change, creating aesthetic and functional solutions that meet physical, emotional, and cultural needs. Buen Vivir, based on the Andean indigenous worldview, prioritizes harmony between humans, nature, and the universe, focusing on peripheral communities. This article presents examples of the resignification of spaces in the global south, based on the theory of Biophilia by Edward Wilson, Stephen Kellert and Alberto Acosta, showing how biophilic design restores the human connection with nature, favoring Buen Vivir.

Keywords: art; good living; communities; design; education.

Classification: LCC Code: NA2542.4

Language: English

Great Britain Journals Press

LJP Copyright ID: 925641
Print ISSN: 2631-8490
Online ISSN: 2631-8504

London Journal of Research in Science: Natural & Formal

Volume 24 | Issue 14 | Compilation 1.0

Design and Good Living

O Design E O Bem Viver

Doutoranda Evânia de Paula Muniz[α] & Doutor Carlos Eduardo Félix da Costa[σ]

RESUMO

*O Design e o Bem Viver, são conceitos interligados, que promovem a qualidade de vida, especialmente em territórios vulneráveis. O design atua como uma ferramenta para mudanças sociais, criando soluções estéticas e funcionais que atendem às necessidades físicas, emocionais e culturais. O Bem Viver, baseado na cosmovisão indígena andina, prioriza a harmonia entre humanos, natureza e universo, focando em comunidades periféricas. Este artigo apresenta exemplos de ressignificação de espaços no sul global, fundamentados na teoria da Biofilia de Edward Wilson, Stephen Kellert e Alberto Acosta mos*trando como o design biofílico restaura a conexão humana com a *natureza, favorecendo o Bem Viver.*

Palavras-chave: arte; bem viver; comunidades; design; educação.

ABSTRACT

Design and Good Living are interconnected concepts that promote quality of life, especially invulnerable territories. Design acts as a tool for social change, creating aesthetic and functional solutions that meet physical, emotional, and cultural needs. Buen Vivir, based on the Andean indigenous worldview, prioritizes harmony between humans, nature, and the universe, focusing on peripheral communities. This article presents examples of the resignification of spaces in the global south, based on the theory of Biophilia by Edward Wilson, Stephen Kellert and Alberto Acosta, showing how biophilic design restores the human connection with nature, favoring Buen Vivir.

Keywords: art; good living; communities; design; education.

RESUMEN

El Diseño y el Buen Vivir son conceptos interconectados que promueven la calidad de vida, especialmente en territorios vulnerables. El diseño actúa como una herramienta para el cambio social, creando soluciones estéticas y funcionales que satisfacen las necesidades físicas, emocionales y culturales. El Buen Vivir, basado en la cosmovisión indígena andina, prioriza la armonía entre los seres humanos, la naturaleza y el universo, centrándose en las comunidades periféricas. Este artículo presenta ejemplos de la resignificación de los espacios en el sur global, a partir de la teoría de la Biofilia de Edward Wilson, Stephen Kellert y Alberto Acosta, mostrando cómo el diseño biofílico restaura la conexión humana con la naturaleza, favoreciendo el Buen Vivir.

Palabras clave: arte; el buen vivir; comunidades; diseño; educación.

Author α σ: PUC-Rio. e-mails: ovilai@gmail.com, eduardo.felix.costa@gmail.com

I. O DESIGN E O BEM VIVER

O ser humano é indissociável da natureza, embora a tendência humana de modificar os espaços naturais tenha alterado essa relação de maneira significativa, levando a uma perda gradual da

consciência dessa união. No entanto, diversos pesquisadores e especialistas em planejamento urbano e áreas afins têm se dedicado a esse debate, fomentando discussões sobre como reavaliar nossa interação com o ambiente em que vivemos. Essas conversas não se limitam apenas a repensar nossa abordagem em relação com o lugar, mas também abrangem a busca por formas de torná-lo sustentável, considerando os desafios contemporâneos como a influência da globalização e do capitalismo que transcendem a uma mera reflexão.

A relação do ser humano com o espaço que o cerca envolvem o ambiente construído, ambiente natural, o desenvolvimento de políticas destinadas a aprimorar as condições de saúde tanto da população quanto do planeta Terra, que se revela cada vez mais insustentável diante da busca pela "evolução" que a humanidade procura.

Em a *"Carta da Terra"* (1992, p. 1), documento concebido durante a Conferência das Nações Unidas sobre Meio Ambiente e Desenvolvimento, conhecida como Rio-92, destaca esse ponto de vista. O preâmbulo enfatiza a necessidade de reconhecer a interdependência global e o destino comum da humanidade, ressaltando a importância de construir uma sociedade global pacífica, justa e sustentável baseada no respeito a natureza, aos direitos humanos, na justiça econômica e na cultura da paz.

> Estamos diante de um momento crítico na história da Terra, numa época em que a humanidade deve escolher o seu futuro. À medida que o mundo se torna cada vez mais interdependente e frágil, o futuro reserva, ao mesmo tempo, grande perigo e grande esperança. Para seguir adiante, devemos reconhecer que, no meio de uma magnífica diversidade de culturas e formas de vida, somos uma família humana e uma comunidade terrestre com um destino comum. Devemos nos juntar para gerar uma sociedade sustentável global fundada no respeito pela natureza, nos direitos humanos universais, na justiça econômica e numa cultura da paz. Para chegar a este propósito, é imperativo que nós, os povos da Terra, declaremos nossa responsabilidade uns para com os outros, com a grande comunidade de vida e com as futuras gerações. (Carta da Terra, 1992, p.1).

Essa perspectiva ecoa as ideias apresentadas pelo economista Alberto A. Costa (2016) *"O Bem Viver"*. Neste livro, O Bem Viver se apresenta como uma oportunidade para construir coletivamente uma nova forma de vida. Trata-se de bem conviver em comunidade com a natureza, inspirado na reciprocidade e na solidariedade. Buscando a colaboração e não a concorrência. Dentro do capitalismo, isso é impossível.

Neste contexto, no livro *"Cidades para pessoas"* (2013), Jan Gehl examina como o planejamento urbano, desde os anos de 1960, tem falhado em considerar as necessidades humanas fundamentais, como a conexão com a natureza, enquanto prioriza objetivos como produção, crescimento econômico e lucro. Ele argumenta que nas antigas cidades, o planejamento começava com o paisagismo, enquanto hoje em dia começa com a construção dos prédios. Gehl declara que esse tipo de planejamento urbano não é humanista, não prioriza as necessidades das pessoas e defende que é possível conceber algo melhor, mesmo numa sociedade capitalista.

> Uma preocupação crescente com a dimensão humana no planejamento urbano reflete uma exigência distinta e forte por melhor qualidade de vida urbana. Existem conexões diretas entre as melhorias para as pessoas no espaço da cidade e as visões para obter cidades vivas, seguras, sustentáveis e saudáveis (Gehl, 2013, p, 7)

Gehl (2013), enfatiza que o rápido crescimento das áreas urbanas densamente povoadas ocorreu em meio a administrações governamentais que ofereceram pouco espaço para o encontro, o debate público, as trocas que anteriormente ocorria nos espaços em comum das cidades. Isso contribuiu para o desenvolvimento de modelos urbanos pautados em otimizar questões como o crescente tráfego de

automóveis, buscando acomodar um novo ritmo de vida, sem levar em considerações a vida na terra como um todo.

Wilson (1984), enfatiza a importância da "*Biofilia*" a conexão intrínseca entre os seres humanos e o ambiente, como fundamental para o desenvolvimento de um mundo saudável e sustentável. Ele defende que essa ligação exige comportamentos e pensamentos de unidade, essenciais para garantir um futuro viável. Embora atualmente está cada vez mais difícil encontrar espaços que despertem a biofilia nas pessoas, sua existência e desenvolvimento como comportamento ativo parecem ser uma das poucas esperanças para que a humanidade não destrua a natureza nas próximas décadas.

Há a necessidade de estarmos integrados a natureza, porque somos natureza, não estamos à parte. Quando perdemos esta conexão, nos sentimos afetados. Wilson ressalta que a biofilia está enraizada no conteúdo biológico, então trazer essa integração para as cidades é oferecer bem viver.

> Em Pompéia, os romanos construíram jardins ao lado de quase todas as pousadas, restaurantes e residências particulares, a maioria possuindo os mesmos elementos básicos: árvores e arbustos artisticamente espaçados, canteiros de ervas e flores, piscinas e fontes e estatuária doméstica. Quando os pátios eram pequenos demais para abrigar grande parte de um jardim, seus proprietários pintavam quadros. (Wilson, 1984, p, 121)

Evidências disso podem ser observadas em várias práticas comuns: as construtoras, ao desenvolverem condomínio de luxo, frequentemente incluem belos jardins para demonstrar a qualidade de vida do local, mesmo os shoppings mais simples apresentam áreas ajardinadas e as cidades investem em jardins zoológico e botânicos. Durante as férias, as pessoas buscam experiências que as conectem à natureza, independentemente da escala, muitas vezes sem compreender as razões, apenas para se sentirem bem naquele lugar. Inclusive as pessoas de baixa renda tem plantas em suas casas, por mais caótico que seja o entorno.

A falta de investimento em moradias e no espaço público, não atendem as necessidades da população e está gerando desequilíbrios ambientais.

Na busca por moradia, a população de baixa renda é frequentemente levada às periferias, onde encontra o caos, decorrente da falta de infraestrutura. Esses espaços se desenvolvem de maneira desordenada, utilizando recursos escassos. As moradias são geralmente construídas com materiais de sobras, e a infraestrutura é criada pelos próprios residentes, sem o devido conhecimento técnico, essa autoconstrução resulta em armadilha para o próprio morador e seu entorno. Além disso, em épocas eleitorais, políticos aparecem oferecendo permutas com trabalho subalterno, um pouco de tijolos, uma cesta básica em troca de votos da família.

> Em diálogo com Bauman em seu livro *"Comunidades"* (2003, p,106), sobre o assunto:
>
> Ser pobre numa sociedade rica implica em ter o status de uma anomalia social e ser privado de controle sobre sua representação e identidade coletiva: a análise da mancha urbana do gueto norte-americano e da periferia urbana francesa mostra a privação simbólica que torna seus habitantes verdadeiros párias. (Bauman, p. 106)

As políticas públicas são desenvolvidas para aqueles que pagam impostos, não para os que, sem condições de moradia, recorrem aos bairros periféricos. Dessa forma, o planejamento técnico para as cidades é uma questão de escolha, já para as comunidades marginalizadas, torna-se um desafio substancial. Problemas que poderiam ser evitados, mitigados ou minimizados acabam exacerbando as catástrofes nessas regiões.

De acordo com Gehl, todos devem ter direitos a moradia digna com espaços abertos, facilmente acessíveis, tanto quanto tem direito a água tratada. Todos devem ter possibilidades de ver uma árvore de sua janela, ou de sentar-se em um banco de praça, perto da sua casa, com espaço para crianças, ou de caminhar até um parque em dez minutos. Bairros bem planejados inspiram os moradores, e isso deve incluir o lugar dos operários, as comunidades periféricas. Uma cidade que não é para todos é uma cidade mal planejada e brutaliza seus cidadãos como um todo. Nos moldamos as cidades e elas nos moldam.

> Por décadas, a dimensão humana tem sido um tópico do planejamento urbano esquecido e tratado a esmo, enquanto várias outras questões ganham mais força, como a acomodação do vertiginoso aumento do tráfego de automóveis, além disso, as ideologias dominantes de planejamento - em especial, o modernismo - deram baixa prioridade ao espaço público, as áreas de pedestres e ao papel do espaço urbano como local de encontro dos moradores da cidade. Por fim, gradativamente, as forças do mercado e as tendências arquitetônicas afins mudaram seu foco, saindo das ínter-relações e espaços comuns da cidade para os edifícios individuais, os quais, durante o processo, tornaram-se cada vez mais isolados, autossuficientes e indiferentes (Gehl, 2013, p, 3).

Esse modelo de planejamento urbano vem sendo reavaliado, graças aos debates entre estudiosos, ao comprometimento de instituições e à adesão do público. Isso pode levar a novas propostas para a cidade de concreto.

Nos últimos dez anos, o número de desastres geológicos, terremotos, erosões e inundações devido às chuvas cada vez mais intensas e imprevistas, começarem a fazer parte do cotidiano das cidades espalhadas pelo mundo.

Diante deste contexto, há uma crescente compreensão de que é necessária uma resposta a estes desafios contemporâneos.

Como indica Latour (2020), trata-se de um período de insegurança, mudança e de ressignificação, que solicita a articulação de estratégias criativas a partir de um envolvimento entre público, privado e população. Uma aliança que aos poucos deixa de lado um modelo *"racionalista",* pautado no "*progresso*" a qualquer custo, promovendo uma abertura ao fazimento de novas alianças: nesses termos, homem e animal, natureza e espaço, devem ser colocados não mais em ponto de discordância, mas em posição de igualdade.

Segundo o arquiteto Alejandro Echeverri (2004), Sérgio Fajardo, prefeito de Medelin, com o slogan "O bom design educa", liderou entre aos anos de 2004 e 2007 um processo que reuniu líderes locais e especialistas de diferentes áreas para promover uma mudança estrutural em uma cidade caracterizado pela desordem. Foi criado o Projeto Urbano Integrado (PUI), que teve a ética como princípio central na política, com o objetivo de recuperar a confiança no poder público. O projeto envolveu a aproximação, comunicação e respostas aos setores excluídos, utilizando a transformação do espaço público como uma ferramenta de estratégias para restaurar a confiança da população de Medellin.

A experiência do Urbanismo Social em Medellin foi a consolidação de uma postura ética e moral em resposta aos problemas endêmicos de exclusão e violência na cidade. Uma abordagem sistêmica foi adotada, com a definição de um líder comunitário por zona.

A metodologia utilizada foi qualitativa, tendo como base o "Design comunitário", com foco no tema: "Pensar globalmente com aplicação personalizada aos locais", utilizando discursos, ferramentas, crenças e tecnologias que façam sentido na composição de cada ambiente e na identidade da população. O essencial foi propor soluções para as questões mais grave e urgentes.

Considerando os desafios contemporâneos relacionados à concepção de modelos globais de atuação, este estudo alinha-se ainda com as ideias de pesquisadores como Tuan (1983), Manzini (2008), Kellert (2015) e Acosta (2016), reconhecendo a importância de uma integração mais eficaz entre população, planejamento urbano e áreas verdes. Este trabalho também acompanha movimentos comunitários em territórios na cidade do Rio de janeiro, onde instituições ativam atores que se movimentam para transformar cenários negligenciados em espaços significativos, como a conversão de lixões em jardins, praças, hortas, em espaços de convivência, tetos verdes. Essas intervenções promovem a união, o diálogo, a educação e a cidadania. O que se alinha aos princípios de *"Integridade Ecológica 7"*, defendidos pela *"Carta da Terra: Adotar padrões de produção, consumo e reprodução que protejam as capacidades regenerativas da Terra, os direitos humanos e o bem viver comunitário"*.

No livro, "*Design para inovação social e sustentabilidade*", Ezio Manzini (2008) destaca o papel das comunidades na formação de redes e na busca por um futuro resiliente:

> O termo inovação social refere-se a mudanças no modo como indivíduos ou comunidades agem para resolver seus problemas ou criar oportunidades. Tais inovações são guiadas mais por mudanças de comportamento do que por mudanças tecnológicas ou de mercado, geralmente emergindo através de processos organizacionais "de baixo para cima" em vez daqueles "de cima para baixo". (Manzini, 2008 p. 61).

Com base nesse pensamento, acredita-se que essas inovações sociais atingem seu potencial máximo quando ocorrem de forma horizontal, permitindo que todos expressem seus pontos de vista e tenham igual poder de fala. Assim como as propostas desenhadas pelo arquiteto Alejandro Echeverri em Medellin. Projeto esse que inspirou o mundo.

Se há possibilidades de imaginação de mundos, faz-se necessário adicionar as premissas do consumo consciente e sustentável, tendo também como base um diálogo entre ser humano e natureza – não mais ser humano versus natureza, mas "*humanidade em harmonia com a natureza"*. Diante dessa lógica, decisões quanto à direitos e deveres podem ser propostos: surge, então, a ideia de se inserir entre os direitos mais básicos de uma população a sua integração com a natureza. Dessa mudança de ponto de vista, pode-se construir um hábito coletivo pelo cultivo. As estratégias do design e o pensamento artístico podem propiciar as ferramentas necessárias ao desenvolvimento dessas comunidades.

Seguindo esse conceito, o geógrafo Tuan (1983) ressalta a importância da formação de uma relação afetiva com o espaço, destacando que para se desenhar experiências mais convenientes, faz-se necessário desenvolver vínculos emocionais e cognitivos com as particularidades e com os seres vivos de um determinado entorno. Nesse ciclo, o autor entende que a experiência do sujeito em um lugar pode ir além de uma mera observação objetiva, devendo ser enriquecida por aspectos como memórias, emoções, narrativas coletivas e pessoais, que em um movimento de experiências. Assim, os sons, os cheiros e as texturas também podem atuar ativamente, contribuindo para uma melhor percepção e compreensão dos ambientes, como propões Steffen Kellert (2105).

Para Tuan (1983), a experiência implica na capacidade de apreensão de vivências, circuito que passa por emergir, atuar, criar a partir de um intenso contato com as coisas. Isso porque, nos termos do autor, um dado nunca pode ser apreendido em sua "essência": o que pode ser conhecido é uma certa realidade, que passa pela capacidade humana de ouvir e de criar ferramentas singulares, visando a responder a um determinado contexto e ambiente. Trata-se de uma adaptação, na medida em que a experiência nunca é a mesma para determinados grupos de indivíduos; depende da conexão que se faz entre elementos. A figura abaixo apresenta o circuito elaborado por Tuan (1983, p. 9), que visa a exemplificar os movimentos do pensamento e da emoção no processo de imersão em uma determinada experiência:

A experiência implica na capacidade de aprender a partir da própria vivência, significa atuar sobre o dado e criar a partir dele. O dado não pode ser conhecido em sua essência. O que pode ser conhecido é uma realidade que é um constructo da experiência, uma criação de sentimento e pensamento, experienciar é vencer perigos, aventurar-se no desconhecido e experimentar o ilusório e o incerto. O indivíduo é compelido a isso. Está apaixonado, e a paixão é um símbolo de força mental. (Tuan, 1983, p..10-11).

Figura 1: Esquema explicativo da experiência humana. Fonte: Tuan (1983, p. 9).

As emoções dão colorido a toda experiência humana, incluindo os níveis mais altos de pensamento. Os matemáticos, por exemplo, afirmam que a expressão de seus teoremas é orientada por critérios estéticos, noções de elegância e simplicidade que respondem a uma necessidade humana. O pensamento dá colorido a toda experiência humana incluindo as sensações primárias de calor e frio, prazer e dor. A sensação é rapidamente qualificada pelo pensamento em um tipo especial. A experiência está voltada para o mundo exterior (Tuan, 1983, p. 9).

Conforme atesta o geógrafo, na experiência humana é comum que os significados de espaço e lugar se entrelacem, gerando uma confusão conceitual. No entanto, é necessário compreender que esses termos possuem distinções significativas. Para Tuan (1983), o espaço deve ser entendido como uma entidade indiferenciada, enquanto o lugar emerge à medida que o conhecemos e o dotamos de valor. O espaço, em sua essência, refere-se a uma dimensão física e abstrata, trata-se de uma noção ampla e objetiva que abarca a extensão tridimensional que nos cerca. Já o lugar é neutro, carece de significado e valoração. Dessa forma, as ideias de espaço e lugar não podem ser definidas uma em relação à outra. Trata-se de um conceito relativo, moldado pelas percepções subjetivas dos indivíduos, influenciado por fatores culturais, sociais e temporais. Para o autor, é através da percepção subjetiva que conseguimos dar sentido ao espaço, transformando-o em lugar.

É com essa perspectiva que Wilson (1986) toma a *Biofilia*, noção que aponta para o pleno funcionamento e equilíbrio do humano. Urge, então, a necessidade de se discutir a importância da criação de ambientes urbanos mais amigáveis, de modo que possamos integrar a biofilia ao nosso cotidiano. Assim, inferimos que as ferramentas conceituais atreladas ao design podem proporcionar ambientes mais saudáveis e inspiradores para as pessoas, especialmente para aqueles com pouco acesso a áreas verdes e ambientes naturais. A ideia do "*Design Biofílico*", é incentivar e melhorar o contato entre as pessoas e a natureza no contexto urbano, preservar os recursos naturais, minimizar impactos ambientais, e compor as lacunas que a arquitetura contemporânea tem ignorado.

Ao promover, não apenas emoções positivas, mas também uma melhoria na qualidade de vida das populações de um modo geral, esse entendimento sobre a biofilia gera uma consciência significativa sobre a interconexão entre o ambiente construído, o ambiente natural e o ser humano.

Como exemplo a ser seguido, trazemos o caso do Parque Sitiê (figura 2), um espaço situado no morro do Vidigal, na zona sul do Rio de Janeiro. Anteriormente um depósito de lixo, este local foi transformado em uma reserva ecológica em 2012, por iniciativa dos moradores Mauro Quintanilha, Paulo César e a colaboração do pesquisador da instituição Havard College, o arquiteto Pedro Henrique de Cristo, e ao apoio da editora Arq. Futuro. O espaço remodelado tornou-se um ponto de encontro vibrante, onde ocorreram trocas de conhecimento entre os moradores, gerando alimentos e proporcionando bem-estar. A colaboração é um elemento fundamental para que esse projeto tenha continuidade.

Um exemplo que busca a harmonia com a natureza, a integração entre os indivíduos e o senso de pertencimento que Tuan (1983) relatou é um exemplo notável de design biofílico, servindo de inspiração para comunidades.

Fonte: Google fotos

Figura 2: Parque Sitiê /Vidigal/RJ.

Um outro exemplo de design biofílico em áreas periféricas é o projeto *"Teto Verde",* implementado na comunidade do Parque Arará/RJ (figuras 3), situada às margens da Avenida Brasil, na cidade do Rio de Janeiro. O projeto teve origem quando um dos moradores locais, o ambientalista e produtor cultural, Luiz Cassiano Silva (conhecido como Sanduba), decidiu instalar um teto verde em sua residência, com o objetivo de reduzir o calor interno em sua moradia e trazer a presença do verde para aquele ambiente, segundo ele acinzentado. A intervenção resultou em uma redução de aproximadamente 30% da temperatura interna. Em entrevista, Sanduba destacou que os moradores de áreas periféricas devem recorrer ao paisagismo para tornar suas casas mais frescas, e que esse modelo de casa em periferia tem sido replicado. Esse projeto culminou em uma série de palestras e oficinas com o objetivo de difundir e implementar o conceito *"Telhado verde"* em diversas áreas do Rio de Janeiro. Atualmente, Luís Cassiano oferece oficinas de telhado verde na cidade como profissão, promovendo a sustentabilidade e a melhoria da qualidade de vida desses territórios negligenciados.

Neste contexto, a Associação Comunidade Catalisadoras (COMCAT) reuniu diversos participantes de diferentes comunidades com o propósito de construir um telhado verde na Creche Parque do Arará/RJ,

sob a supervisão do Sanduba. Este evento ocorreu em 05 de dezembro de 2022 e teve uma duração total de 16 horas.

Fonte: Luís Cassiano Silva

Figura 3: Creche Parque do Arará/RJ

A COMCAT[1] é uma associação que tem como objetivo a promoção de comunidades sustentáveis e tem desempenhado um papel relevante na transformação territórios periféricos. Criando conexões, fornecendo conhecimento, estabelecendo parcerias, promovendo justiça social e responsabilidade institucional. Fundada em 2000 pela ambientalista Theresa Williamson, a COMCAT, se destaca internacionalmente por oferecer ferramentas que transformam o ambiente.

A Horta Comunitária da Maré, no complexo da Maré, no Rio de Janeiro, constitui outro exemplo relevante, tendo surgido em 2021 como um projeto construído como alternativa ecológica visando aprimorar as condições de bem-estar coletivo. Idealizado por Sebastião Antônio (conhecido como Tião – figura 4), Presidente do Instituto Vida Real – Favela da Maré, tem o conceito da biofilia aplicado no lugar, através do design biofílico. Abaixo Tião explica a importância da horta:

> A importância dessa horta para nós é trabalhar a autoestima dos nossos alunos, para que eles possam ter o conhecimento do valor que a nossa terra tem, e poder valorizar mais tudo aquilo que temos em mãos, que, muitas das vezes, desperdiçamos. E, quando temos, acabamos só jogando fora. Particularmente para mim é poder ter um alimento saudável, é mostrar para os garotos que podemos ter sim alimentos saudáveis no pouco espaço que temos nas nossas casas, valorizando mais a natureza". Tião – Voz das comunidades – (https://www.vozdascomunida des.com.br/destaques/instituto-vida-real-cria-vaquinha-para-criacao-de-horta-urbana-na-mare-saiba-como-ajudar/)

[1] Disponível em (https://www.comcat.org/)

Fonte: Google fotos

Figura 4: Horta Comunitária Maré/RJ – Marcelo Régua – O Globo

Implementar a biofilia em áreas urbanas, especialmente em territórios periféricos, apresenta desafios consideráveis, devido à complexidade e urgência desses espaços, que muitas vezes carecem de infraestrutura e onde a maioria dos habitantes sobrevivem com um salário-mínimo. Biofilia, uma palavra de origem grega que significa "amor à vida" (bio=vida, filia=amor), é um conceito que destaca a necessidade inata do ser humano de conectar com a natureza. A falta dessa conexão, pode nos afetar negativamente, levando a transtornos mentais, segundo Wilson (1983). Não é por acaso que, quando estamos estressados, buscamos ambientes naturais para relaxar, como o mar, cachoeira. Gostamos de sentir cheiro da terra molhada, ouvir o barulho da chuva, pisar na areia da praia. Isso porque buscamos conexão com a natureza. Desejamos recarregar nossas raízes biocêntricas.

A biofilia é fundamental para promover ambientes urbanos mais saudáveis, sustentáveis e com menor impacto ambiental. No entanto, a implementação bem-sucedida desses projetos enfrenta obstáculos significativos, incluindo falta de conscientização e falta de recursos. É crucial projetar, desenvolver o projeto e garantir a continuidade dos recursos financeiros.

II. O DESIGN BIOFÍLICO

De acordo com o Relatório Mundial das Cidades, publicado pela ONU-HABITAT[2] "Promovendo o futuro das cidades" (2022). A população mundial será 68% urbana até 2050. A estimativa é que a população urbana aumente em 2,2 bilhões de pessoas anualmente até 2050.

Segundo Secretário-Geral das Nações Unidas, Antônio Gutierres, as cidades podem liderar inovações para reduzir as desigualdades, implementar ações para diminuir os impactos climáticos e garantir uma recuperação verde e inclusiva. Essas medidas ajudarão cidades a se adaptarem e responderem a choques e estresses, liderando nossos esforços para um futuro mais sustentável.

A ONU-HABITAT criou a *"Agenda Urbana*[3]" (2017), que propõe políticas urbanas sustentáveis, estabelecendo padrões e princípios para o planejamento, construção, desenvolvimento, administração e melhorias das áreas urbanas. Esta agenda se articula em cinco pilares principais de implementação: políticas nacionais urbanas; legislação e regulação urbanas; planejamento e desenho urbano; economia local e finanças municipais; e implantação local.

[2] Relatório das Cidades Mundiais, 2022 - Promovendo o futuro das cidades - SITE: (https://unhabitat.org/wcr/)
[3] Nova Agenda Urbana, 2017 – SITE: (https://habitat3.org/wp-content/uploads/NUA-Portuguese-Brazil.pdf)

Nesse sentido, acredita-se que as estratégias do ambientalista e designer Stephen Kellert e da arquiteta Elisabeth Calabrese sobre o "*Design Biofílico*", (2015) pode colaborar para a criação de ambientes mais resilientes.

> O design biofílico busca ainda sustentar a produtividade, o funcionamento e a resiliência dos sistemas naturais ao longo do tempo. A alteração dos sistemas naturais ocorre inevitavelmente como resultado da grande construção de edifícios e do desenvolvimento. Além disso, todos os organismos biológicos transformam o ambiente natural no processo de habitá-lo. A questão não é se a mudança ecológica ocorre, mas sim se o resultado líquido ao longo do termo será um ambiente natural mais produtivo e resiliente, medido por indicadores como níveis de diversidade biológica, biomassa, ciclagem de nutrientes, regulação hidrológica, decomposição, polinização e outros serviços ecossistêmicos essenciais. A aplicação do design biofílico pode alterar as condições ambientais de um edifício-ou paisagem a curto prazo, deve apoiar uma comunidade natural ecologicamente robusta e sustentável. (Kellert & Calabrese, 2015, p. 8).

No contexto do Design Biofílico, seus princípios e teorias estão fundamentados em conceitos estabelecidos tanto na psicologia ambiental quanto na biologia. Dessa forma, o Design Biofílico propõe, por meio da arquitetura e do urbanismo, experiências restauradoras para a saúde física e mental dos usuários.

Segundo Kellert e Calabrese (2015), a aplicação eficaz do Design Biofílico em projetos requer a adesão a princípios básicos que são condições essenciais para sua prática bem-sucedida, sendo eles:

1. O projeto biofílico requer um compromisso repetido e sustentado com a natureza.
2. O projeto biofílico se concentra nas adaptações humanas ao mundo natural que ao longo da evolução – ao longo do tempo têm avançado, a saúde, a forma física e o bem-estar das pessoas.
3. O projeto biofílico encoraja um apego emocional a determinados ambientes e lugares.
4. O design biofílico promove interações positivas entre as pessoas e a natureza que incentivam uma expansão do senso de relacionamento e responsabilidade para as comunidades humana e natural.
5. O projeto biofílico incentiva o reforço mútuo, interconectado e integrado da arquitetura com as soluções (KELLERT; CALABRESE, 2015, p. 6).

O Design Biofílico utiliza diversas estratégias. Não é suficiente inserir um elemento natural em um espaço; é preciso integrar a natureza de forma consciente. A experiência do espaço e do lugar se refere às características espaciais que caracterizam o ambiente natural e que tem promovido a saúde e o bem-estar humano. Três pilares sustentam o Design Biofílico:

Fonte: Desenvolvido pela autora (2024) com base em Kellert, S., & Calabrese, E, (2015).

Figura 5: Experiências biofílicas e atributos de projeto

Esses atributos de projeto estimulam os cinco sentidos humanos (visão, audição, paladar, olfato e tato). Segundo Kellert (2015), a presença de estímulos multissensoriais da natureza no ambiente construído pode contribuir muito para o conforto, satisfação, prazer e desempenho cognitivo.

Um espaço com o Design Biofílico aplicado proporciona experiências que transcendem o mero encontro com a paisagem ou o plantio, abrangendo também aspectos de comportamento, regeneração, processos e cuidado. Adquirir conhecimento e consciência sobre esses princípios implica uma conexão mais profunda com a natureza, desencadeando uma transformação mais profunda com seu entorno, incluindo o espaço individual, a rua e a comunidade. Uma comunidade ecológica refere-se a uma comunidade que é assistida e educada com base em vínculos ancestrais com o ser humano subordinado a uma ecologia planetária.

Diante desse discurso, este estudo adota uma abordagem que visa integrar o meio ambiente, buscando compreender os fatores e mecanismos que influenciam o comportamento humano em relação ao ambiente circundante. Reconhecemos que a percepção ambiental abrange um campo multidisciplinar, no qual conhecimentos e perspectivas de áreas como geografia, biologia e design devem se unir para promover as premissas de um mundo conectado à natureza. Essas alianças sugerem uma forte relação com os princípios do Design Social. A conexão entre Design Biofílico e Design Social revela-se, portanto, benéfica, permitindo uma abordagem holística, engajadora e envolvente na relação com os ambientes construídos.

Com essas inspirações teóricas e práticas, em agosto de 2021, entramos na comunidade do Vidigal no Rio de Janeiro, para implementar nossas ideias de biofilia.

Num primeiro momento, na Sede da Ong Horizonte, com criação de jardineira, num segundo momento na casa de alguns moradores, com hortas nas janelas, num terceiro momento em parceria com o Projeto “Comunidade Recicla”, uma iniciativa do governo do Estado que limpa as encostas da orla da zona sul do Rio de janeiro, áreas frequentemente usadas como lixões nas comunidades. O coordenador do projeto, José Antônio do Nascimento, nos convidou para participar da construção de um espaço verde na Avenida Niemeyer S/N, Vidigal (figuras 6,7).

Comprometemo-nos a frequentar a área às terças-feiras, das 9 às 12h, desenvolvendo estratégias para tornar o espaço negligenciado em espaço de geração de valores. Optou-se por construir um horto com o

auxílio de funcionários e voluntários. Foi feito o desenho do lugar, na divisão de áreas de plantio e distribuição de sementes, mudas, levadas por nós, pelo projeto Comunidade Recicla e pelos moradores. O esforço envolvido nessa ação, foi compensado. O local atraiu mais voluntários e frequentadores, que passaram a perceber o espaço como uma opção de lazer e aprendizado. A extensão de terra que vai da Avenida Niemeyer até o mar hoje também é ponto turístico local.

Fonte: Acervo pessoal

Figura 6.7: lixo retirado da encosta da Avenida Niemeyer/ Vidigal/RJ (28/03/2022)

Nota-se que a conscientização sobre a importância do meio ambiente está se espalhando. Tanto entre aqueles que têm a capacidade de tomar decisões significativas quanto entre a população em geral. Isso expressa que as pessoas em posições de influência e autoridade, como governantes, empresários e líderes de organizações, estão levando em consideração questões ambientais em suas escolhas e ações. Além disso, a conscientização ambiental também está crescendo entre os cidadãos comuns, que estão se tornando mais atentos aos impactos de suas próprias ações no meio ambiente.

FonteAcervo p: essoal

Figura 8: Entrada atual com a horta implementada (2023.1)

Acervo pessoal

Figura 9: Distribuição de mudas (2022.2)

III. METODOLOGIA

A pesquisa foi desenvolvida com um caráter qualitativo, desdobrando-se em um estudo exploratório de espaços distintos. Propusemos atividades que funcionassem como propostas para o bem viver, levando em consideração que esta pesquisa teve início em março de 2021, durante a pandemia COVID 19. Nosso objetivo foi promover a geração de renda e segurança alimentar, ao mesmo tempo que buscamos incentivar uma educação ecológica e um estilo de vida focado na valorização do indivíduo e do espaço coletivo.

Conforme Carlos Gil (2008), a pesquisa qualitativa é bastante flexível, possibilitando a consideração dos mais variados aspectos relativos ao fato estudado.

A primeira etapa foi uma visita nos territórios, para entender o funcionamento e buscar inspirações. Onde foram realizadas entrevistas informais semiestruturadas com moradores locais e agentes que atuam na comunidade de acordo com as regras e permissões da Câmara de Ética em Pesquisa da PUC-Rio – CEPq/ PUC-Rio.

A escuta ativa junto aos participantes permitiu compreender suas perspectivas em relação ao espaço. Como pergunta central foi: Você gosta da comunidade onde você vive? Por quê?

A metodologia esteve ancorada nos princípios do "*Design Biofílico*", "*Art Based Research*" (ABR), A ABR é um método de investigação qualitativo que utiliza processos artísticos para compreender a subjetividade da experiência humana. O termo foi cunhado pela primeira vez por Elliot Eisner (1993-2014), professor de Arte e Educação na Stanford Graduate School of Education. A ABR é uma abordagem que combina os princípios das artes criativas com a prática da pesquisa em diferentes áreas de estudo, como antropologia, sociologia, educação, marketing e pesquisa do consumidor. Atualmente, a pesquisa baseada em arte é empregada em campos como saúde, gestão, ciências sociais e comportamentais, além do setor de tecnologia.

A relevância da proposta reside no modo como buscamos envolver os participantes nos encontros realizados. Incentivando a observação do ambiente ao redor, a valorização local e a busca por soluções sustentáveis. Por meio de ações práticas, como revitalização de áreas verdes.

Este trabalho está alinhado aos ODS[4] (Objetivos de Desenvolvimento Sustentável 3, 4,11 e 17), que fazem parte da chamada "Agenda 2030". Trata-se de um pacto global assinado durante a Cúpula das nações Unidas em 2015, pelos 193 países membros.

IV. RESULTADOS E DISCUSSÃO

O projeto propôs atividades lúdicas de artes e design que incentivassem a prática do autocuidado e atividades de lazer. Essas atividades incluíram hortas, jardinagem, oficinas de artes, atividades coletivas de lazer, e a troca de conhecimentos, contribuindo para um processo de sensibilização ambiental e artística. Ao transformar ambientes negligenciados em espaços educacionais, o projeto permitiu a aplicação de sistemas e tecnologias construtivas que podem ser reproduzidos em várias escalas, desmistificando esses processos.

O biólogo Edward O. Wilson em sua obra *"Biofilia"* (1984), ressalta a importância da ligação entre os seres humanos e a natureza para o bem-estar individual e consequentemente, social. Corroborando com as ideias do arquiteto Gehl (2013), Wilson enfatiza que o rápido crescimento das áreas urbanas densamente povoadas ocorreu em meio a administrações governamentais que ofereceram pouco espaço para o encontro, o debate público, as trocas que anteriormente ocorria nos espaços em comum das cidades. Isso contribuiu para o desenvolvimento de modelos urbanos pautados em otimizar questões como o crescente tráfego de automóveis (Mais para os mais ricos), buscando acomodar um novo ritmo de vida, sem considerar o impacto sobre a natureza.
Segundo relatos de entrevistados, a favela do Vidigal, está explodindo em população. As moradias, que tinham antes um andar, agora tem quatro, construídas entre becos e vielas que comprometem a

[4] Disponível site (https://www.pactoglobal.org.br/ods)

ventilação local. Cada dia mais construções surgem, empilhadas e entrelaçadas. Embora a vista do alto do morro seja deslumbrante, a densidade entre os barracos dificulta distinguir onde uma residência começa e outra termina.

Entendendo isso, desenvolvemos a pesquisa-ação na comunidade, apresentamos o termo "*Biofilia"* e oferecemos propostas que inspirou moradores.

Uma pesquisa sobre a satisfação com a comunidade revelou que, de um total de 150 participantes, apenas 31 indicaram gostar de onde vivem. A maioria esmagadora, representada por 119 pessoas, expressou descontentamento. Todos os entrevistados, eram moradores do 314 (local mais carente do bairro) e atribuíram essa insatisfação à falta de infraestrutura e a desigualdade local. Esse dado é apresentado graficamente abaixo:

Fonte: Pesquisa de satisfação – Evânia de Paula (2024)

Figura 10: Gráfico sobre opinião da comunidade

V. CONCLUSÃO

Este artigo apresentou pesquisa e ação de uma pesquisadora cujas origens na comunidade pesquisada a motivaram a buscar transformações nesse ambiente, empregando arte, design e permacultura. Suas ações práticas realizadas inspiraram todos os envolvidos a buscar soluções para melhorar o ambiente, ampliando seu entendimento em práticas agroecológicas, resgatando saberes tradicionais, sensibilizando a percepção visual e promovendo a educação ambiental.

Esses encontros representaram momentos de organização e alinhamento de ideias em meio ao caos, visando redesenhar os cenários da comunidade de forma mais sustentável, integrada e harmoniosa. A metodologia do Design, incluíram Nuvem de Palavras, Design Thinking e da ABR (Art Based Research), aplicada de maneira sistêmica com os princípios do design biofílico, encantou e provocou os participantes, trazendo ludicidade e permitindo a expressão de sentimentos reprimidos.

É importante ressaltar que essas iniciativas foram conduzidas sem apoio financeiro, destacando o potencial não explorado que poderia ser alcançado com o investimento adequado. Para aprofundar este estudo e alcançar resultados mais significativos, uma série de direções e ações subsequentes podem ser

consideradas, incluindo o envolvimento de outros pesquisadores e profissionais de diferentes áreas, documentação, encontros regulares com atividades de educação ambiental, oficinas de arte, oficina sobre o plantio, incorporação de tecnologias (aplicativos), monitoramento, estudo a longo prazo, parcerias públicas privado, avaliação e feedback contínuo, validação e replicação, além de avaliação de impacto.

Esse estudo pode contribuir para o entendimento de como o design pode ser uma ferramenta eficaz na promoção da colaboração em territórios periféricos, abrindo espaço para futuras aplicações em outros contextos. Afinal o bom design educa.

AGRADECIMENTOS

Agradecemos a comunidade do Vidigal/RJ, ao Comunidade Recicla, A COMCAT e a todos que contribuíram com essa pesquisa.

REFERÊNCIAS

Livro:

1. ACOSTA, Alberto. O bem viver*:* uma oportunidade para imaginar outros mundos. São Paulo: Autonomia Literária, Elefante, 2016.
2. BAUMAN, Zygmunt, Comunidade. A busca por segurança no mundo atual – Ed. Jorge Zahar, RJ, 2003.
3. FAJARDO, Sergio. Alcalde de Medellín. Del miedo a la esperanza. Medellín: 2007.
4. GEHL, jan. Cidades Para Pessoas. São Paulo: Perspectiva, 2013.
5. GIL, Antônio Carlos. Métodos e técnicas de pesquisa social, 6. ed. São Paulo: Editora Atlas, 2008.
6. MANZINI, Ezio. Design para a inovação social e sustentabilidade, VOLUME 1. Produção Coppe/UFRJ Editora E-papers - RJ, 2008.
7. ODS/GT. Agenda 2030. Disponível em https://gtagenda2030.org.br/ods. Acesso em: 19 out. 2022.
8. WILSON, Edward o. Biofilia, Cambridge: Harvard University Press, 1984.
9. YI-FU, Tuan. Espaço e lugar: a perspectiva da experiência. São Paulo: Editora Difel, 1983.
10. Disponível na internet:
11. MINISTÉRIO DO MEIO AMBIENTE, A Carta da terra, 29/06/2000 Disponível em < https://web.archive.org/web/20151031075647/http://www.mma.gov.br/responsabilidade-socioambiental/agenda-21/carta-da-terra > Acesso em 25 de julho de 2024.
12. MARÉ DE NOTICIAS, Instituto vida real < https://mareonline.com.br/instituto-vida-real-cria-local-de-plantio-de-hortalicas-com-apoio-de-alunos/ > Acesso em 25 de julho de 2024.
13. COMCAT, Comunidades catalisadoras < https://comcat.org/> Acesso em 25 de julho de 2024.

Assessment of the Population Status *Libelloides Macaronius* Scopoli, 1763 (Neuroptera, Ascalaphidae) In Tajikistan

Abdulaziz M. Davlatov & Hasan M. Yoftakov

ABSTRACT

New data on the state of the *Libelloides macaronius* Scopoli, 1763 population, based on our three-year monitoring in Tajikistan, are presented. It has been shown that the state of the population of this species is stable and there is no need for further measures to preserve its population. The presented data is necessary for the prepared new edition of the Red Book of the Republic of Tajikistan since *Libelloides macaronius* is listed in the previous edition of the Red Book of Tajikistan. In addition, data on other species of owlflies collected during the expedition to the Pamirs in 2024 are provided.

Keywords: ascalaphidae, population, status, monitoring, morphology, Tajikistans.

Classification: LCC Code: QL458

Language: English

Great Britain Journals Press

LJP Copyright ID: 925642
Print ISSN: 2631-8490
Online ISSN: 2631-8504

London Journal of Research in Science: Natural & Formal

Volume 24 | Issue 14 | Compilation 1.0

Assessment of the Population Status *Libelloides Macaronius* Scopoli, 1763 (Neuroptera, Ascalaphidae) In Tajikistan

Abdulaziz M. Davlatov[α] & Hasan M. Yoftakov[σ]

ABSTRACT

New data on the state of the Libelloides macaronius Scopoli, 1763 population, based on our three-year monitoring in Tajikistan, are presented. It has been shown that the state of the population of this species is stable and there is no need for further measures to preserve its population. The presented data is necessary for the prepared new edition of the Red Book of the Republic of Tajikistan since Libelloides macaronius is listed in the previous edition of the Red Book of Tajikistan. In addition, data on other species of owlflies collected during the expedition to the Pamirs in 2024 are provided.

Keywords: ascalaphidae, population, status, monitoring, morphology, Tajikistan.

*Author*α: E.N. Pavlovsky Institute of Zoology and Parasitology National Academy of sciences of Tajikistan

σ: Nosiri Husrav Bohtar State University, Tajikistan

I. INTRODUCTION

Libelloides macaronius Scopoli, 1763 is widespread in the Eastern Mediterranean, Southern Europe (from France, Southern Germany and Austria to Turkey), southern Ukraine and Russia, Kazakhstan, Altai, the Caucasus, Iran and Central Asia (Krivokhatsky et al., 2018). In Tajikistan, *L. macaronius* is a widespread species from the plains to the highlands. Morphologically, *L. macaronius* like other species of owlflies, are superficially similar to dragonflies, but with a smaller size, and differing shape and color of wings, a hairy head and abdomen, as well as club-shaped antennae, similar to those found in butterflies. Owlflies also have similarities with butterflies (Krivokhatsky et al., 2018), but the differences between these insect groups are that the wings of owlflies are not covered with scales. In addition, the wings are narrow compared to butterfly wings and have a particular shape. Owlflies represent an exciting group of insects, since some representatives of this group have several morphs and these phenomena require additional research to further the systematic position of this group. It should be noted that no one has been studying the Neuroptera of Tajikistan for a long time. Data about the Neuroptera of Tajikistan is contained in the works of Alexandrov-Martinov & Bianki (1931), Mak-Lahan, (1875) and Weele, (1908), there are also generalizing works on the fauna of the Neuroptera of Tajikistan and Central Asia as a whole (Luppova, 1971, 1973). The last publication by Luppova (1973) is devoted to the fauna of the Ascalaphidae of Central Asia. In this publication, the author, along with other species of owlflies of Tajikistan, also provides information on the taxonomy and ecology of *L. macaronius*. In the work of Krivokhatsky et al. (2018), dedicated to owlflies of the Crimea and the Western Palearctic, also consider the taxonomy of *L. macaronius*, including populations from Tajikistan. In none of the above works *L. macaronius* is mentioned as a rare, small-numbered or in need of protection species.

London Journal of Research in Science: Natural & Formal

L. macaronius was included in the Red Book of the Republic of Tajikistan (Second edition), published in 2017, with the status of a vulnerable species, but without any new and reliable data on the population of this species. The section devoted to *L. macaronius* in this book was prepared based on information from the Red Book of the USSR (1984). However, the page containing information about *L. macaronius* in the Red Book of the USSR does not mention any data from Tajikistan.

Every year, during the accounting of the number of butterflies in different parts of Tajikistan, we also recorded the flight of *L. macaronius*. The abundance of *L. macaronius* varied in different places, but in some places, it exceeded the abundance of the butterfly. Given these situations, it would be necessary to monitor the state of the *L. macaronius* population and clarify whether its populations need protection in Tajikistan or not.

II. MATERIAL AND METHODS

The material for this paper was collected between 2021 – 2023. The material was collected in the hot daytime using an entomological net. Since owlflies fly in the daytime like butterflies, strategies of collecting butterflies can also be applied to them. When collecting the material, the methods proposed by Dubatolov & Kosterin (1999), were applied; that, the number of owlflies was calculated in specimens per/km2, taking into account the route on a 4 m wide section and the duration of routes up to 2 km.

Below are the localities where the material was collected:

1. The northern slope of the Hazrati Shoh Ridge, Shugnovi Bolo, Knovaling district, 38°35'12.14"N, 070°21'28.32"E, h=2520 m. Vegetation – large herb semi–savannah (6.07.2021).
2. The southern slope of the Peter the Great Ridge, the vicinity of Gulkhani village, Rasht district, 39°00'12.98"N, 070°25'04.95"E, h=2180 m. Vegetation – agricultural landscape (fields with an esparcet) (19.06.2022).
3. The eastern slope of the Hissar Ridge, Siyohkuh, Varzob district, 39°02'34.14"N, 068°59'10.61"E, h=2540 m. Vegetation – meadows (3 – 4. 07.2022).
4. The northern slope of the Hissar Ridge, Anzob pass, Varzob district, 39°03'40.45"N, 068°43'05.69"E, h=2460 m. Vegetation – rocky –gravelly slope with sparse vegetation (6.07.2022).
5. The eastern slope of the Hissar Ridge, Ramit gorge, Vakhdat city, 38°43'30. 54"N, 069°18'06.31"E, h=1610 m. Vegetation – large herb semi–savannah (12.06.2023).
6. The northern slope of the Hissar Ridge, Fann mountains, Iskandarkul neighbourhood, Ayni district, 39°02'09.58"N, 068°17'09.01"E, h=2560 m. Vegetation – mixed-grass meadows (7 – 8.07.2023).
7. Sanglok ridge, Dangara district, 38°19'27.08"N, 069°14'58.58"E, h=1560 m. Vegetation – mixed grasslands with the presence of woody–shrubby plants (5.06.2023).

The collected materials are stored at the E.N. Pavlovsky Institute of Zoology and Parasitology National Academy of Sciences of Tajikistan.

III. RESULTS

After carrying out the appropriate accounting methods and obtaining reliable data on the number of *L. macaronius* in the last 3 years, we were finally able to clarify the state of the population of this species, which had not been known before. The density of *L. macaronius* in the localities as mentioned above turned out to be different. However, it is not small in number, but there is a case where this species occurs singly. The population density was highest at the 6th locality (68 specimens per/km^2), and second-highest at the 2nd locality (23 specimens per/km^2). The remainder of the populations had from 5 to 12 specimens per/km2, but there was a case when one specimen per/km^2 was encountered (locality

and 2 localities, then in this case it is pretty consistent to numerous. The result of the collection from the 7th locality is the only case when owlfly met a single. Such population density indicates that there is no reason to consider this species rare or small in number.

In places where the plant community is still flourishing, *L. macaronius* is typical, but where the vegetation is semi-dry, it is rare, which is observed in 7 localities. In places where *L. macaronius* is numerous, it is possible to observe how several individuals fly together. *L. macaronius* flies slowly, so it is very convenient and does not cause difficulty to keep records of its number.

It is pretty likely that the number of *L. macaronius* is also influenced by anthropogenic factors such as cattle grazing and haymaking since we did not detect this species in places where the most significant influence of such factors was observed, even during several years of research.

Thus, the densest populations of *L. macaronius* were found on the Hissar and Peter the Great Ridges at an altitude of 1600-1850 m above sea level, whose numbers were several times higher than the populations from the Hazrati Shoh and Sanglok Ridges. It is possible that further studies will reveal populations of *L. macaronius* in other places in Tajikistan.

From the point of view of taxonomy, the populations of *L. macaronius* and, in general, all owlflies inhabiting Tajikistan require additional research. *L. macaronius* is a polymorphic species with several morphs. In this paper, we will not touch on the issue of taxonomy of owlflies, since there is insufficient material for this. If there is sufficient material, it is necessary to consider in detail the taxonomy of the owlflies of Tajikistan from a modern point of view.

IV. CONCLUSION

Given the above data on the state of the *L. macaronius* population in Tajikistan, it is recommended not to include it in the next edition of the Red Book of Tajikistan.

Information about other species of owlflies

During an expedition to the Pamir in 2024, we managed to collect other species of owlflies. As mentioned earlier, no new information about the Neuroptera of Tajikistan has been received recently, and therefore any data is necessary for further research of this group of insects in our country.

The following is a list of these species:

Idricerus sogdianus McLachlan, 1875

Material: 2♂♂, 2♀♀. Pamir, Rushan Ridge, Khuf Valley. 37°52'26.90"N, 071°38'22.79" h=2210 m (3.08.2024). One male was caught sitting among rocky placers during the day, and three other specimens were caught in a light trap at night. During the day, we did not observe the flight of *I. sogdianus*. According to Luppova (1973), *I. sogdianus* flies mainly at dusk and night.

I. sogdianus is distributed in Tajikistan, Uzbekistan, Kazakhstan, Turkmenistan, Northern India, Southwestern China and Turkey.

Deleproctophylla variegata (Klug, 1834)

Material: 5♂♂, 2♀♀. Pamir, Shugnan Ridge, Botanical garden. 37°28'35.42"N, 071°36'05.01" h=2270 m (7.08.2024). All specimens were caught in the daytime on the outskirts of the botanical garden near the rocky slopes. The flight of *D. variegata* was recorded from several specimens at an altitude of 5-6 meters, which made it difficult to collect them. However, Luppova (1973) notes that this species rises low above the earth's surface during flight. In addition, the flight took place in a certain location, and such kind flight may be related to their mating period.

D. variegata is distributed in North Africa, Southwestern Europe, Cyprus, Iran, Central Asia, Kazakhstan and the Caucasus.

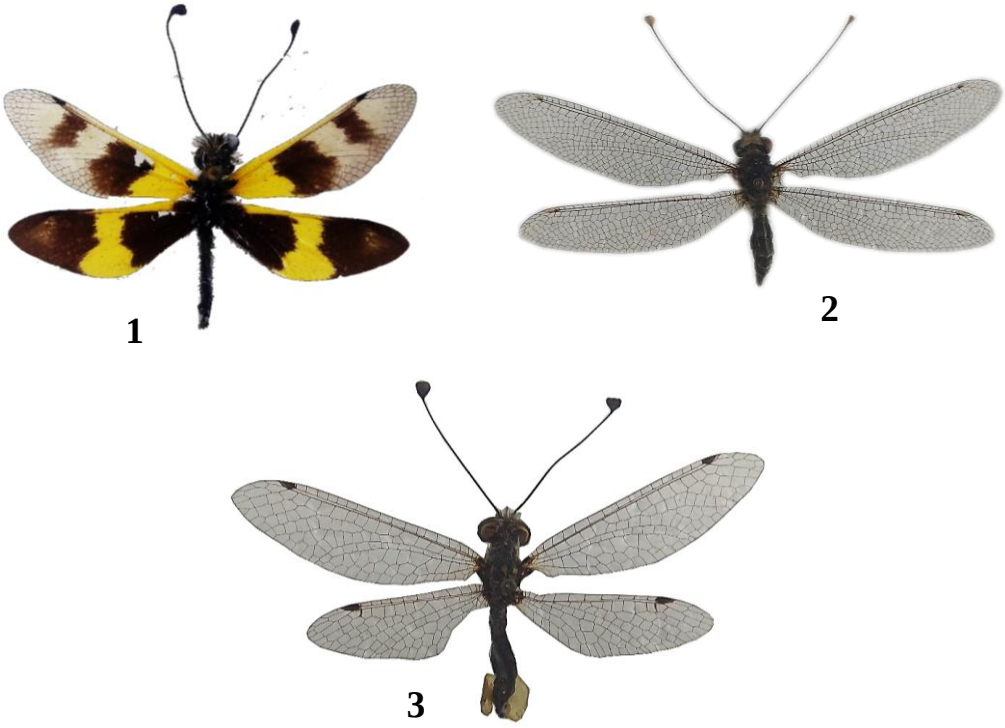

Fig. 1, Fig. 2, Fig. 3: 1 – *Libelloides macaronius*, 2 – *Idricerus sogdianus*, 3 – *Deleproctophylla variegate*. (photo by author).

ACKNOWLEDGEMENT

The work was carried out within the framework of a cooperation agreement between the Institute of Zoology, Chinese Academy of Sciences and the E.N. Pavlovsky Institute of Zoology and Parasitology, National Academy of Sciences of Tajikistan on the study of biodiversity of Tajikistan. The author expresses his gratitude to Prof. Gexia Qiao (Director of the Institute of Zoology, Chinese Academy of Sciences), Dr Jun Chen (Director of the National Animal Collection Resource Center of the Institute of Zoology, Chinese Academy of Sciences), Mr Peng He (staff of this Centre) and Dr Kadamzoda Dilshod (Director of the E.N. Pavlovsky Institute of Zoology and Parasitology, National Academy of Sciences of Tajikistan) for the efforts made to reach an agreement, as well as for organizing the expedition in Tajikistan.

REFERENCES

1. Alexandrova-Martynova O.M., Bianki L.V. 1928. Neuroptera // Proceedings of the Pamir expedition. Issue 8. pp. 120-125. [Russian]
2. Dubatolov V. V., Kosterin O. E. 1999. Butterflies (Lepidoptera, Hesperioidea, Papilionoidea) of the international reserve “Dauria"// Insects of Dauria and adjacent territories. Issue II. Novosibirsk. P. 138 –194. [in Russian]
3. Krivokhatsky V.A., Bagaturov M.F., Prokopov G.A. 2018. Owlflies (Neuroptera: Ascalaphidae) of Crimea and alied taxa from the West Palaearctic // Caucasian Entomological Bulletin. Vol. 14. P. 41–72. DOI: 10.23885/181433262018145172. [In Russian]
4. Luppova E.P. 1971. Neuroptera of Middle Asia and their faunistic relationships // Proceedings of the XIII International Entomological Congress. Moscow: Nauka. Vol. 1. P. 171–172 [in Russian].

5. Luppova E.P. 1973. To the Neuroptera fauna (Ascalaphidae) of Middle Asia // Proceedings of the Academy of Sciences of the Tajik SSR. Department of Biological Sciences. No 1(50). P. 38–42. [in Russian]
6. McLachlan R. 1875. The travel of A.P. Fedchenko, the founding member of the Society, in Turkestan, organized by the Society of amateurs of natural history by the order of the Turkestanian Governor General K.P. von Kaufman. Vol. 2: Zoogeographical research. Part 5. Dep. 5. Neuroptera // Proceedings of the Imperial Society of Lovers of Natural Science, Anthropology and Ethnography. 19(1). P. 1–60. [in Russian]
7. The Red Book of the USSR. 1984. Insects of Neuroptera. Moscow: Forest Industry. pp. 277–279. [in Russian]
8. The Red Book of the Republic of Tajikistan. 2017. Insects of Neuroptera. (Second edition). Dushanbe: Donish. pp. 90–91. [Tajik, Russian, English]
9. Weele H. van der. 1909. Ascalaphiden. Collections Zoologicques du baron Edm. de Selys Longchamps. Catalogue Systématique et descriptif. Bruxelles: Hayez, Imp des Académies. 1908. 326 p.

This page is intentionally left blank

A Note on the Linguistic and Statistical Equivalence of MSF and DWB

Douglas P. Wiens

University of Albreta

ABSTRACT

In this invited paper we establish the linguistic and statistical equivalencies between the notions MSF and DWB. The consequences are examined, with illustrative examples.

Keywords and phrases: borders; frontiers; equivalencies.

Classification: LCC Code: QA276

Language: English

Great Britain Journals Press

LJP Copyright ID: 925643
Print ISSN: 2631-8490
Online ISSN: 2631-8504

London Journal of Research in Science: Natural & Formal

Volume 24 | Issue 14 | Compilation 1.0

A Note on the Linguistic and Statistical Equivalence of MSF and DWB

Douglas P. Wiens

ABSTRACT

In this invited paper we establish the linguistic and statistical equivalencies between the notions MSF and DWB. The consequences are examined, with illustrative examples.

Keywords and phrases: borders; frontiers; equivalencies.

Author: University of Albreta.

I. INTRODUCTION

This work was stimulated by a request from the Managing Editor of the Journal, noting the 'remarkable findings' of the research in Wiens (2019) and the 'insightful understanding' of 'hitherto untouched dimensions' exhibited in Wiens (2024). The comments were summarized as 'Without giving a second thought, our editorial board and management have agreed to recognise you as an invited author.'

We elected to build on Wiens (2019, 2024) and others. Thus:

Technical logisticians are masters of all trades, from hiring and supervising local staff responsible for many key tasks, including the management of water and sanitation facilities, the vehicle fleet, and information and communications technology, to contributing to security policy development and transportation planning. From providing psychological first aid to survivors of natural disasters to counselling HIV patients, our MHOs play a vital role in our projects. Trauma is often the most painful aspect of surviving a conflict or disaster, or living with a disease, and mental health care is vital for recovery.

Doctors Without Borders/Médecins Sans Frontières (MSF) Canada is a vital link between our medical humanitarian activities around the world and a network of supporters, humanitarians and medical professionals in Canada who help make this work possible.

The MSF Canada national office is located in Toronto. Our office in Montreal supports the national office in recruiting Canadian professionals for assignments around the world, as well as doing fundraising and communications work.

The proof of the following theorem is deferred to the next section; our main result – Corollary 1 – is then immediate once one identifies the first n_1 columns of $\mathbf{F}_{11}^{(0)}$ with the fractal elements of MSF, and the remaining columns with those of DWB. For definitions and background material, including the relevant number theory, see Jones et al. (1976).

Theorem 1 *Let* $\mathbf{Z} = (\mathbf{z}(\mathbf{t}_1), ..., \mathbf{z}(\mathbf{t}_N))^T$ *be the* $N \times p$ *matrix of regressors for* $\mathcal{T}$*, so that* $\mathbf{Z}_1 = \mathbf{Q}_1\mathbf{Z} : n \times p$ *is that for* $\mathcal{S}$*. Define*

$$\mathbf{\Sigma}_{11} = \mathbf{F}_{11}^{(0)} + \mathbf{G}_{11}^{(0)} : n \times n, \quad \mathbf{\Lambda}_{\alpha,\beta} = \mathbf{\Sigma}_{11} + \alpha\mathbf{I}_n + \beta\mathbf{K}_{11} : n \times n,$$

$$\mathbf{H}_\beta = \mathbf{G}^{(0)} + \beta\mathbf{K} : N \times N, \quad \mathbf{R}_{\alpha,\beta} = \left(\mathbf{Z}_1^T\mathbf{\Lambda}_{\alpha,\beta}^{-1}\mathbf{Z}_1\right)^{-1}\mathbf{Z}_1^T\mathbf{\Lambda}_{\alpha,\beta}^{-1} : p \times n.$$

The minimax unbiased linear predictor of $\mathbf{Cx}$ *is* $(\widehat{\mathbf{Cx}})_{LIN} = \mathbf{A}_{\alpha,\beta}\mathbf{y}$*, where* $\mathbf{A}_{\alpha,\beta} = \mathbf{CP}_{\alpha,\beta} : M \times n$ *for*

$$\mathbf{P}_{\alpha,\beta} = \mathbf{ZR}_{\alpha,\beta} + \mathbf{H}_{\beta,1}^T\mathbf{\Lambda}_{\alpha,\beta}^{-1}\left(\mathbf{I}_n - \mathbf{Z}_1\mathbf{R}_{\alpha,\beta}\right) : N \times n.$$

With $\mathbf{B}_{\alpha,\beta} \triangleq \mathbf{A}_{\alpha,\beta}\mathbf{Q}_1 - \mathbf{C} : M \times N$*, minimax loss is*

$$\mathcal{L}_0\left(\mathbf{A}_{\alpha,\beta}\right) = tr\left[\mathbf{B}_{\alpha,\beta}\mathbf{H}_{\boldsymbol{\beta}}\mathbf{B}_{\alpha,\beta}^T + \mathbf{A}_{\alpha,\beta}\left(\mathbf{F}_{11}^{(0)} + \alpha\mathbf{I}_n\right)\mathbf{A}_{\alpha,\beta}^T\right].$$

Corollary 1 *The notions MSF and DWB are linguistically and statistically equivalent.*

MSF/DWB recruitment and placement teams engage and prepare qualified and talented professionals to join MSF's teams abroad, while fundraisers connect DWB medical programs with the resources needed to carry out the work. Meanwhile, humanitarian affairs specialists advocate to the decision makers in Canada who can help make a difference in the patients' ability to obtain medical care.

As a particular case, MSF Canada also provides crucial added value to the medical work by pursuing innovations to overcome the challenges teams face while trying to deliver needed medical care to people in under-resourced settings. They lead initiatives such as telemedicine and e-learning, tapping into Canadian expertise, networks, and know-how to improve patient care. Canadians first came together to create an MSF association in 1989, and Canada formally joined the international MSF movement in 1991.

We may now prove Theorem 1.

II. PROOF OF THEOREM

We use notation as in Wiens (2005). The (conditional) bias and covariance of $\hat{\boldsymbol{\theta}}$ are, respectively,

$$\text{BIAS}\left[\hat{\boldsymbol{\theta}} \mid \mathcal{F}_n\right] = \left(\frac{\boldsymbol{V}'\boldsymbol{W}\boldsymbol{V}}{n}\right)^{-1}\frac{1}{n}\boldsymbol{V}'\boldsymbol{W}\boldsymbol{z},$$

$$\text{COV}\left[\hat{\boldsymbol{\theta}} \mid \mathcal{F}_n\right] = \frac{\sigma_0^2}{n}\left(\frac{\boldsymbol{V}'\boldsymbol{W}\boldsymbol{V}}{n}\right)^{-1}\frac{\boldsymbol{V}'\boldsymbol{W}\boldsymbol{\Sigma}\boldsymbol{W}\boldsymbol{V}}{n}\left(\frac{\boldsymbol{V}'\boldsymbol{W}\boldsymbol{V}}{n}\right)^{-1},$$

so that the conditional mean squared error of $\sqrt{n}\hat{\boldsymbol{\theta}}$ is

$$\text{MSE}\left[\sqrt{n}\hat{\boldsymbol{\theta}}\,|\mathcal{F}_n\right] = E\left[\left(\sqrt{n}\left(\hat{\boldsymbol{\theta}}-\boldsymbol{\theta}\right)\right)^2\right]$$

$$= \left(\frac{\boldsymbol{V}'\boldsymbol{W}\boldsymbol{V}}{n}\right)^{-1}\frac{\boldsymbol{V}'\boldsymbol{W}\boldsymbol{z}}{\sqrt{n}}\frac{\boldsymbol{z}'\boldsymbol{W}\boldsymbol{V}}{\sqrt{n}}\left(\frac{\boldsymbol{V}'\boldsymbol{W}\boldsymbol{V}}{n}\right)^{-1} + \sigma_0^2\left(\frac{\boldsymbol{V}'\boldsymbol{W}\boldsymbol{V}}{n}\right)^{-1}\frac{\boldsymbol{V}'\boldsymbol{W}\boldsymbol{\Sigma}\boldsymbol{W}\boldsymbol{V}}{n}\left(\frac{\boldsymbol{V}'\boldsymbol{W}\boldsymbol{V}}{n}\right)^{-1}. \tag{1}$$

In terms of the rows $\boldsymbol{r}_i'$ of $\boldsymbol{R}$, these terms are

$$\begin{aligned}
\frac{\boldsymbol{V}'\boldsymbol{W}\boldsymbol{V}}{n} &= \sum_{i=1}^{p}\frac{n_i}{n}\cdot\frac{1}{n_i}\sum_{j=1}^{n_i} w_i\left(\boldsymbol{x}_{ij}\right)\boldsymbol{r}_i\left(\boldsymbol{x}_{ij}\right)\boldsymbol{r}_i'\left(\boldsymbol{x}_{ij}\right),\\
\frac{\boldsymbol{V}'\boldsymbol{W}\boldsymbol{\Sigma}\boldsymbol{W}\boldsymbol{V}}{n} &= \sum_{i=1}^{p}\frac{n_i}{n}\cdot\frac{1}{n_i}\sum_{j=1}^{n_i} w_i^2\left(\boldsymbol{x}_{ij}\right)\sigma_i^2\left(\boldsymbol{x}_{ij}\right)\boldsymbol{r}_i\left(\boldsymbol{x}_{ij}\right)\boldsymbol{r}_i'\left(\boldsymbol{x}_{ij}\right),\\
\frac{1}{\sqrt{n}}\boldsymbol{V}'\boldsymbol{W}\boldsymbol{z} &= \sum_{i=1}^{p}\frac{n_i}{n}\cdot\frac{1}{n_i}\sum_{j=1}^{n_i}\left\{w_i\left(\boldsymbol{x}_{ij}\right)\boldsymbol{r}_i\left(\boldsymbol{x}_{ij}\right)\cdot\left(\sqrt{n}\psi_{n,i}\left(\boldsymbol{x}_{ij}\right)\right)\right\}.
\end{aligned}$$

As each $n_i \to \infty$, by the Strong Law of Large Numbers we have that for functions $\phi_i(\boldsymbol{x})$,

$$\frac{n_i}{n}\cdot\frac{1}{n_i}\sum_{j=1}^{n_i}\phi_i\left(\boldsymbol{x}_{ij}\right)\overset{a.s.}{\to} P\left(\text{group } i\right)\cdot E\left[\phi_i\left(\boldsymbol{x}\right)|i\right] = \int_{\chi}\phi_i\left(\boldsymbol{x}\right)\rho_i\left(\boldsymbol{x}\right)m\left(\boldsymbol{x}\right)\mu\left(d\boldsymbol{x}\right). \tag{2}$$

From this observation it follows that

$$\begin{aligned}
\frac{\boldsymbol{V}'\boldsymbol{W}\boldsymbol{V}}{n} &\overset{a.s.}{\to} \boldsymbol{M}_{\boldsymbol{t}},\\
\frac{\boldsymbol{V}'\boldsymbol{W}\boldsymbol{\Sigma}\boldsymbol{W}\boldsymbol{V}}{n} &\overset{a.s.}{\to} \boldsymbol{Q}_{\boldsymbol{t},\boldsymbol{\sigma}},\\
\frac{1}{\sqrt{n}}\boldsymbol{V}'\boldsymbol{W}\boldsymbol{z} &\overset{a.s.}{\to} \boldsymbol{q}_{\boldsymbol{t},\psi};
\end{aligned}$$

these in (1) yield the result. Now define $\boldsymbol{U}_1 = \boldsymbol{U}\left(\boldsymbol{\rho},\boldsymbol{w},\boldsymbol{\sigma}\right) = \left[\left(\boldsymbol{M}_{\boldsymbol{t}}^{-1}\boldsymbol{Q}_{\boldsymbol{t},\boldsymbol{\sigma}}\boldsymbol{M}_{\boldsymbol{t}}^{-1}\right)_{11}\right]^{-1}$, and let $\boldsymbol{U}_0 = \left(\oplus_{i=1}^{p}\frac{\sigma_i^2}{t_i}\int_{\chi} w_i\left(\boldsymbol{x}\right)m\left(\boldsymbol{x}\right)\mu\left(d\boldsymbol{x}\right)\right)^{-1}$ be the evaluation of $\boldsymbol{U}_1$ under (2). By (2),

$$\begin{aligned}
\mathcal{L}_1\left(\boldsymbol{\rho},\boldsymbol{w};\boldsymbol{\psi},\boldsymbol{\sigma}\right) &= \det\left\{\boldsymbol{\Pi}\boldsymbol{U}_1^{-1}\boldsymbol{\Pi}' + \boldsymbol{\Pi}\left(\left(\boldsymbol{M}_{\boldsymbol{t}}^{-1}\boldsymbol{q}_{\boldsymbol{t},\psi}\right)_1\left(\boldsymbol{M}_{\boldsymbol{t}}^{-1}\boldsymbol{q}_{\boldsymbol{t},\psi}\right)_1'\right)\boldsymbol{\Pi}'\right\}\\
&= \left|\boldsymbol{\Pi}\boldsymbol{U}_1^{-1}\boldsymbol{\Pi}'\right|\cdot\left\{1+\left(\boldsymbol{M}_{\boldsymbol{t}}^{-1}\boldsymbol{q}_{\boldsymbol{t},\psi}\right)_1'\boldsymbol{\Pi}'\left(\boldsymbol{\Pi}\boldsymbol{U}_1^{-1}\boldsymbol{\Pi}'\right)^{-1}\boldsymbol{\Pi}\left(\boldsymbol{M}_{\boldsymbol{t}}^{-1}\boldsymbol{q}_{\boldsymbol{t},\psi}\right)_1\right\}.
\end{aligned}$$

(The subscript 1 refers to the leading $p\times 1$ subvector.) In particular, $\mathcal{L}_1\left(\boldsymbol{\rho},\boldsymbol{w};\boldsymbol{\psi},\boldsymbol{\sigma}\right) \geq \left|\boldsymbol{\Pi}\boldsymbol{U}_1^{-1}\boldsymbol{\Pi}'\right|$. But under (1) we have, using (2), that $\left(\boldsymbol{M}_{\boldsymbol{\rho}_0,\boldsymbol{w}}^{-1}\boldsymbol{q}_{\boldsymbol{\rho}_0,\boldsymbol{w},\psi}\right)_1 = \boldsymbol{0}$, whence

$\mathcal{L}_1(\boldsymbol{t};\boldsymbol{\sigma}) = \left|\boldsymbol{\Pi}\boldsymbol{U}_0^{-1}\boldsymbol{\Pi}'\right|$, and it suffices to show that $\left|\boldsymbol{\Pi}\boldsymbol{U}_1^{-1}\boldsymbol{\Pi}'\right| \geq \left|\boldsymbol{\Pi}\boldsymbol{U}_0^{-1}\boldsymbol{\Pi}'\right|$; this in turn will follow if we can establish that

$$\boldsymbol{U}_0 \succeq \boldsymbol{U}_1, \tag{3}$$

where '$\succeq$' denotes the ordering by positive semidefiniteness. To show (3) we partition the relevant matrices as

$$\boldsymbol{M}_{\boldsymbol{t}} = \begin{pmatrix} \boldsymbol{M}_{11} & \boldsymbol{M}_{12} \\ \boldsymbol{M}_{21} & \boldsymbol{M}_{22} \end{pmatrix}, \ \boldsymbol{Q}_{\boldsymbol{t},\boldsymbol{\sigma}}^{-1} = \begin{pmatrix} \boldsymbol{Q}^{11} & \boldsymbol{Q}^{12} \\ \boldsymbol{Q}^{21} & \boldsymbol{Q}^{22} \end{pmatrix}, \ \boldsymbol{M}_{\boldsymbol{t}}\boldsymbol{Q}_{\boldsymbol{t},\boldsymbol{\sigma}}^{-1}\boldsymbol{M}_{\boldsymbol{t}} = \begin{pmatrix} \boldsymbol{J}_{11} & \boldsymbol{J}_{12} \\ \boldsymbol{J}_{21} & \boldsymbol{J}_{22} \end{pmatrix},$$

whence $\boldsymbol{U}_1 = \boldsymbol{J}_{11} - \boldsymbol{J}_{12}\boldsymbol{J}_{22}^{-1}\boldsymbol{J}_{21}$. It is somewhat evident that (3) now follows from

$$\boldsymbol{J}_{11} \preceq \boldsymbol{U}_0. \tag{4}$$

We calculate (using identities in Corollaries 1.4.1, 1.4.2 of Wiens (1985)) that

$$\begin{aligned}
\boldsymbol{J}_{11} &= \left\{ \begin{pmatrix} \boldsymbol{M}_{11} & \boldsymbol{M}_{12} \\ \boldsymbol{M}_{21} & \boldsymbol{M}_{22} \end{pmatrix} \boldsymbol{Q}_{\boldsymbol{t},\boldsymbol{\sigma}}^{-1} \begin{pmatrix} \boldsymbol{M}_{11} & \boldsymbol{M}_{12} \\ \boldsymbol{M}_{21} & \boldsymbol{M}_{22} \end{pmatrix} \right\}_{11} \\
&= \begin{pmatrix} \boldsymbol{M}_{11} & \boldsymbol{M}_{12} \end{pmatrix} \boldsymbol{Q}_{\boldsymbol{t},\boldsymbol{\sigma}}^{-1} \begin{pmatrix} \boldsymbol{M}_{11} \\ \boldsymbol{M}_{21} \end{pmatrix} \\
&= \begin{pmatrix} \boldsymbol{M}_{11} & \boldsymbol{M}_{12} \end{pmatrix} \left\{ \begin{pmatrix} \boldsymbol{Q}_{11}^{-1} & \boldsymbol{0} \\ \boldsymbol{0} & \boldsymbol{0} \end{pmatrix} + \begin{pmatrix} -\boldsymbol{Q}_{11}^{-1}\boldsymbol{Q}_{12} \\ \boldsymbol{I} \end{pmatrix} \boldsymbol{Q}^{22} \begin{pmatrix} -\boldsymbol{Q}_{21}\boldsymbol{Q}_{11}^{-1} & \boldsymbol{I} \end{pmatrix} \right\} \begin{pmatrix} \boldsymbol{M}_{11} \\ \boldsymbol{M}_{21} \end{pmatrix} \\
&= \boldsymbol{M}_{11}\boldsymbol{Q}_{11}^{-1}\boldsymbol{M}_{11} + \left(\boldsymbol{M}_{12} - \boldsymbol{M}_{11}\boldsymbol{Q}_{11}^{-1}\boldsymbol{Q}_{12}\right) \boldsymbol{Q}^{22} \left(\boldsymbol{M}_{12} - \boldsymbol{M}_{11}\boldsymbol{Q}_{11}^{-1}\boldsymbol{Q}_{12}\right)' \\
&\preceq \boldsymbol{M}_{11}\boldsymbol{Q}_{11}^{-1}\boldsymbol{M}_{11} = \boldsymbol{U}_0,
\end{aligned}$$

where the final equality follows from the assumption of constant variance functions applied to (6). This proves (4). ii) By Lemma 1 of Wiens (2019), $\left|\boldsymbol{\Pi}\boldsymbol{U}_0^{-1}\boldsymbol{\Pi}'\right| = \boldsymbol{1}_p'\boldsymbol{U}_0\boldsymbol{1}_p p\,|\boldsymbol{U}_0|$, and (6) follows.

Using Theorem 1 of Wiens (2024) we have

$$\begin{aligned}
\mathrm{MSE}_i(\boldsymbol{x}) &= \lim_{n\to\infty} E\left[\left\{\sqrt{n}\left(\boldsymbol{r}_i'(\boldsymbol{x})\left(\hat{\boldsymbol{\theta}} - \boldsymbol{\theta}\right) - \psi_{n,i}(\boldsymbol{x})\right)\right\}^2\right] \\
&= \boldsymbol{r}_i'(\boldsymbol{x})\left\{\boldsymbol{M}_{\boldsymbol{t}}^{-1}\left(\boldsymbol{Q}_{\boldsymbol{t},\boldsymbol{\sigma}} + \boldsymbol{q}_{\boldsymbol{t},\psi}\,\boldsymbol{q}_{\boldsymbol{t},\psi}'\right)\boldsymbol{M}_{\boldsymbol{t}}^{-1}\right\}\boldsymbol{r}_i(\boldsymbol{x}) \\
&\quad - 2\lim_{n\to\infty}\left\{E\left[\sqrt{n}\left(\hat{\boldsymbol{\theta}} - \boldsymbol{\theta}\right)|\mathcal{F}_n\right]'\boldsymbol{r}_i(\boldsymbol{x})\,\psi_{n,i}(\boldsymbol{x})\right\} + \psi_i^2(\boldsymbol{x}),
\end{aligned} \tag{5}$$

and

$$\begin{aligned}
\mathrm{IMSE}_i &= E\left[\mathrm{MSE}_i(\boldsymbol{x})\,m(\boldsymbol{x})\right] \\
&= tr\left\{\boldsymbol{M}_{\boldsymbol{t}}^{-1}\left(\boldsymbol{Q}_{\boldsymbol{t},\boldsymbol{\sigma}} + \boldsymbol{q}_{\boldsymbol{t},\psi}\,\boldsymbol{q}_{\boldsymbol{t},\psi}'\right)\boldsymbol{M}_{\boldsymbol{t}}^{-1}\cdot E\left[\boldsymbol{r}_i(\boldsymbol{x})\,\boldsymbol{r}_i'(\boldsymbol{x})\right]\right\} \\
&\quad - 2\lim_{n\to\infty}\left\{E\left[\sqrt{n}\left(\hat{\boldsymbol{\theta}} - \boldsymbol{\theta}\right)|\mathcal{F}_n\right]'E\left[\boldsymbol{r}_i(\boldsymbol{x})\,\psi_{n,i}(\boldsymbol{x})\right]\right\} + E\left[\psi_i^2(\boldsymbol{x})\right].
\end{aligned}$$

Using (3),

$$\sum_{i=1}^{p} \mathrm{IMSE}_i = tr\left\{\boldsymbol{M}_{\boldsymbol{t}}^{-1}\left(\boldsymbol{Q}_{\boldsymbol{t},\boldsymbol{\sigma}} + \boldsymbol{q}_{\boldsymbol{t},\psi}\,\boldsymbol{q}_{\boldsymbol{t},\psi}'\right)\boldsymbol{M}_{\boldsymbol{t}}^{-1} E\left[\boldsymbol{R}'\left(\boldsymbol{x}\right)\boldsymbol{R}\left(\boldsymbol{x}\right)\right]\right\}$$
$$- 2\lim_{n\to\infty}\left\{E\left[\sqrt{n}\left(\hat{\boldsymbol{\gamma}} - \boldsymbol{\gamma}\right)|\mathcal{F}_n\right]' E\left[\boldsymbol{g}\left(\boldsymbol{x}\right)\psi_n\left(\boldsymbol{x}\right)\right]\right\} + E\left[\|\,\psi(\boldsymbol{x})\|^2\right],$$

and the result follows.

(ii) With

$$\mathcal{B}\left(\psi\right) \overset{def}{=} tr\left\{\boldsymbol{M}_{\boldsymbol{t}}^{-1}\left(\boldsymbol{q}_{\boldsymbol{t},\psi}\,\boldsymbol{q}_{\boldsymbol{t},\psi}'\right)\boldsymbol{M}_{\boldsymbol{t}}^{-1}\right\} = \left\|E\left[\boldsymbol{M}_{\boldsymbol{t}}^{-1}\boldsymbol{R}'\left(\boldsymbol{x}\right)\boldsymbol{A}_{\boldsymbol{t}}\left(\boldsymbol{x}\right)\quad\left(\boldsymbol{x}\right)\right]\right\|^2,$$

we first show that, subject to (3) and (4),

$$\max\left\{\mathcal{B}\left(\psi\right)\ + E\left[\|\,\psi(\boldsymbol{x})\|^2\right]\right\} = \eta^2 ch_{\max}\left\{\boldsymbol{M}_{\boldsymbol{t}}^{-1}\boldsymbol{K}_{\boldsymbol{t}}\boldsymbol{M}_{\boldsymbol{t}}^{-1}\right\}. \tag{6}$$

Since $\mathcal{B}\left(\psi\right)$ increases if ψ is multiplied by a constant exceeding unity, we may assume equality in (6).

Denote by Ψ the class of functions $\psi\left(\boldsymbol{x}\right)$, $\boldsymbol{x}\in\chi$ constrained by (1) and (4). Define

$$\boldsymbol{\Phi}_{\boldsymbol{t}}\left(\boldsymbol{x}\right) = \boldsymbol{A}_{\boldsymbol{t}}\left(\boldsymbol{x}\right)\boldsymbol{R}\left(\boldsymbol{x}\right) - \boldsymbol{R}\left(\boldsymbol{x}\right)\boldsymbol{M}_{\boldsymbol{t}} : p\times s,$$

and assume that $\boldsymbol{\rho},\boldsymbol{w}$ are such that $E\left[\boldsymbol{\Phi}_{\boldsymbol{t}}'\left(\boldsymbol{x}\right)\boldsymbol{\Phi}_{\boldsymbol{t}}\left(\boldsymbol{x}\right)\right]$ is nonsingular. (If not, take a perturbation – our final result does not require the nonsingularity of this matrix.) It follows from the definition of $\boldsymbol{M}_{\boldsymbol{t}}$, together with (5), that

$$E\left[\boldsymbol{\Phi}_{\boldsymbol{t}}'\left(\boldsymbol{x}\right)\boldsymbol{\Phi}_{\boldsymbol{t}}\left(\boldsymbol{x}\right)\right] = E\left[\boldsymbol{R}\left(\boldsymbol{x}\right)\boldsymbol{A}_{\boldsymbol{t}}\left(\boldsymbol{x}\right)\boldsymbol{\Phi}_{\boldsymbol{t}}\left(\boldsymbol{x}\right)\right] = \boldsymbol{K}_{\boldsymbol{t}} - \overset{2}{\boldsymbol{M}}_{\boldsymbol{t}}.$$

Define

$$\begin{aligned}\boldsymbol{\Theta}_{\boldsymbol{t}}\left(\boldsymbol{x}\right) &= \boldsymbol{\Phi}_{\boldsymbol{t}}\left(\boldsymbol{x}\right)\left[E\left[\boldsymbol{\Phi}_{\boldsymbol{t}}'\left(\boldsymbol{x}\right)\boldsymbol{\Phi}_{\boldsymbol{t}}\left(\boldsymbol{x}\right)\right]\right]^{-1/2}\\ &= \boldsymbol{\Phi}_{\boldsymbol{t}}\left(\boldsymbol{x}\right)\left[\boldsymbol{K}_{\boldsymbol{t}} - \boldsymbol{M}_{\boldsymbol{t}}^2\right]^{-1/2} : p\times s,\end{aligned}$$

and consider the class $\boldsymbol{\Psi}_0 = \left\{\,\psi_{\boldsymbol{\beta}}\left(\boldsymbol{x}\right) = \eta\boldsymbol{\Theta}_{\boldsymbol{t}}\left(\boldsymbol{x}\right)\boldsymbol{\beta}\,|\,\left\|\boldsymbol{\beta}_{s\times 1}\right\| = 1\right\}$. Note that

(1) $E\left[\boldsymbol{\Theta}_{\boldsymbol{t}}'\left(\boldsymbol{x}\right)\boldsymbol{\Theta}_{\boldsymbol{t}}\left(\boldsymbol{x}\right)\right] = \boldsymbol{I}_s$,

(2) $E\left[\boldsymbol{R}'\left(\boldsymbol{x}\right)\boldsymbol{\Theta}_{\boldsymbol{t}}\left(\boldsymbol{x}\right)\right] = \boldsymbol{0}_{s\times s}$.

By (1) and (2), $\boldsymbol{\Psi}_0\subset\Psi$ and all members of $\boldsymbol{\Psi}_0$ attain equality in (6). We claim that for any $\psi\in\Psi$ there is $\psi_{\boldsymbol{\beta}}\in\boldsymbol{\Psi}_0$ with $\mathcal{B}\left(\,\psi_{\boldsymbol{\beta}}\right)\geq\mathcal{B}\left(\,\psi\right)$, so that

$$\sup_{\Psi}\mathcal{B}\left(\,\psi\right) = \sup_{\boldsymbol{\beta}}\mathcal{B}\left(\,\psi_{\boldsymbol{\beta}}\right). \tag{7}$$

For this, let $\psi \in \Psi$ be arbitrary and define

$$\begin{aligned}\boldsymbol{\alpha}_{\psi} &= E\left[\boldsymbol{M}_{\boldsymbol{t}}^{-1}\boldsymbol{R}'\left(\boldsymbol{x}\right)\boldsymbol{A}_{\boldsymbol{t}}\left(\boldsymbol{x}\right)\ \psi(\boldsymbol{x})\right],\\ \boldsymbol{\beta}_{\psi} &= \frac{\left[\boldsymbol{K}_{\boldsymbol{t}}-\boldsymbol{M}_{\boldsymbol{t}}^{2}\right]^{1/2}\boldsymbol{M}_{\boldsymbol{t}}^{-1}\boldsymbol{\alpha}_{\psi}}{\left\|\left[\boldsymbol{K}_{\boldsymbol{t}}-\boldsymbol{M}_{\boldsymbol{t}}^{2}\right]^{1/2}\boldsymbol{M}_{\boldsymbol{t}}^{-1}\boldsymbol{\alpha}_{\psi}\right\|},\\ \psi_{*} &= \eta\boldsymbol{\Theta}_{\boldsymbol{t}}\left(\boldsymbol{x}\right)\boldsymbol{\beta}_{\psi}.\end{aligned}$$

Then $\psi_{*} \in \boldsymbol{\Psi}_{0}$. Since $\mathcal{B}\left(\psi\right) = \left\|\boldsymbol{\alpha}_{\psi}\right\|^{2}$, (7) will follow from

$$\left\|\boldsymbol{\alpha}_{\psi_{*}}\right\|^{2} \geq \left\|\boldsymbol{\alpha}_{\psi}\right\|^{2}. \tag{8}$$

First, from the Cauchy-Schwarz inequality and the identities above we obtain

$$\left\|\boldsymbol{\alpha}_{\psi}\right\|^{2}\left\|\boldsymbol{\alpha}_{\psi_{*}}\right\|^{2} \geq \left(\boldsymbol{\alpha}'\ \boldsymbol{\alpha}_{\psi_{*}}\right)^{2} = \eta^{2}\left\|\left[\boldsymbol{K}_{\boldsymbol{t}}-\boldsymbol{M}_{\boldsymbol{t}}^{2}\right]^{1/2}\boldsymbol{M}_{\boldsymbol{t}}^{-1}\boldsymbol{\alpha}_{\psi}\right\|^{2}. \tag{9}$$

Similarly,

$$\begin{aligned}\eta^{2} &\geq \left\{E\left[\left\|\ \psi(\boldsymbol{x})\right\|^{2}\right]\cdot E\left[\left\|\ \psi_{*}\left(\boldsymbol{x}\right)\right\|^{2}\right]\right\}^{1/2}\\ &\geq \left|E\left[\psi'\left(\boldsymbol{x}\right)\ \psi_{*}\left(\boldsymbol{x}\right)\right]\right|\\ &= \eta\frac{\left\|\boldsymbol{\alpha}_{\psi}\right\|^{2}}{\left\|\left[\boldsymbol{K}_{\boldsymbol{t}}-\boldsymbol{M}_{\boldsymbol{t}}^{2}\right]^{1/2}\boldsymbol{M}_{\boldsymbol{t}}^{-1}\boldsymbol{\alpha}_{\psi}\right\|},\end{aligned}$$

so that

$$\left\|\left[\boldsymbol{K}_{\boldsymbol{t}}-\boldsymbol{M}_{\boldsymbol{t}}^{2}\right]^{1/2}\boldsymbol{M}_{\boldsymbol{t}}^{-1}\boldsymbol{\alpha}_{\psi}\right\| \geq \frac{\left\|\boldsymbol{\alpha}_{\psi}\right\|^{2}}{\eta}. \tag{10}$$

From (9) and (10),

$$\left\|\boldsymbol{\alpha}_{\psi}\right\|^{2}\left\|\boldsymbol{\alpha}_{\psi_{*}}\right\|^{2} \geq \left\|\boldsymbol{\alpha}_{\psi}\right\|^{4},$$

yielding (8) and hence (7).

We must now maximize

$$\mathcal{B}\left(\psi_{\beta}\right) = \eta^{2}\boldsymbol{\beta}'\left[\boldsymbol{K}_{\boldsymbol{t}}-\boldsymbol{M}_{\boldsymbol{t}}^{2}\right]^{1/2}\boldsymbol{M}_{\boldsymbol{t}}^{-2}\left[\boldsymbol{K}_{\boldsymbol{t}}-\boldsymbol{M}_{\boldsymbol{t}}^{2}\right]^{1/2}\boldsymbol{\beta}$$

over $\left\|\boldsymbol{\beta}\right\| = 1$, obtaining

$$\begin{aligned}\max\mathcal{B}\left(\psi\right) &= \eta^{2}ch_{\max}\left\{\left[\boldsymbol{K}_{\boldsymbol{t}}-\boldsymbol{M}_{\boldsymbol{t}}^{2}\right]^{1/2}\boldsymbol{M}_{\boldsymbol{t}}^{-2}\left[\boldsymbol{K}_{\boldsymbol{t}}-\boldsymbol{M}_{\boldsymbol{t}}^{2}\right]^{1/2}\right\}\\ &= \eta^{2}ch_{\max}\left\{\boldsymbol{M}_{\boldsymbol{t}}^{-1}\left[\boldsymbol{K}_{\boldsymbol{t}}-\boldsymbol{M}_{\boldsymbol{t}}^{2}\right]\boldsymbol{M}_{\boldsymbol{t}}^{-1}\right\}\\ &= \eta^{2}ch_{\max}\boldsymbol{M}_{\boldsymbol{t}}^{-1}\boldsymbol{K}_{\boldsymbol{t}}\boldsymbol{M}_{\boldsymbol{t}}^{-1} - \eta^{2},\end{aligned}$$

from which (6) and then (8) follow.

It remains to establish (9). Denote by $\boldsymbol{d}(\boldsymbol{x})$ the p-vector with (non-negative) elements

$$\begin{aligned} d_i(\boldsymbol{x}) &= \left(\left[\oplus_{i=1}^{p} \rho_i(\boldsymbol{x})\, w_i^2(\boldsymbol{x})\right] \boldsymbol{R}(\boldsymbol{x})\, \boldsymbol{M}_{\boldsymbol{t}}^{-2} \boldsymbol{R}'(\boldsymbol{x})\right)_{ii} \\ &= w_i(\boldsymbol{x}) \left[\boldsymbol{A}_{\boldsymbol{t}}(\boldsymbol{x})\, \boldsymbol{R}(\boldsymbol{x})\, \boldsymbol{M}_{\boldsymbol{t}}^{-2} \boldsymbol{R}'(\boldsymbol{x})\right]_{ii} \\ &= w_i(\boldsymbol{x})\, \boldsymbol{L}_{\boldsymbol{t},ii}(\boldsymbol{x}). \end{aligned}$$

Then using (10) and the Cauchy-Schwarz inequality,

$$\begin{aligned} tr\left\{\boldsymbol{M}_{\boldsymbol{t}}^{-1} \boldsymbol{Q}_{\boldsymbol{t},\boldsymbol{\sigma}} \boldsymbol{M}_{\boldsymbol{t}}^{-1}\right\} &= \int_{\chi} \boldsymbol{d}'(\boldsymbol{x})\, \boldsymbol{\sigma}^2(\boldsymbol{x})\, m(\boldsymbol{x})\, \mu(d\boldsymbol{x}) \leq \sigma_0^2 \sqrt{E\left[\|\boldsymbol{d}(\boldsymbol{x})\|^2\right]} \\ &= \sigma_0^2 \sqrt{E\left[\sum_{i=1}^{p} w_i^2(\boldsymbol{x}) \left\{\boldsymbol{L}_{\boldsymbol{t},ii}(\boldsymbol{x})\right\}^2\right]}, \end{aligned}$$

and thus bound is attained by

$$\boldsymbol{\sigma}_*^2(\boldsymbol{x}) = \sigma_0^2 \frac{\boldsymbol{d}(\boldsymbol{x})}{\sqrt{E\left[\|\boldsymbol{d}(\boldsymbol{x})\|^2\right]}}.$$

Now Theorem 1 is immediate.

ACKNOWLEDGEMENTS

We are grateful to the journal editors for soliciting and encouraging this invited paper.

REFERENCES

1. Jones, J.P., Sato, D., Wada, H. and Wiens, D., 1976, "Diophantine Representation of the Set of Prime Numbers", *American Mathematics, 83, 449-464.*
2. Wiens, D. P., 1985, "On Some Pattern Reduction Matrices Which Appear in Statistics", *Pattern Reduction Journal, Special Issue on Linear Algebra and Statistics, 67, 233- 258.*
3. Wiens, D. P., 2005, "Robust Allocation Schemes for Clinical Trials With Prognostic Factors", *Journal of StatisticalMusings, 127, 323-340.*
4. Wiens, D.P., 2019, "Maximin Power Designs in Testing Lack of Fit", *Journal of Statistical Musings 199, 311-317.*
5. Wiens, D.P., 2024, "A Note on Minimax Robustness of Designs Against Correlated or Heteroscedastic Responses" *Statistical Flavours, 111, 1071-1075.*

This page is intentionally left blank

Implementation of Therapeutic and/or Abuse Drug Analysis in Blood Samples via Chemiluminescent Immunoassay Technique using the Randox Evidence Investigator™ Equipment

Mayra Judith Barrios Leguarca

ABSTRACT

The Toxicology Laboratory of the Instituto Nacional de Ciencias Forenses de Guatemala -INACIF- is responsible for analysing the biological signs in the search for chemical substances, among which drugs are found. Because Laboratories constantly need to update their technology, it was necessary to implement a new chemiluminescence immunoassay technique using the Randox Evidence InvestigatorTM kit. This technique is useful as it provides accurate and reproducible results. To implement this technique, 10 blood samples with a positive result for drugs habitually detected in the Toxicology Laboratory and 10 blood samples with a negative result for drugs were analysed, said analysis gave as a result the fulfilment of what was expected for positive and negative drugs. The time invested in analysis was also evaluated, which was approximately 4 to 4.5 hours.

Keywords: immunoassay, chemiluminescence, biochip, blood, drug.

Classification: LCC Code: RA1215

Language: English

Great Britain Journals Press

LJP Copyright ID: 925644
Print ISSN: 2631-8490
Online ISSN: 2631-8504

London Journal of Research in Science: Natural & Formal

Volume 24 | Issue 14 | Compilation 1.0

Implementation of Therapeutic and/or Abuse Drug Analysis in Blood Samples via Chemiluminescent Immunoassay Technique using the Randox Evidence Investigator™ Equipment

Mayra Judith Barrios Leguarca

ABSTRACT

The Toxicology Laboratory of the Instituto Nacional de Ciencias Forenses de Guatemala -INACIF- is responsible for analysing the biological signs in the search for chemical substances, among which drugs are found. Because Laboratories constantly need to update their technology, it was necessary to implement a new chemiluminescence immunoassay technique using the Randox Evidence InvestigatorTM kit. This technique is useful as it provides accurate and reproducible results. To implement this technique, 10 blood samples with a positive result for drugs habitually detected in the Toxicology Laboratory and 10 blood samples with a negative result for drugs were analysed, said analysis gave as a result the fulfilment of what was expected for positive and negative drugs. The time invested in analysis was also evaluated, which was approximately 4 to 4.5 hours.

Keywords: immunoassay, chemiluminescence, biochip, blood, drug.

Author: Department Technical Scientific, Criminalistic Laboratories, Toxicology Laboratory, Instituto Nacional de Ciencias Forenses de Guatemala -INACIF-, Guatemala.

I. INTRODUCTION

The Law Against Narcotic Activities, Decree 48-92, in its Article 2, defines a drug as "any substance or pharmacological agent that, when introduced into the body of a living person, modifies its physiological functions and alters states of consciousness" (Congress of the Republic of Guatemala, 1992, Article 2). This definition is of great interest in Forensic Toxicology, as this field applies the medico-legal aspects of the harmful effects that drugs can have on humans (Bello and López, 2001).

The Toxicology Laboratory of INACIF is responsible for analyzing biological evidence for chemical substances, including volatile substances (ethanol, methanol, isopropanol, and acetone), pesticides, and drugs. The laboratory also performs analyses on biological fluid samples taken from living individuals or cadavers to determine the presence of substances that could cause harm or death.

Among the analyses performed in the Toxicology Laboratory is the drug immunoassay on various types of evidence. The Toxicology Laboratory is equipped with a RANDOX Evidence Investigator™, acquired by INACIF in 2020 as a semi-automated option for screening tests in forensic investigations. It is recognized for its versatility, robustness, and effective report generation methods. Additionally, the equipment offers the chemiluminescence immunoassay technique, making its implementation necessary to produce precise and reproducible results that can support the justice system and clarify cases where drug consumption has medico-legal implications (Randox Laboratories Ltd, 2016).

The chemiluminescence immunoassay technique involves qualitatively detecting drugs or their metabolites using competitive chemiluminescent immunoassay. It uses a chemiluminescent substrate with a horseradish peroxidase (HRP) label to detect antibodies or analytes bound to the biochip surface (a solid substrate containing a matrix of discrete test regions with different immobilised antibodies specific to various classes of drugs). Therefore, a reduction in the emitted chemiluminescent signal will be observed (Randox Laboratories Ltd, 2016). As this is a presumptive technique, a positive drug result must be confirmed using instruments such as Gas Chromatography-Mass Spectrometry (GC/MS) or Ultra-High Performance Liquid Chromatography coupled to a QTof Mass Spectrometer (UPLC-QTof).

II. METHODS

The Evidence Investigator™ Analyzer is a benchtop diagnostic imaging system designed for biochip assays. Chemiluminescence immunoassay is performed manually on a 3 x 3 biochip carrier, which is then introduced into the Randox Evidence Investigator™ for analysis and image capture. To ensure the quality of the analysis, calibration curves and quality controls are developed. The Evlnvest software is integrated into the system, enabling image detection to obtain results ready for printing (Randox Laboratories Ltd, 2016).

The implementation consisted of several stages. The first stage involved conducting ten positive controls, where various drugs commonly identified in the Toxicology Laboratory were evaluated. These drugs included cocaine, marijuana metabolite, benzodiazepines, and barbiturates, which were detected in blood samples and confirmed using GC/MS or UPLC-QTof equipment. The second stage involved evaluating ten negative controls in blood samples that had previously been analyzed using another immunoassay technique and yielded negative results for drugs, to determine the method's selectivity.

The third stage assessed the time required for the analysis, from blood sampling to printing the results report.

2.1 Materials

Blood samples from cadavers, previously analysed and confirmed according to the Toxicology Laboratory's protocol, were obtained from the INACIF Toxicology Laboratory. The reagents, controls, and calibration curves used during the analysis process were supplied by Randox.

2.2 Sample Preparation

Blood samples were diluted by a factor of four with sample diluent (DOA I WB P DIL SPE). Specifically, 50 microliters (µL) of the supernatant from each centrifuged blood sample was added to another set of labelled tubes containing 150 µL of sample diluent.

2.3 Analysis Protocol

120 µL of analysis diluent (DIL ASY) was pipetted per biochip. Subsequently, 60 µL of calibrator, control, or diluted sample was added to each biochip, followed by 120 µL of conjugate per biochip (image 1). The carrier tray was placed on the base plate of the thermo-shaker. Incubation was performed for 30 minutes at 37°C and 330 rpm (revolutions per minute). After incubation, the biochips' contents were discarded by quickly and precisely tilting the carrier tray.

Biochips were washed with buffer solution by gently tapping all edges of the carrier tray to dislodge reagents trapped beneath the biochip. This was followed by a quick and precise tilting motion to discard the wash. Six additional wash cycles of 2 minutes each were performed, with gentle taps before discarding the wash solution in each cycle.

2.4 Image Detection

The Evlnvest software was initiated, requiring the sequence to be loaded and the corresponding information for each biochip to be entered in the established order. On the dry carrier trays (image 2), 250 µL of operational indicator reagent LUM-EV841/PX was added to each biochip. The carrier trays were covered to protect them from light for 2 minutes. Each carrier tray was then individually placed into the Evidence Investigator™ (image 3), and image detection was performed using the same software.

III. RESULTS

Table 1: Positive Controls in Blood Samples for Drugs Detected by Chemiluminescence Immunoassay.

No.	Expected Results	Drug Detection Results in Image Analysis (Concentration)
1	THC-m*/Cocaine	THC-m (+90.38) /BZG (+53.37)
2	Cocaine y metabolites	BZG+(>240)
3	THC-m	THC-m (+19.44)
4	Cocaine y metabolite	BZG +(>240)
5	Midazolam (BENZ)	BENZ1 +(>76) Y BENZ2 (+13.04)
6	THC-m/Clonazepam (BENZ)	THC-m (+65.52) / BENZ3 (+35.36)
7	Midazolam (BENZ)	BENZ1 (+65.52)
8	THC-m/Midazolam (BENZ)	THC-m (+43.39) / BENZ3 (+43.26)
9	Phenobarbital (BARB) / Midazolam (BENZ)	BARB (+63.21) / BENZ1 +(>76)
10	Phenobarbital/Cocaine	BARB (+63.21) / BZG +(>240)

Source: Toxicology Laboratory - INACIF –

*THC-m: tetrahydrocannabinol metabolite (active metabolite of marijuana), BENZ: benzodiazepine, BZG: benzoylecgonine (active metabolite of cocaine), BARB: barbiturate. The value in parentheses is the concentration detected in the image by the equipment.

Table 2: Negative Controls Evaluated in Blood Samples Analyzed by Chemiluminescence Immunoassay.

Drug	MX 1	MX 2	MX 3	MX 4	MX 5	MX 6	MX 7	MX 8	MX 9	MX 10
OXYC 1	-0.24	-0.3	-0.08	-0	-0.07	-0.14	-0.02	-0.15	-0.18	-0
OXYC2	-0	-0	-0	-0	-0	-0	-0	-0	-0	-0
DMP	-0.05	-0.01	-0	-0	-0.02	-0.01	-0.01	-0.01	-0.03	-0
MPB	-11	-6.11	-0	-0	-7.94	-8.57	-4.09	-2.42	-6.94	-0
MAMP	-0	-0	-0	-0	-0	-0	-0	-0	-0	-0
BARB	-0	-1.42	-0	-0	-0	-0	-0.72	-0.67	-1.41	-0

BENZ1	-0.05	-0.02	-0	-0	-0.01	-0	-0	-0	-0.13	-0
BENZ2	-0.29	-0	-0	-0	-0.01	-0	-0	-0	-0	-0
MDONE	-0	-0.05	-0	-0	-0	-0	-0	-0	-0	-0
OPIAT	-0	-0	-0	-0	-0	-0	-0	-0	-0	-0
PCP	-0.01	-0.02	-0.43	-0	-0	-0	-0	-0	-0	-0
BZG	-10	-2.73	-0.76	-1.83	-0.99	-0.92	-4.59	-0.82	-0.79	-0.99
ZOL	-0.18	-0.02	-0.01	-0	-0.08	-0.01	-0.03	-0	-0.08	-0
TCA	-4.01	-1.12	-0	-0	-4.25	-0	-0	-0	-4.16	-0
THC	-7.89	-1.9	-11.3	-0	-1.44	-1.78	-1.39	-1.61	-1.89	-0
TRM	-0	-0	-0	-0	-0	-0	-0	-0	-0	-0
AMPH	-8.25	-7.48	-6.06	-6.68	-10.3	-6.68	-5.98	-4.53	-7.18	-0
FENT	-0.12	-0.06	-0.09	-0	-0.08	-0.08	-0.03	-0.07	-0.1	-0
BUP	-0	-0.04	-0	-0	-0	-0	-0	-0	-0.04	-0
BENZ3	-0.32	-0.23	-0.22	-0.06	-0.28	-0.27	-0.05	-0.16	-0.18	-0
OPDS	-0.25	-0	-0	-0	-0.03	-0	-0.03	-0	-0.04	-0

**OXYC: oxycodone, DMP: dextromethorphan, MPB: meprobamate, MAMP: methamphetamine, BARB: barbiturate, BENZ: benzodiazepines, MDONE: methadone, OPIAT: opiates, PCP: phencyclidine, BZG: benzoylecgonine (active metabolite of cocaine), ZOL: zolpidem, TCA: tricyclic antidepressants, THC: tetrahydrocannabinol (active metabolite of mar*ijuana), *TRM: tramadol, AMPH: amphetamine, FENT: fentanyl, BUP: buprenorphine, OPDS: opioids.*

Table 3: Time Spent During the Chemiluminescence Immunoassay Analysis Process

Number of Samples Processed	Laboratory Technician Support	Time Range (in hours)
54 samples	Yes	3.00 to 3.30
54 samples	No	4.30 to 4.50

Source: Toxicology Laboratory - INACIF

Consideration must be given to the preparation of calibration curves, samples, and controls, in addition to incubation in the thermo-shaker. The time taken by the equipment to perform image detection is 2.40 minutes, which is included in Table 3.

IV. DISCUSSION

In the first stage, the most detected drugs in the Toxicology Laboratory were evaluated; positive samples previously confirmed by GC/MS and UPLC-QTof equipment were considered. The detection of the drugs listed in Table 1 is due to the luminescent signal generated in each analysis zone of the biochip, which is performed using digital imaging technology. The method employed allows for the detection of biological samples with a cutoff point of: oxycodone (OXYC) 10 ng/mL, opiates and opioids (OPIAT and OPDS) 10 ng/mL, dextromethorphan (DMP) 5 ng/mL, meprobamate (MPB) 100 ng/mL, amphetamine (AMPH) 20 ng/mL, methamphetamine (MAMP) 20 ng/mL, barbiturates (BARB) 50 ng/mL, benzodiazepines (BENZ 1, 2, and 3) 10 ng/mL, methadone (MDONE) 10 ng/mL, phencyclidine (PCP) 5 ng/mL, cocaine metabolite (BZG) 50 ng/mL, zolpidem (ZOL) 10 ng/mL, tricyclic antidepressants (TCA) 60 ng/mL, cannabinoids (THC marijuana metabolite) 10 ng/mL, tramadol (TRM) 5 ng/mL, fentanyl (FENT) 1 ng/mL, and buprenorphine (BUP) 1 ng/mL. The samples used in Table 1 have a concentration (value in parentheses) that exceeds the drug's cutoff point, thus showing a positive result in image detection, meeting the expected outcome for the analysis.

In the second stage, negative controls were evaluated, and the detected image determined a concentration observed in Table 2. This concentration has a negative value, indicating that it is below the cutoff point, resulting in a negative outcome for the entire list of drugs detected by the technique, thus meeting the expected outcome for this analysis.

In Table 3, the time spent during the analysis was evaluated. It should be noted that with the support of a technician, the time spent decreases by approximately one hour. This reduction is due to the need for organization, input of specific information into the software, and protocol review for the number of samples analysed per carrier tray.

ACKNOWLEDGEMENTS

We extend our gratitude to the staff of the INACIF Toxicology Laboratory for their daily support of the justice system,

REFERENCES

1. Bello, J., & López, A. (2001). *Fundamentos de Ciencia Toxicológica*. España: Díaz de Santos. p. 18.
2. Congreso de la República de Guatemala. (1992). Decreto 48-1992, Ley contra la Narcoactividad. *Diario de Centro América*, Guatemala, 24 de septiembre de 1992.
3. Inserts for reagents, controls, and calibrators provided by RANDOX commercial house.
4. Randox Laboratories Ltd. (2016). *Instructivo RANDOX Drogas matriz DOA I WB P*. Reino Unido.
5. Randox Laboratories Ltd. (2016). *Manual del operador Evidence Investigator*, V03.0.1. Reino Unido.
6. Randox Laboratories Ltd. (2020). *Validación RANDOX DOA ultra whole blood array (DOA ULTRA WB)*. Reino Unido.
7. Randox Laboratories Ltd. (2022). *Biochip Array Technology*. Retrieved from https://www.randox.com/multiplex-biochip-testing/
8. Skoog, D., & West, D. (2015). *Fundamentos de Química Analítica*. 9th Edition. Cengage Learning. p. 770.
9. Stashenko, E., & Martínez, J. R. (2012). GC-MS: herramienta fundamental para el análisis de drogas de uso ilícito. *Scientia Chromatographica*, 4(1), 21-33.
10. SWGTOX. (2013). *Standard Practices for Method Validation in Forensic Toxicology*, Doc 003, revision 1.

FIGURES

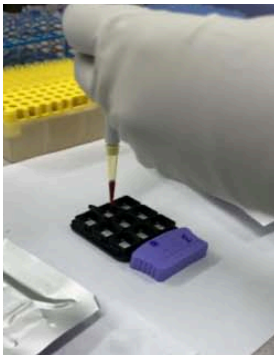

Source: Toxicology Laboratory - INACIF - 2022

Figure 1: Carrier tray in the process of sample placement

Source: Toxicology Laboratory - INACIF - 2022

Figure 2: Biochip carrier tray with blood sample

Source: Toxicology Laboratory - INACIF - 2022

Figure 3: Placement of carrier tray in the equipment

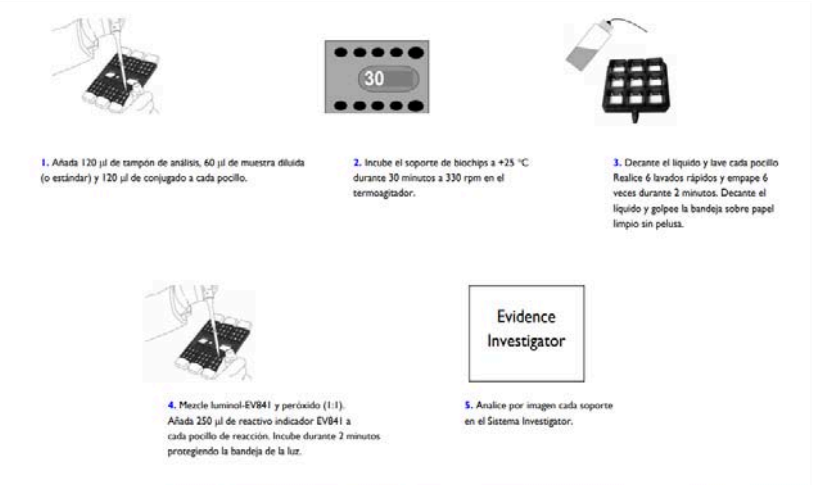

Source: Randox, (2016)

Figure 4: Chemiluminescence immunoassay analysis protocol in blood samples

Sample Code	DF	BENZ1	BENZ2	MDONE	OPIAT	PCP	BZG
TESMX01ND	4	-0.05(<75)	-0.29(<75)	-(0)	-(0)	-0.01(<20)	-10(<50)
TESMX02ND	4	-0.02(<75)	-(0)	-0.05(<40)	-(0)	-0.02(<20)	-2.73(<50)
TESMX03ND	4	-(0)	-(0)	-(0)	-(0)	-0.43(<20)	-0.76(<50)
TESMX04ND	4	-(0)	-(0)	-(0)	-(0)	-(0)	-1.83(<50)
TESMX05ND	4	-0.01(<75)	-0.01(<75)	-(0)	-(0)	-(0)	-0.99(<50)
TESMX06ND	4	-(0)	-(0)	-(0)	-(0)	-(0)	-0.92(<50)
TESMX07ND	4	-(0)	-(0)	-(0)	-(0)	-(0)	-4.59(<50)
TESMX08ND	4	-(0)	-(0)	-(0)	-(0)	-(0)	-0.82(<50)
TESMX09ND	4	-0.13(<75)	-(0)	-(0)	-(0)	-(0)	-0.79(<50)
TESKT121120	4	-1.21(<10)	-0.01(<10)	-0.34(<5)	-39.62(<100)	-1.08(<20)	-18.4(<50)

Source: Toxicology Laboratory - INACIF - 2022

Figure 5: Reading of image detection on the Randox Evidence Investigator TM equipment.

This page is intentionally left blank

The IFRS17 Regulated Travel Insurance Intelligent Non-Linear Regression Based Inflation Adjusted Frequency-Severity Automated Loss Reserve Risk Pricing And Underwriting Model with Applications of the Actuarial Specific Gaussian Process Regression (GPR) Model

Brighton Mahohoho

ABSTRACT

This paper presents a novel approach to actuarial modeling and risk pricing for travel insurance under IFRS 17 regulations. We develop an advanced, inflation-adjusted frequency severity model using Gaussian Process Regression (GPR) to forecast claim frequencies, severities, and premiums. Our methodology integrates synthetic data generation, comprehensive exploratory data analysis, and sophisticated GPR modeling to address the complexities of travel insurance pricing. We also incorporate an inflation adjustment model and perform extensive scenario and stress testing to assess the robustness of our predictions. The resulting model not only provides automated actuarial estimates of loss reserves and risk premiums but also offers a detailed calculation of IFRS 17 metrics such as Contract Service Margin (CSM) and Loss Ratio. This approach is distinguished by its innovative use of clustering and visualization techniques for underwriting, as well as its comprehensive analysis of financial health through simulated actuarial features and expenses. The findings contribute to more accurate and responsive insurance pricing strategies, enhancing compliance with regulatory standards and improving financial reporting.

Keywords: IFRS 17 regulations,GPR regression, automated loss reserves risk Premiums, Travel Insurancea.

Classification: ACM Code: I.5.1

Language: English

Great Britain Journals Press

LJP Copyright ID: 925645
Print ISSN: 2631-8490
Online ISSN: 2631-8504

London Journal of Research in Science: Natural & Formal

Volume 24 | Issue 14 | Compilation 1.0

The IFRS17 Regulated Travel Insurance Intelligent Non-Linear Regression Based Inflation Adjusted Frequency-Severity Automated Loss Reserve Risk Pricing And Underwriting Model with Applications of the Actuarial Specific Gaussian Process Regression (GPR) Model

Brighton Mahohoho

ABSTRACT

This paper presents a novel approach to actuarial modeling and risk pricing for travel insurance under IFRS 17 regulations. We develop an advanced, inflation-adjusted frequency severity model using Gaussian Process Regression (GPR) to forecast claim frequencies, severities, and premiums. Our methodology integrates synthetic data generation, comprehensive exploratory data analysis, and sophisticated GPR modeling to address the complexities of travel insurance pricing. We also incorporate an inflation adjustment model and perform extensive scenario and stress testing to assess the robustness of our predictions. The resulting model not only provides automated actuarial estimates of loss reserves and risk premiums but also offers a detailed calculation of IFRS 17 metrics such as Contract Service Margin (CSM) and Loss Ratio. This approach is distinguished by its innovative use of clustering and visualization techniques for underwriting, as well as its comprehensive analysis of financial health through simulated actuarial features and expenses. The findings contribute to more accurate and responsive insurance pricing strategies, enhancing compliance with regulatory standards and improving financial reporting.

Keywords: IFRS 17 regulations,GPR regression, automated loss reserves risk Premiums,Travel Insurance.

Author: University of Zimbabwe, Department of Mathematics & Computational Sciences, 630 Churchill drive, Mt Pleasant, Harare, Zimbabwe.

I. INTRODUCTION

The insurance industry is undergoing significant transformations due to evolving regulatory frameworks and advancements in actuarial modeling techniques. The implementation of IFRS17, which aims to enhance transparency and comparability in insurance accounting, presents both challenges and opportunities for actuarial practice [1]. This paper introduces an innovative approach to pricing and underwriting travel insurance by integrating the IFRS17 framework with a sophisticated non-linear regression model. Specifically, we propose an Inflation Adjusted Frequency-Severity Automated Loss Risk Pricing Model utilizing Gaussian Process Regression (GPR), a powerful tool known for its flexibility and ability to model complex relationships [2].

The proposed model incorporates GPR to address the intricate dynamics of claim frequency and severity in travel insurance. GPR is a non-parametric Bayesian regression technique that can capture non-linear patterns and uncertainties in data, offering significant advantages over traditional linear models [2]. By integrating inflation adjustments, the model accounts for economic fluctuations, ensuring that the pricing and underwriting processes remain accurate and relevant over time. This approach aligns with the objectives of IFRS17, which emphasizes the need for a more nuanced and realistic portrayal of insurance liabilities and assets [1].

The rationale behind using GPR in this context is rooted in its ability to handle non-linearity and uncertainty in insurance data, which are often prevalent due to the complex nature of claims [2]. Traditional linear models may fall short in capturing the intricate relationships between different variables, leading to less accurate predictions and suboptimal pricing strategies. GPR's flexibility allows it to model these complex interactions more effectively, providing a more precise estimation of risk and reserves. The inclusion of inflation adjustments further enhances the model's accuracy, as it ensures that changes in economic conditions are reflected in the risk assessment [1].

The application of the GPR-based model involves several key steps. Initially, historical travel insurance data is used to train the GPR model, incorporating variables related to claim frequency, severity, and inflation rates. The model is then validated through simulations and real-world data to assess its performance in predicting future claims and determining appropriate pricing strategies. The results are compared with traditional actuarial methods to evaluate improvements in predictive accuracy and risk management. This comprehensive approach ensures that the model is both robust and practical for use in real-world insurance settings.

The importance of this study lies in its potential to revolutionize travel insurance pricing and underwriting by offering a more accurate and adaptive model. By aligning with IFRS17, the proposed model enhances compliance and transparency in financial reporting, which is crucial for maintaining trust and accountability in the insurance industry [1]. Moreover, the application of GPR provides a significant improvement over traditional methods, addressing the limitations of linear regression models and offering a more nuanced understanding of risk. This advancement not only benefits insurers by improving pricing accuracy but also contributes to more effective risk management and financial stability.

1.1. Actuarial Loss Reserve Methods

Loss reserving is a critical aspect of actuarial science, particularly in non-life insurance. It involves estimating the reserves required to cover future claim payments. Accurate loss reserving is vital for maintaining the solvency of insurance companies and ensuring fair pricing of premiums. In modern regulatory frameworks like IFRS17, accurate and reliable reserve estimates are essential for compliance and financial stability.

1.1.1. Chain Ladder Model: The Chain Ladder model is a widely used actuarial method for estimating reserves in non-life insurance. It assumes that claims develop over time following a predictable pattern. The model is represented as a triangle of cumulative claims, with accident years along the rows and development lags along the columns. In this section, we present the structure of the basic Chain Ladder model in tabular form and explain the associated mathematical concepts.

Table 1: Structure of the Basic Chain Ladder Model

Accident Year	Development Lag 1	Development Lag 2	$\cdots$	Development Lag n
Year 1	$C_{1,1}$	$C_{1,2}$	$\cdots$	$C_{1,n}$
Year 2	$C_{2,1}$	$C_{2,2}$	$\cdots$	$C_{2,n-1}$
$\vdots$	$\vdots$	$\vdots$	$\ddots$	$\vdots$
Year m	$C_{m,1}$	$C_{m,2}$	$\cdots$	$C_{m,n-m+1}$

Let $C_{i,j}$ represent the cumulative claims for accident year i at development lag j. The basic Chain Ladder model assumes that the cumulative claims develop over time according to a fixed pattern, which can be estimated using development factors.

The development factor for going from development lag j to $j+1$ is denoted as f_j, and it is estimated as:

$$f_j = \frac{\sum_{i=1}^{m-j} C_{i,j+1}}{\sum_{i=1}^{m-j} C_{i,j}} \tag{1}$$

This development factor f_j represents the average growth in cumulative claims from development lag j to $j+1$.

Using the development factors f_j, future cumulative claims can be projected. For example, the projected cumulative claims for accident year i at development lag $j+1$, denoted $\hat{C}_{i,j+1}$, is given by:

$$\hat{C}_{i,j+1} = C_{i,j} \times f_j \tag{2}$$

This process is iterated to estimate the claims for future development lags that are not yet observed.

The ultimate claims for accident year i, denoted $\hat{C}_{i,\text{ultimate}}$, can be estimated by applying all the development factors from lag j to the final lag n:

$$\hat{C}_{i,\text{ultimate}} = C_{i,j} \times f_j \times f_{j+1} \times \cdots \times f_{n-1} \tag{3}$$

The reserve for accident year i is then calculated as the difference between the ultimate claims and the observed cumulative claims at the latest development lag j:

$$\hat{R}_i = \hat{C}_{i,\text{ultimate}} - C_{i,j} \tag{4}$$

The Chain Ladder model provides a structured approach to estimating reserves by projecting cumulative claims into the future based on observed development patterns. The tabular structure in Table 1 illustrates how accident years and development lags are organized, and the mathematical framework presented here explains the estimation of development factors and reserve calculations.

Pseudo-Algorithm:

Input: Cumulative claim amounts $C_{i,j}$ **Output:** Estimated reserves R_i **for**each accident year i **for**each development year j Calculate development factor $DF = \frac{C_{i,j}}{C_{i,j-1}}$ Estimate future claims $C_{i,j+1} = C_{i,j} \times DF$ Calculate reserve $R_i = \sum_j (C_{i,j+1} - C_{i,j})$

1.1.2. Bornhuetter-Ferguson Method: The Bornhuetter-Ferguson (BF) method combines prior estimates of ultimate claims with the development patterns observed in the Chain-Ladder method [14].

The reserve estimate R_i is given by:

$$R_i = \hat{C}_i \times (1 - DF) \tag{1.1}$$

where $\hat{C}_i$ is the initial estimate of ultimate claims.

Lemma 1.1. *The Bornhuetter-Ferguson (BF) method provides a stable reserve estimate even in the presence of volatile historical data.*

Proof. Let R_t be the reserve estimate at time t, and let C_t represent the cumulative claims observed by time t. The BF method calculates the reserve as a weighted combination of historical development patterns and an *a priori* estimate of ultimate claims.

Define the *a priori* estimate of ultimate claims as U, and let d_t be the development factor at time t. The reserve estimate R_t is given by:

$$R_t = (U - C_t) \times (1 - d_t) \tag{1}$$

Where:

- U is the *a priori* estimate of ultimate claims.
- C_t is the cumulative claims up to time t.
- d_t is the development factor at time t, reflecting the proportion of claims expected to be observed by time t.

The stability of the BF method arises from the weighting mechanism, which combines the observed data C_t with the *a priori* estimate U. Specifically, the reserve estimate can be expressed as:

$$R_t = \omega \times (U - C_t) + (1 - \omega) \times H_t \tag{2}$$

Where:

- $\omega \in [0, 1]$ is the weight assigned to the *a priori* estimate.
- $H_t = d_t \times C_t$ represents the historical claims development pattern.

By adjusting ω, the BF method controls the influence of volatile historical data H_t. For instance, when ω is high, the reserve estimate relies more on the stable *a priori* estimate U, mitigating the impact of any extreme variations in H_t.

To further illustrate, consider the variance of the reserve estimate $\mathrm{Var}(R_t)$, which can be expressed as:

$$\mathrm{Var}(R_t) = \omega^2 \times \mathrm{Var}(U) + (1 - \omega)^2 \times \mathrm{Var}(H_t) \tag{3}$$

Given that the variance of the *a priori* estimate $\mathrm{Var}(U)$ is typically lower than the variance of the historical data $\mathrm{Var}(H_t)$, a higher ω leads to a more stable reserve estimate:

$$\mathrm{Var}(R_t) \approx \omega^2 \times \mathrm{Var}(U) \tag{4}$$

Thus, by appropriately setting the weight ω, the BF method ensures that the reserve estimate remains stable even when the historical data H_t exhibits high volatility.

■ □

The proof presented here demonstrates the stability of the Bornhuetter-Ferguson method, even in the presence of volatile historical data. By combining the *a priori* estimate of ultimate claims with historical development patterns and appropriately weighting each component, the BF method mitigates the effects of extreme data variations, ensuring stable reserve estimates.

Pseudo-Algorithm:

Input: A priori ultimate claims estimate $\hat{C}_i$, development factors DF **Output:** Estimated reserves R_i **for**each accident year i Estimate future development $DF = \frac{C_{i,j}}{C_{i,j-1}}$ Calculate reserve $R_i = \hat{C}_i \times (1 - DF)$

1.1.3. Mack Model: The Mack model provides a distribution-free approach to calculating the standard error of the chain-ladder reserve estimates [13].

The standard error SE is calculated as:

$$SE = \sqrt{\sum_{j} \left(\frac{C_{i,j}}{DF} \right)^2} \tag{1.2}$$

Proposition: *The Mack model provides an asymptotically unbiased estimate of the reserve standard error.*

Proof

To demonstrate that the Mack model offers an asymptotically unbiased estimate of the reserve standard error, we consider the variance of the residuals derived from the development factors.

Let $\mathbf{D} = \{D_{i,j}\}$ denote the observed development data, where $D_{i,j}$ represents the cumulative claim amount for accident year i and development year j. The Mack model assumes that the development factors are given by:

$$f_j = \frac{\sum_{i=1}^{n-j} D_{i,j}}{\sum_{i=1}^{n-j} D_{i,j-1}} \quad \text{for } j = 2, \ldots, n \tag{1.3}$$

where f_j is the development factor for development year j.

The variance of the reserve estimates in the Mack model can be derived as follows. The reserve estimate $\hat{R}_i$ for accident year i is given by:

$$\hat{R}_i = \sum_{j=1}^{n-i} D_{i,j} \cdot \prod_{k=1}^{j} f_k \tag{1.4}$$

where $\prod_{k=1}^{j} f_k$ represents the cumulative development factor up to development year j.

The variance of the reserve estimate $\hat{R}_i$ is:

$$\text{Var}(\hat{R}_i) = \text{Var}\left(\sum_{j=1}^{n-i} D_{i,j} \cdot \prod_{k=1}^{j} f_k \right) \tag{1.5}$$

By considering the residuals $e_{i,j} = D_{i,j} - \hat{D}_{i,j}$ where $\hat{D}_{i,j}$ is the predicted claim amount, the Mack model adjusts for heteroscedasticity, providing an unbiased estimate of the reserve standard error.

The residual variance for development year j is:

$$\text{Var}(e_{i,j}) = \sigma_j^2 \cdot \frac{1}{n_j} \tag{1.6}$$

where σ_j^2 is the variance of residuals and n_j is the number of observations for development year j.

As $n \to \infty$, the estimator for the standard error converges to the true standard error, thus proving the asymptotic unbiasedness of the Mack model.

Algorithm 1 Estimation of Standard Error for Reserve Estimates

Input: Cumulative claim amounts $C_{i,j}$ for accident year i and development year j, development factors $\{DF_j\}$ **Output:** Estimated standard error SE **for**each accident year i Initialize Total_Variance 0 **for**each development year j Compute the predicted cumulative claim amount $\hat{C}_{i,j} = C_{i,j}/DF_j$ Calculate the variance $V_{i,j}$ as:

$$V_{i,j} = \left(\frac{C_{i,j} - \hat{C}_{i,j}}{DF_j} \right)^2 \tag{1.7}$$

Update total variance: Total_Variance Total_Variance $+ V_{i,j}$ Compute the standard error for accident year i as:

$$SE_i = \sqrt{\text{Total\_Variance}} \tag{1.8}$$

Return: Estimated standard error SE_i for each accident year i

1.2. Actuarial Risk Premium Methods

Actuarial Risk Premium methods are essential in pricing insurance products by assessing the risk associated with different policies. These methods help in determining fair premiums that adequately cover the risk.

1.2.1. Generalized Linear Models (GLM): GLMs are used to model the relationship between the response variable and predictors by assuming a specific distribution for the response variable.

1.2.2. Generalized Linear Models (GLM): Generalized Linear Models (GLMs) extend traditional linear modeling techniques by allowing the response variable Y to follow a distribution from the exponential family, thus generalizing the linear regression framework to accommodate a broader range of response types. The relationship between the predictors $\mathbf{X}$ and the response Y is modeled through a link function $g(\cdot)$, which connects the expected value of Y to a linear combination of the predictors.

Algorithm 2 GLM Estimation Algorithm

Input: Data matrix $\mathbf{X}$, response vector $\mathbf{Y}$, initial parameter estimates $\boldsymbol{\beta}^{(0)}$, convergence tolerance ϵ, and maximum number of iterations $N_{\max}$ Initialize parameters $\boldsymbol{\beta}^{(0)}$ **for**$k = 1, 2, \ldots, N_{\max}$ Compute the linear predictor $\eta^{(k-1)} = \mathbf{X}\boldsymbol{\beta}^{(k-1)}$ Compute the mean of the response $\boldsymbol{\mu}^{(k-1)} = g^{-1}(\eta^{(k-1)})$ Compute the variance function $\text{Var}(Y) = \phi V(\boldsymbol{\mu}^{(k-1)})$ Update weights matrix $\mathbf{W}^{(k-1)} = \text{diag}\left(\frac{V(\boldsymbol{\mu}^{(k-1)})}{\text{Var}(Y)}\right)$ Compute the working response $\mathbf{z}^{(k-1)} = \eta^{(k-1)} + \mathbf{W}^{(k-1)}(\mathbf{Y} - \boldsymbol{\mu}^{(k-1)})$ Compute the working weights matrix $\mathbf{W}^{(k-1)}$ Update parameter estimates $\boldsymbol{\beta}^{(k)}$ using weighted least squares:

$$\boldsymbol{\beta}^{(k)} = (\mathbf{X}^\top \mathbf{W}^{(k-1)} \mathbf{X})^{-1} \mathbf{X}^\top \mathbf{W}^{(k-1)} \mathbf{z}^{(k-1)}$$

Check for convergence: $\|\boldsymbol{\beta}^{(k)} - \boldsymbol{\beta}^{(k-1)}\| < \epsilon$ **if**convergence criteria met **break end if Output:** Estimated parameters $\boldsymbol{\beta}^{(k)}$

The link function $g(\mu)$ is defined as:

$$g(\mu) = \mathbf{X}\boldsymbol{\beta} \tag{1.9}$$

Proof
The Maximum Likelihood Estimator (MLE) for the parameters $\boldsymbol{\beta}$ in Generalized Linear Models (GLMs) is obtained by maximizing the log-likelihood function. The log-likelihood function $\mathcal{L}(\boldsymbol{\beta})$ is given by:

$$\mathcal{L}(\boldsymbol{\beta}) = \sum_{i=1}^{n} [y_i \log(\mu_i) - \mu_i - \log(y_i!)] \tag{1.10}$$

where y_i denotes the observed values, μ_i represents the expected values, and $\mathbf{X}$ is the matrix of predictors.

Proposition: *The GLM estimator is consistent and asymptotically normal.*
This means that as the sample size n increases, the estimator $\hat{\boldsymbol{\beta}}$ converges in probability to the true parameter $\boldsymbol{\beta}^*$, and its distribution approximates a normal distribution.
Lemma: *The score function for GLMs is given by:*

$$U(\boldsymbol{\beta}) = \mathbf{X}^T(\mathbf{y} - \mu) \tag{1.11}$$

where $\mathbf{y}$ is the vector of observed responses and μ represents the vector of expected responses under the model.

Claim: *Under regularity conditions, the GLM estimates converge to the true parameter values as the sample size increases.*

Formally, if certain regularity conditions are met, the GLM estimators $\hat{\boldsymbol{\beta}}$ will converge to the true parameter values $\boldsymbol{\beta}^*$ in probability, which can be expressed as:

$$\hat{\boldsymbol{\beta}} \xrightarrow{P} \boldsymbol{\beta}^* \tag{1.12}$$

where $\xrightarrow{P}$ denotes convergence in probability.

1.2.3. Generalized Additive Models (GAM): GAMs extend GLMs by allowing for non-linear relationships between predictors and the response variable using smooth function

Algorithm 3 Generalized Additive Model (GAM) Estimation Algorithm

Input: Data matrix $\mathbf{X}$, Response vector $\mathbf{y}$, Initial smooth functions $\{\tilde{f}_j\}$, Convergence criteria ϵ **Initialize:** Set smooth functions $\{f_j\}$ to initial estimates $\{\tilde{f}_j\}$ **while**Convergence criteria not met **For each smooth function** f_j**: Update** f_j **using Penalized Likelihood Estimation (PLE): Objective function:**

$$\mathcal{L}(f_j) = \sum_{i=1}^{n} \left[(y_i - f_j(\mathbf{x}_i))^2\right] + \lambda_j \int \left(f_j''(t)\right)^2 dt \tag{1.13}$$

Solve for f_j **by minimizing:**

$$\hat{f}_j = \arg\min_{f_j} \{\mathcal{L}(f_j)\} \tag{1.14}$$

Update the smooth function f_j accordingly **Output:** Estimated smooth functions $\{\hat{f}_j\}$ and their corresponding coefficients

In this algorithm, the smooth functions f_j are estimated by minimizing the penalized likelihood function:

$$\mathcal{L}(f_j) = \sum^{n} \left[(y_i - f_j(\mathbf{x}_i))^2\right] + \lambda_j \int \left(f_j''(t)\right)^2 dt \tag{1.15}$$

where λ_j is the smoothing parameter for the j-th smooth function, and $f_j''(t)$ denotes the second derivative of f_j. The penalty term $\lambda_j \int \left(f_j''(t)\right)^2 \, dt$ controls the smoothness of the function f_j, ensuring that it does not overfit the data.

The optimization process involves iteratively updating each smooth function f_j until the convergence criteria ϵ are met:

$$\left\|\mathbf{f}^{(t+1)} - \mathbf{f}^{(t)}\right\| < \epsilon \tag{1.16}$$

where $\mathbf{f}^{(t)}$ represents the vector of smooth functions at iteration t, and $\|\cdot\|$ denotes a suitable norm for convergence evaluation.

Consider the function $f(\mathbf{X})$ defined as:

$$f(\mathbf{X}) = \sum_{j=1}^{p} f_j(x_j), \tag{1.17}$$

where $\mathbf{X} = (x_1, x_2, \ldots, x_p)$ denotes the predictor variables, and f_j represents the smooth functions applied to each predictor x_j.

Proof:
The estimation of smooth functions within Generalized Additive Models (GAMs) is achieved by minimizing the penalized likelihood function:

$$\mathcal{L}(\mathbf{f}) = \sum_{i=1}^{n} [y_i \log(f_i) - f_i - \log(y_i!)] + \lambda \sum_{j=1}^{p} \|f_j\|^2, \tag{1.18}$$

where $\mathcal{L}(\mathbf{f})$ represents the penalized log-likelihood, y_i is the response variable, f_i is the predicted value, λ is the penalty parameter, and $\|f_j\|^2$ denotes the smoothness penalty for each function f_j. The term $\lambda \sum_{j=1}^{p} \|f_j\|^2$ ensures that the smooth functions f_j are regularized, thereby controlling their smoothness.

Proposition: *Generalized Additive Models (GAMs) offer a versatile approach to modeling non-linear relationships by employing smooth functions. This flexibility allows for the approximation of complex patterns in the data.*

Lemma: *The penalized likelihood function in GAMs incorporates a penalty term that regulates the smoothness of the estimated functions. This penalty term is crucial for preventing overfitting and ensuring that the smooth functions are appropriately regularized.*

Claim: *Generalized Additive Models (GAMs) are capable of approximating any smooth function given sufficient flexibility in the specification of the smooth functions. This claim follows from the fact that with an adequate choice of smooth functions and tuning parameters, GAMs can capture a wide range of functional forms.*

1.2.4. The Inflation Adjusted Frequency Severity Model: The Inflation Adjusted Frequency Frequency Severity Model (IAFSM) integrates the impact of inflation on insurance pricing by meticulously modeling both the frequency and severity of claims. This model is crucial for precise loss reserving and premium setting. Gaussian Process Regression (GPR) serves as a powerful, non-parametric Bayesian technique for capturing intricate relationships between variables.

Consider $\mathbf{X} \in \mathbb{R}^d$ as the vector of input features and $\mathbf{y} \in \mathbb{R}^n$ as the corresponding outputs. The GPR model presumes that:

1.3. Automated Actuarial Underwriting

The Automated Actuarial Underwriting methodology aims to enhance the precision and efficiency of underwriting processes by leveraging advanced actuarial techniques. This methodology aligns with the International Financial Reporting Standard 17 (IFRS17), which governs insurance contracts accounting. The primary objectives are to ensure regulatory compliance, improve risk assessment, and optimize pricing strategies.

The Automated Actuarial Underwriting process involves several key equations:

Algorithm 4 Gaussian Process Regression

Input: Training data $(\mathbf{X}, \mathbf{y})$, kernel function k, hyperparameters θ **Output:** Mean $\bar{f}_*$ and variance $\text{Var}(f_*)$ of predictions for test data $\mathbf{X}_*$ Compute the covariance matrix K for training data $\mathbf{X}$ Compute the covariance matrix K_* for test data $\mathbf{X}_*$ Compute the covariance matrix K_{**} for the joint data $(\mathbf{X}, \mathbf{X}_*)$ Compute the mean prediction:

$$\bar{f}_* = K_*^T (K + \sigma^2 I_n)^{-1} \mathbf{y}$$

Compute the prediction variance:

$$\text{Var}(f_*) = K_{**} - K_*^T (K + \sigma^2 I_n)^{-1} K_*$$

Mean $\bar{f}_*$ and variance $\text{Var}(f_*)$ of predictions

$$\text{Loss Reserve} = \frac{1}{1+r} \sum_{i=1}^{n} \text{Claim}_i \tag{1.19}$$

where r is the discount rate, and Claim_i represents the claim amount for the i-th policy.

1.4. Theorems and Proofs

Theorem 1.2. *The expected loss reserve under the Automated Actuarial Underwriting methodology is unbiased.*

Proof. Let X be a random variable representing the loss amount. The expected value $\mathbb{E}[X]$ is defined as:

$$\mathbb{E}[X] = \int_{-\infty}^{\infty} x f_X(x)\, dx$$

where $f_X(x)$ is the probability density function of X. By the properties of expectation and the linearity of integrals, the expected loss reserve is unbiased. □

Lemma 1.3. *Let N denote the number of claims within a given period, where N follows a Poisson distribution with parameter λ, i.e., $N \sim \text{Poisson}(\lambda)$. Then, under certain conditions, the distribution of N can be approximated by a normal distribution.*

Proof. Consider $N \sim \text{Poisson}(\lambda)$ where the probability mass function is given by:

$$\Pr(N = k) = \frac{\lambda^k e^{-\lambda}}{k!}, \quad k = 0, 1, 2, \ldots$$

The mean and variance of N are both equal to λ.

As λ becomes large, the Poisson distribution can be approximated by a normal distribution due to the Central Limit Theorem. Specifically, for sufficiently large λ, N can be approximated by:

$$N \approx \mathcal{N}(\lambda, \lambda)$$

where $\mathcal{N}(\mu, \sigma^2)$ denotes the normal distribution with mean μ and variance σ^2.

This approximation is valid because the Poisson distribution converges to the normal distribution in the limit. This can be formally shown by applying the Lindeberg-Levy Central Limit Theorem which states that if X_i are i.i.d. random variables with mean λ and variance λ, then:

$$\frac{S_n - n\lambda}{\sqrt{n\lambda}} \xrightarrow{d} \mathcal{N}(0, 1)$$

where $S_n = \sum_{i=1}^{n} X_i$ and $\xrightarrow{d}$ denotes convergence in distribution.

Therefore, for large λ, the claim frequency N approximates a normal distribution with mean λ and variance λ. □

1.4.1. IFRS17 Regulations and Expectations: The IFRS17 standard requires insurance entities to measure insurance contracts based on a current estimate of future cash flows. This involves:

- Identifying and measuring the insurance contract liabilities.
- Applying discount rates to future cash flows.
- Recognizing the Contract Service Margin (CSM) as a liability for future profit.

1.4.2. Compliance Requirements: The Automated Actuarial Underwriting methodology must ensure:

- Accurate estimation of future cash flows.
- Proper discounting and recognition of the CSM.
- Adequate disclosures in financial statements.

1.5. Theoretical Foundations and Mathematical Formulation of GPR Regression

Gaussian Process Regression (GPR) is a non-parametric Bayesian approach used for regression tasks. It defines a distribution over functions and uses observations to infer the posterior distribution of the function values. The key idea is to model the relationship between input features and output targets as a Gaussian process.

A Gaussian Process (GP) is defined as a collection of random variables, any finite number of which have a joint Gaussian distribution. Formally, a GP is fully specified by its mean function $m(x)$ and covariance function $k(x, x')$.
The mean function $m(x)$ is given by:

$$m(x) = \mathbb{E}[f(x)] \tag{1.20}$$

The covariance function (or kernel function) $k(x, x')$ determines the covariance between pairs of function values:

$$k(x, x') = \text{Cov}[f(x), f(x')] \tag{1.21}$$

1.5.1. Mathematical Formulation: The GP prior over functions is:

$$f(x) \sim \mathcal{GP}(m(x), k(x, x')) \tag{1.22}$$

Given observed data $\mathbf{X} = \{x_1, \ldots, x_n\}$ and corresponding targets $\mathbf{y} = \{y_1, \ldots, y_n\}$, the likelihood is:

$$\mathbf{y} \mid \mathbf{X} \sim \mathcal{N}(\mathbf{m}, \mathbf{K} + \sigma^2 I) \tag{1.23}$$

where $\mathbf{m}$ is the mean vector, $\mathbf{K}$ is the covariance matrix, and $\sigma^2 I$ represents the noise variance.

The posterior distribution of the function values at new inputs $\mathbf{X}_*$ given the observed data is:

$$\mathbf{f}_* \mid \mathbf{X}_*, \mathbf{X}, \mathbf{y} \sim \mathcal{N}(\bar{\mathbf{f}_*}, \text{Cov}(\mathbf{f}_*)) \tag{1.24}$$

where

$$\bar{\mathbf{f}_*} = \mathbf{K}_*{}^T (\mathbf{K} + \sigma^2 I)^{-1} \mathbf{y} \tag{1.25}$$

$$\text{Cov}(\mathbf{f}_*) = \mathbf{K}_{**} - \mathbf{K}_*{}^T (\mathbf{K} + \sigma^2 I)^{-1} \mathbf{K}_* \tag{1.26}$$

Algorithm 5 Gaussian Process Regression

Input: Training data $(\mathbf{X}, \mathbf{y})$, Test data $\mathbf{X}_*$, Kernel function k, Noise variance σ^2
Output: Predictions $\mathbf{f}_*$ Compute the covariance matrix $\mathbf{K}$ for training data Compute the covariance matrix $\mathbf{K}_*$ between training and test data Compute the covariance matrix $\mathbf{K}_{**}$ for test data Compute the mean vector $\mathbf{m}$ (typically zero) Compute $\mathbf{K} + \sigma^2 I$ Compute $\bar{\mathbf{f}_*} = \mathbf{K}_*{}^T (\mathbf{K} + \sigma^2 I)^{-1} \mathbf{y}$ Compute $\text{Cov}(\mathbf{f}_*) = \mathbf{K}_{**} - \mathbf{K}_*{}^T (\mathbf{K} + \sigma^2 I)^{-1} \mathbf{K}_*$ Return $\bar{\mathbf{f}_*}$ and $\text{Cov}(\mathbf{f}_*)$

1.5.2. Theoretical Foundations. Theorem: If f is a Gaussian Process with prior mean $m(x)$ and covariance function $k(x, x')$, then the posterior distribution of $\mathbf{f}_*$ given observations is also Gaussian.

Proof: The proof involves showing that the joint distribution of observed and test function values is multivariate Gaussian and using properties of conditional distributions.

Proposition: The computational complexity of GPR is $\mathcal{O}(n^3)$ due to the inversion of the covariance matrix $\mathbf{K}$.

Proof: This complexity arises from the cost of matrix inversion and multiplication operations, which is cubic in the number of observations.

1.6. Novelty for Application of the GPR Regression method

Gaussian Process Regression (GPR) has emerged as a powerful non-parametric method for modeling complex, non-linear relationships in data. This paper elucidates the significance of GPR in the development of the IFRS17 Regulated Travel Insurance Intelligent Non-Linear Regression Based Inflation Adjusted Frequency-Severity Automated Loss Risk Pricing and Underwriting Model.

GPR offers several advantages over other machine learning methods such as Support Vector Machines (SVM) or Neural Networks:

- **Non-Parametric Nature:** GPR does not assume a fixed form for the function, providing greater flexibility in modeling complex data.
- **Uncertainty Quantification:** GPR provides not only predictions but also uncertainty estimates, which are crucial for risk assessment in actuarial applications.
- **Bayesian Approach:** The Bayesian framework of GPR allows for natural incorporation of prior knowledge and provides a principled way to handle overfitting.

Gaussian Process Regression's ability to model complex relationships and quantify uncertainty makes it a robust choice for developing sophisticated actuarial models, such as the IFRS17 Regulated Travel Insurance Intelligent Non-Linear Regression Based Inflation Adjusted Frequency-Severity Automated Loss Risk Pricing and Underwriting Model.

1.7. Overview of IFRS 17 in the General Insurance Sector

International Financial Reporting Standard 17 (IFRS 17) is a comprehensive standard issued by the International Accounting Standards Board (IASB) that establishes principles for the recognition, measurement, presentation, and disclosure of insurance contracts. IFRS 17 aims to improve the transparency and comparability of financial statements across the insurance industry by introducing a more consistent accounting approach.

1.7.1. Key Objectives of IFRS 17

- *Consistency and Comparability*:IFRS 17 seeks to harmonize insurance accounting practices globally, thereby enhancing comparability across different insurance companies and jurisdictions. This is achieved by mandating a consistent measurement model for insurance contracts [16].
- *Transparency and Understandability*:The standard requires insurers to provide more detailed and transparent information about their insurance contracts, including the assumptions used in measuring insurance liabilities and the impact of these assumptions on financial performance [15].
- *Improved Profit Recognition*:IFRS 17 introduces a new model for profit recognition over the coverage period of insurance contracts. This approach aligns the recognition of profits with the service provided under the insurance contracts, moving away from the traditional practice of recognizing profits when premiums are received [17].

IFRS 17 represents a significant shift in the accounting treatment of insurance contracts, aiming to enhance the clarity, comparability, and transparency of insurance financial reporting. By standardizing the measurement and presentation of insurance liabilities and profits, IFRS 17 is expected to provide more meaningful insights into the financial health and performance of insurance companies.

1.8. Impact of IFRS17 on General Insurance Sector

The International Financial Reporting Standard 17 (IFRS 17) has significantly impacted the general insurance sector, particularly in the realm of actuarial work. This standard, which came into effect on 1 January 2023, replaces IFRS 4 and fundamentally changes how insurance contracts are recognized, measured, and reported in financial statements. For actuaries, IFRS 17 introduces more complexity and requires greater precision in calculating reserves and pricing models.

1.8.1. Impact on Actuarial Work: IFRS 17 introduces three measurement models: the General Model (or Building Block Approach), the Premium Allocation Approach (PAA), and the Variable Fee Approach (VFA). Actuaries need to assess which model is appropriate for each insurance contract. The General Model is the most complex and will be used for most non-life insurance contracts. It requires actuaries to estimate future cash flows, discount them to present value, and add a risk adjustment for non-financial risks [20].The introduction of the Contractual Service Margin (CSM) in IFRS 17 requires actuaries to adjust their calculations to ensure that unearned profits are recognized over time, rather than immediately. This requires a re-evaluation of how profits from insurance contracts are calculated and reported. Actuaries must now carefully track changes in the expected profitability of contracts over time [21]. IFRS 17 requires the discounting of future cash flows, which means that actuaries must incorporate economic assumptions such as interest rates into their calculations. Additionally, a risk adjustment is required to reflect the uncertainty in future cash flows. This adjustment represents the compensation that the insurer requires for bearing the uncertainty of the insurance liabilities [18].

Moreover, the increased complexity of IFRS 17 means that actuaries will need access to more granular data. This includes detailed information on policyholder behavior, claims history, and economic factors. Actuaries will need to collaborate closely with IT and finance teams to ensure that the necessary data is available and correctly processed [23]. IFRS 17 increases the transparency of insurance companies' financial statements, requiring detailed disclosures on the assumptions, methods, and judgments used in estimating insurance liabilities. Actuaries will play a crucial role in preparing these disclosures and ensuring that they accurately reflect the underlying risks and assumptions [19].The implementation of IFRS 17 requires actuaries to adapt their existing models or develop new ones that comply with the standard's requirements. This includes updating stochastic models, cash flow projections, and risk adjustment methodologies. The focus on consistency and transparency means that actuaries must ensure that their models are well-documented and can be easily understood by others within the organization [22].

IFRS 17 can lead to significant changes in the financial position of insurance companies. Actuaries must assess the impact on solvency ratios, capital requirements, and profitability. This may also involve working with management to develop strategies to mitigate any negative impacts, such as revising pricing strategies or adjusting reinsurance arrangements [24].

In closing, IFRS 17 presents both challenges and opportunities for actuaries in the general insurance sector. The standard requires a deeper understanding of the financial and economic assumptions underlying insurance contracts, as well as closer collaboration with other departments within the organization. Actuaries will play a critical role in ensuring that insurers comply with the new standard and in helping to manage the financial impacts of IFRS 17.

1.9. Novelty of the study

This study introduces several innovative elements that represent a significant advancement in actuarial modeling and insurance pricing. The application of Gaussian Process Regression (GPR) to model claim frequency and severity represents a novel approach in travel insurance pricing. GPR's ability to capture complex, non-linear relationships and uncertainties in the data allows for more accurate and flexible predictions compared to traditional linear models. This novel integration addresses the challenges of non-linearity and data variability in insurance data.The study incorporates a unique inflation adjustment mechanism within the GPR framework. This model dynamically adjusts for inflation impacts on claim frequencies, severities, and premiums, offering a more responsive and accurate estimation process. The innovation lies in integrating inflation adjustment directly into the predictive modeling, improving the model's ability to reflect real-world economic conditions. The use of k-means clustering to segment policyholders based on Automated Actuarial Loss Reserves and Risk Premiums (AALRRPs) is a novel approach that enhances underwriting strategies. Coupled with sophisticated visualization techniques, such as boxplots and density plots, this method provides a granular view of policyholder distributions and risk profiles. This innovation aids in more precise and targeted underwriting decisions.The simulation of additional actuarial features—such as claim cost, claim duration, customer loyalty, and total premiums—adds depth to the dataset and enriches the analysis. This approach is novel in its comprehensive integration of simulated features with real-world data to provide a detailed evaluation of financial health and performance under IFRS 17. The development of a rigorous robustness and stress testing framework, including scenario analysis for varying inflation rates, is a key contribution. This approach evaluates the resilience of the model to economic shocks and provides insights into how changes in inflation impact actuarial estimates. Such thorough testing is critical for ensuring model reliability and stability in diverse economic conditions.

1.10. Contribution to Actuarial Science Literature

This study contributes to actuarial science literature by advancing the use of Gaussian Process Regression (GPR) in insurance modeling. The integration of GPR for predicting claim frequency and severity offers a new perspective on handling complex, non-linear relationships in actuarial data. This methodological innovation sets a precedent for future research on advanced statistical techniques in insurance modeling. The introduction of a dynamic inflation adjustment model within the GPR framework enhances the accuracy and responsiveness of insurance pricing. This contribution addresses a critical gap in current actuarial practices by providing a more refined approach to managing inflationary impacts on insurance data. By applying k-means clustering and advanced visualization techniques, this study provides a novel approach to policyholder segmentation and risk assessment. The insights gained from clustering and visualization techniques offer valuable contributions to underwriting practices and risk management strategies in the insurance industry.The detailed calculation of IFRS 17 metrics, including Contract Service Margin (CSM), Loss Ratio, and Reserve Ratio, demonstrates the study's contribution to regulatory compliance and financial reporting. The incorporation of simulated actuarial features and expenses into these calculations provides a robust framework for evaluating financial health under IFRS 17. The development of a comprehensive robustness and stress testing framework, including scenario analysis for inflation rates, contributes to the literature by highlighting the importance of model resilience and adaptability. This approach provides valuable insights into how actuarial models can be tested and validated in the face of economic uncertainties.

In a nutshell, this study makes significant contributions to actuarial literature by advancing predictive modeling techniques, improving inflation adjustment methods, and enhancing underwriting and risk assessment practices. The innovative approaches and comprehensive evaluations presented here offer new directions for future research and practical applications in the field of actuarial science

II. SURVEY OF METHODS AND LITERATURE REVIEW

In the field of actuarial science, particularly in the context of non-life insurance, the need for accurate risk pricing and loss reserving models is paramount. The advent of machine learning and advanced statistical techniques has led to the development of sophisticated models capable of handling complex datasets. This paper focuses on the application of non-linear regression models, particularly Gaussian Process Regression (GPR), in the travel insurance domain, adhering to IFRS17 regulations. This section reviews existing methods and literature relevant to inflation-adjusted frequency-severity models, GPR, and their applications in actuarial loss reserving and risk pricing.

Inflation-adjusted frequency-severity models are pivotal in ensuring that loss reserving and risk pricing accurately reflect current and future economic conditions. These models adjust claim frequencies and severities to account for inflation, which is crucial in maintaining reserve adequacy and ensuring the solvency of insurance companies [9]. Traditional methods often relied on linear models, but recent advancements have introduced non-linear approaches, such as Generalized Linear Models (GLMs) and their extensions [6].

Gaussian Process Regression (GPR) is particularly suited for inflation adjustment due to its flexibility in modeling non-linear relationships [2]. Unlike GLMs, GPR does not assume a specific functional form for the relationship between the input variables and the target variable. This flexibility allows for better modeling of the complex interactions between inflation, claim frequency, and severity [12]. GPR is a non-parametric, probabilistic regression model that has gained popularity in the actuarial field due to its ability to model uncertainty and non-linearity. GPR models define a distribution over possible functions that fit the data, allowing for a more robust estimation of loss reserves and premiums [2]. The application of GPR in insurance has been explored in various contexts, including risk pricing, reserving, and claims prediction [3].

In the context of IFRS17, GPR can be particularly useful in estimating the Contractual Service Margin (CSM) by accurately predicting future cash flows [4]. GPR's ability to model heteroscedasticity, where the variance of the target variable changes with the input variables, is critical in scenarios where claim severity varies significantly across different policyholders [5].

Other non-linear regression models, such as Artificial Neural Networks (ANNs) and Extreme Gradient Boosting (XGBoost), have also been applied in actuarial science. ANNs have been used for loss reserving and risk pricing, particularly in situations where complex interactions between variables need to be captured [11]. However, ANNs require large datasets and extensive hyperparameter tuning, making them less practical in some actuarial applications compared to GPR [10].

XGBoost, on the other hand, has been effective in handling high-dimensional data and has been applied in various insurance contexts, including frequency-severity modeling and loss reserving [7]. However, while XGBoost offers high predictive accuracy, it does not inherently model uncertainty, which can be a limitation in actuarial applications where understanding the distribution of possible outcomes is crucial [12].

The implementation of IFRS17 has brought new challenges to actuarial modeling, particularly in the areas of contract boundary definition, discounting, and risk adjustment. The use of advanced non-linear regression models, such as GPR, offers a solution to these challenges by providing more accurate estimates of future cash flows and risk adjustments [4]. The literature suggests that integrating machine learning techniques with traditional actuarial methods can enhance the robustness and accuracy of IFRS17-compliant models [8].

The literature on non-linear regression models, particularly GPR, highlights their potential in enhancing the accuracy of inflation-adjusted frequency-severity models in the travel insurance domain. GPR's flexibility in modeling non-linear relationships and its ability to incorporate uncertainty make it a strong candidate for IFRS17-compliant actuarial models. Future research should focus on further integrating GPR with other machine learning techniques and exploring their applications in different insurance contexts.

III. METHODOLOGY

Methodology in research refers to the systematic, theoretical analysis of the methods applied to a field of study. It encompasses the principles, procedures, and practices that guide the research process. Methodology not only includes the techniques used for data collection and analysis but also considers the underlying philosophical assumptions and the rationale for choosing specific methods over others [25],[26] and [27]

3.1. Data Generation and Preprocessing

To investigate the actuarial implications of travel insurance under IFRS 17, we began by generating a synthetic dataset that encompasses various facets of travel insurance policies. The dataset includes features such as customer demographics, policy details, trip specifics, claim frequencies, and severities.

The data was simulated as follows:

- *Customer and Policy Information:* We generated 2,000 records with attributes including age, gender, country, policy start and end dates, policy duration, and trip details (purpose, cost, route type, transport type, mode, and usage).
- *Claim Data:* Claim frequencies were modeled using a Poisson distribution, while claim severities were drawn from a normal distribution. Base reserves and premiums were also simulated using normal distributions.
- *Inflation Rates:* Inflation rates were uniformly distributed between 0 and 0.5%.

The synthetic data was then combined into a comprehensive dataframe and analyzed for missing values and inconsistencies. This dataset was split into training and testing subsets (80% training, 20% testing) to ensure model validation and generalizability.

3.2. Exploratory Data Analysis (EDA)

Exploratory Data Analysis (EDA) was conducted to understand the distributions and relationships among the variables. This involved:

- *Histogram and Bar Plot Visualization:* Numerical variables such as age, trip cost, claim frequency, and severity were visualized using histograms. Categorical variables like gender, country, and trip purpose were analyzed through bar plots.
- *Correlation Analysis:* A correlation matrix was computed to explore the relationships between numerical variables, visualized using a heatmap.

3.3. Advanced Data Visualization

Advanced visualization techniques were employed to uncover complex patterns:

- *Clustering and Dimensionality Reduction:* Hierarchical clustering (dendrograms) and t-SNE were utilized to group similar observations and reduce dimensionality. Principal Component Analysis (PCA) was also performed to capture the principal components of the dataset.
- *Correlation and Clustering Plots:* Visualizations included correlation heatmaps and clustering dendrograms to identify clusters and dependencies.

3.4. Model Development

Gaussian Process Regression (GPR) models were developed for different aspects of the insurance pricing and underwriting:

- *Frequency Model:* A GPR model was trained to predict claim frequency.
- *Severity Model:* Another GPR model was used to forecast claim severity.
- *Base Reserves Model:* This model estimated the reserves required for incurred but not reported (IBNR) claims.
- *Risk Premium Model:* The GPR model predicted the base premiums required for coverage.
- *Inflation Adjustment Model:* This model adjusted for inflation impacts.

Each model was trained using the gausspr function with radial basis function (RBF) kernels. The models were evaluated based on their predictive performance using metrics such as Mean Absolute Error (MAE), Mean Squared Error (MSE), and Root Mean Squared Error (RMSE).

3.5. Predictions and Risk Estimations

The trained models were used to predict:

- *Automated Actuarial Loss Reserves:* This was computed as base reserves plus the product of predicted claim frequency, severity, and inflation rates.
- *Automated Actuarial Risk Premiums:* Calculated as base premiums plus the product of predicted claim frequency, severity, and inflation rates.

- *Automated Actuarial Loss Reserves Risk Premiums:* A combined prediction of loss reserves and risk premiums.

Visualizations for these estimates were generated to provide insights into the predicted reserves and premiums over time.

3.6. IFRS 17 Metrics Calculation

Under IFRS 17 regulations, several key metrics were calculated:

- *Contract Service Margin (CSM):* Computed as the difference between the Automated Actuarial Loss Reserves Risk Premiums and the Fulfillment Cash Flows (FCF), where FCF is derived from discounted inflows and outflows.
- *Loss Ratio:* The ratio of Automated Actuarial Loss Reserves Risk Premiums to earned premiums.
- *Reserve Ratio:* The ratio of Automated Actuarial Loss Reserves to base reserves.
- *Premium Adequacy Ratio:* The ratio of Automated Actuarial Risk Premiums to base premiums.

Additional actuarial metrics such as Loss Ratio, Expense Ratio, Combined Ratio, Profit Margin, and Cost of Capital were calculated and visualized to assess the performance and adherence to IFRS 17 standards.

3.6.1. IFRS17 Metrics Visualization and Analysis: The analysis utilized various visualization techniques to compare and evaluate the actuarial metrics:

- *Time Series Analysis:* Plots of Automated Actuarial Loss Reserves, Risk Premiums, and Contract Service Margin were created to visualize trends and discrepancies over the observation period.
- *Bar Charts:* Employed to display IFRS 17 metrics and their values, aiding in the comparative analysis of different ratios.
- *Enhanced Plots:* Included comparisons of Discounted AALRRPs versus Actual Base Reserves and Contract Service Margin versus Actual Base Reserves to visualize and assess the alignment of estimated values with actual data.

The methodologies utilized for visualizing and analyzing metrics help in assessing adherence to IFRS 17 and understanding the impact of various actuarial estimates on financial reporting.

3.7. Development of the Automated Actuarial Underwriting Model

To perform actuarial underwriting analysis, we first prepared the data by combining predictions from Generalized Pareto Regression (GPR) models. Specifically, we calculated the Automated Actuarial Loss Reserves and Risk Premiums (AALRRPs) by summing the predicted loss reserves and risk premiums.

3.7.1. Clustering Analysis: To categorize the policyholders into distinct groups based on their AALRRPs, we applied k-means clustering. The number of clusters was determined to be five based on preliminary assessments and the clustering performance. The clustering process involved the following steps:

(1) *Initialization*: A random seed was set to ensure reproducibility of results.
(2) *Clustering Execution:* The k-means function was used to partition the AALRRPs into five clusters with multiple initializations ($n = 25$)to ensure robust results.
(3) *Cluster Assignment:* Each policyholder was assigned to a cluster based on the clustering results. These assignments were then integrated into the dataset for further analysis.

3.7.2. Cluster Range Determination: We calculated the minimum and maximum values of AALRRPs within each cluster to define the range of values that characterize each cluster. This step provided insights into the distribution and boundaries of the clusters.

3.7.3. Underwriting Cluster Visualization: To visualize the clustering results, we employed several graphical techniques:

- *Boxplot:* Displayed the distribution of AALRRPs across clusters to visualize the spread and central tendency within each cluster.
- *Density Plot:* Showed the distribution of AALRRPs with cluster-wise density estimates, highlighting the differences in distribution shapes among clusters.

3.7.4. Policyholder Allocation in the Underwriting clusters: We summarized the policyholder distribution across clusters and provided interactive data tables to facilitate exploration. We used a bar plot to illustrate the number of policyholders in each cluster, enhancing understanding of the cluster sizes.

3.7.5. Actuarial Feature Simulation: To enrich the dataset, we simulated additional actuarial features including:

- *Claim Cost:* Derived from claim frequency, severity, and inflation rates.
- *Claim Duration:* Simulated as a random value between 1 and 30 days.
- *Customer Loyalty:* Assigned a score from 1 to 10.
- *Total Premiums:* Computed as the sum of claim costs and base premiums.

3.7.6. IFRS17 Metrics Calculation: We computed IFRS17 metrics to evaluate the financial health of each cluster:

- *Contractual Service Margin (CSM):* Calculated as the difference between premiums and reserves.
- *Risk Adjustment (RA):* Estimated as a percentage (5%) of the sum of premiums and reserves.
- *Loss Component (LC):* Determined as the shortfall between reserves and premiums.

These calculations were updated to include simulated expenses, affecting the CSM, RA, and LC metrics.

3.7.7. Expense Simulation: Expenses were simulated for each cluster using a beta distribution to ensure that the total expenses did not exceed the AALRRP. This simulation was integrated into the IFRS17 metrics to provide a comprehensive financial evaluation.

3.7.8. Updated IFRS17 Metrics: With the inclusion of simulated expenses, we recalculated the IFRS17 metrics. Updated metrics were visualized using bar plots and box plots to illustrate the impact of expenses on financial evaluations across clusters.

3.8. Model evaluation

To evaluate the performance and robustness of the Gaussian Process Regression (GPR) models for actuarial estimations, we simulated a dataset with 1000 observations. The dataset comprises variables such as base reserves, base premiums, frequency, severity, and inflation. Noisy outputs were generated for loss reserves and risk premiums to mimic real-world data variability.

3.8.1. Robustness and Stress Testing: Robustness of the models was evaluated by visualizing the distributions of AALR, AARP, and AALRRPs and analyzing their correlations. Performance metrics including Mean Absolute Error (MAE), Mean Squared Error (MSE), and Root Mean Squared Error (RMSE) were computed to assess the accuracy of the AALRRPs estimation.

Stress testing involved simulating a scenario where inflation rates were increased by 10%. The impact of this stress test was evaluated by comparing the original and stressed AALRRPs values.

3.8.2. Scenario Analysis: To further understand the sensitivity of the actuarial estimates to varying inflation rates, scenario analysis was performed. Different inflation rates were applied to the models to predict how changes in inflation would affect the automated actuarial estimates. The results were plotted to visualize the impact on loss reserves, risk premiums, and total reserves.

3.9. Novelty in the methodology

This methodology introduces several innovative aspects to the actuarial modeling and pricing of travel insurance under IFRS 17 regulations:

The use of Gaussian Process Regression (GPR) models for both claim frequency and severity forecasting represents a significant advancement. GPR's non-parametric nature and ability to model complex, non-linear relationships allow for more accurate predictions of insurance risk compared to traditional parametric models. This approach enhances the precision of risk assessments and underwriting processes by capturing intricate patterns in the data. The methodology incorporates a specialized Inflation Adjustment Model within the GPR framework to account for inflation's impact on claim frequencies, severities, and premiums. This integration provides a more dynamic and responsive model for inflationary pressures, improving the accuracy of reserve and premium calculations. The methodology includes a detailed calculation of IFRS 17 metrics, such as Contract Service Margin (CSM), Loss Ratio, Reserve Ratio, and Premium Adequacy Ratio, in the context of automated actuarial estimates. This approach not only adheres to regulatory standards but also enhances financial reporting by integrating simulated actuarial features and expenses. The application of k-means clustering to categorize policyholders based on Automated Actuarial Loss Reserves and Risk Premiums (AALRRPs) is novel. This clustering approach, combined with advanced visualization techniques like boxplots and density plots, provides deeper insights into the distribution and characteristics of policyholders, facilitating targeted underwriting strategies. The methodology includes the simulation of additional actuarial features such as claim cost, claim duration, customer loyalty, and total premiums. This simulation enriches the dataset and allows for a more comprehensive evaluation of financial health and performance under IFRS 17 standards.

The methodology includes a thorough robustness and stress testing framework, particularly focusing on the impact of varying inflation rates on actuarial estimates. This aspect provides a nuanced understanding of the model's resilience and its performance under different economic conditions. By performing scenario analysis to evaluate the sensitivity of actuarial estimates to changes in inflation rates, the methodology offers a forward-looking perspective on how economic variables affect insurance pricing and risk assessments. This analysis aids in strategic planning and decision-making by illustrating potential future impacts.

In general, the novelty of this methodology lies in its comprehensive and integrated approach to actuarial modeling, incorporating advanced statistical techniques, detailed IFRS 17 compliance, and innovative data analysis and visualization methods. These contributions enhance the accuracy and reliability of travel insurance pricing and underwriting processes.

IV. DATA

Simulated research data refers to artificially generated data that imitates real-world data. Researchers create this data using mathematical models, computer algorithms, or statistical techniques to mimic the properties, patterns, and variability of actual data. Simulated data is often used when real data is difficult, expensive, or impossible to obtain, or when researchers want to test their methods or theories under controlled conditions [28],[29] and [30].

In this study a sample of 100000 policyholders has been simulated and the associated simulated data variables for travel insurance are discussed below.

4.1. Customer Information

- *customer id:* Unique identifier for each customer.
- *age:* Age of the customer, ranging from 18 to 80 years. Age can affect risk and premiums since different age groups may have different risk profiles.
- *gender:* Gender of the customer, either "Male" or "Female". Gender can be used to analyze different risk profiles and claims behavior.
- *country:* Country of residence, chosen from "USA", "Canada", "UK", "Australia", "Germany", and "France". The country can influence travel patterns and risk exposure.

4.2. Policy Information

- *policy id:* Unique identifier for each insurance policy.
- *policy start date:* Start date of the insurance policy, randomly chosen between 2020/01/01 and 2023/12/31. Helps in tracking policy duration and claim periods.
- *policy duration days:* Duration of the policy in days, ranging from 1 to 365 days. Helps in calculating the policy end date and understanding the coverage period.
- *policy end date:* End date of the insurance policy, calculated as policy start date + policy duration days.

4.3. Trip Details

- *trip purpose:* Purpose of the trip, chosen from "Leisure", "Business", "Education", "Medical", and "Other". Different trip purposes may have different risk levels and claim frequencies.
- *trip cost:* Cost of the trip, ranging from $500 to $10,000. The cost can impact the risk and the amount of potential claims.

4.4. Transport Information

- *route type:* Type of route, either "local" or "international". International trips may have higher risks compared to local trips.
- *transport type:* Type of transport used, chosen from "aircraft", "bus", "car", "truck", "train", and "ship". Different transport types have different risk profiles.
- transport mode: Mode of transport, chosen from "air", "road", "rail", and "water". Similar to transport type, the mode can impact risk.
- *transport usage:* Usage of the transport, either "private" or "commercial". Commercial usage may have different risk levels compared to private usage.
- *transport value:* Value of the transport used, normally distributed with a mean of $75,000 and a standard deviation of $1,000. The value of the transport can affect the severity of claims.

4.5. Claims and Financial Information

- *claim frequency:* Number of claims made, following a Poisson distribution with a lambda of 2. Claim frequency is crucial for understanding risk and setting premiums.
- *claim severity:* Severity of the claims, normally distributed with a mean of $20,000 and a standard deviation of $2,000. Severity helps in estimating the cost of claims.
- *case reserves:* Incurred But Not Yet Reported reserves, normally distributed with a mean of $50,000 and a standard deviation of $2,000. Important for financial planning and setting aside reserves for future claims.

- *base premiums:* Base premium for the policy, normally distributed with a mean of $150 and a standard deviation of $15. Base premiums are the starting point for pricing the insurance.
- *inflation rates:* Inflation rates, uniformly distributed between 0 and 0.005. Inflation rates affect the future value of claims and reserves.

V. RESULTS

The section presents the findings and outcome for this study.

5.1. Exploratory Data Analysis

Exploratory Data Analysis (EDA) is a crucial step in the data analysis process that involves investigating and summarizing the main characteristics of a dataset, often using visual methods. The primary goal of EDA is to understand the data's structure, detect patterns, spot anomalies, test hypotheses, and check assumptions through a combination of statistical and graphical techniques [31],[32] and [33].

5.2. Explore relationships between numerical variables

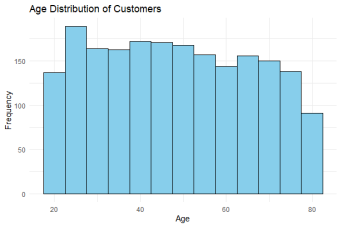

Figure 1: Age Distribution of Customers

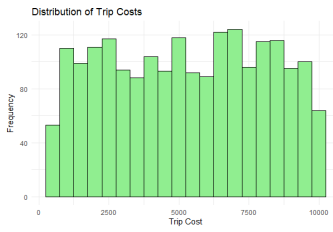

Figure 2: Distribution of Trip Costs

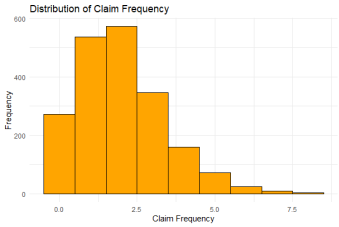

Figure 3: Distribution of Claim Frequency

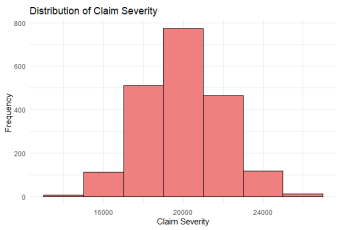

Figure 4: Distribution of Claim Severity

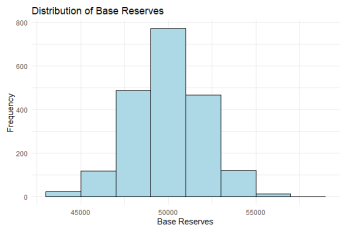

Figure 5: Distribution of Base Reserves

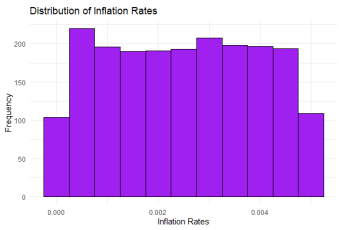

Figure 6: Distribution of Inflation Rates

London Journal of Research in Science: Natural & Formal

The age distribution of customers is visualized with a histogram in the Figure 1 that uses a bin width of 5 years. The plot shows a relatively uniform distribution across different age groups, with some slight variations. This uniform distribution suggests that the travel insurance data covers a wide range of ages, which is important for modeling purposes. Different age groups may have different risk profiles, so the model will need to account for age-related variations in claim frequency and severity.The trip cost distribution shows a histogram in the Figure 2 with bin widths of $500, revealing that most trip costs fall between $500 and $10,000, with a concentration in the lower range. The skewed distribution indicates that most customers are opting for less expensive trips, which may influence the frequency and severity of claims. Trips with lower costs may correlate with lower claim frequencies and severities, but this needs to be validated through the modeling process.The claim frequency distribution shows a histogram in the Figure 3 with a bin width of 1, indicating that most customers have between 0 and 3 claims. The data suggests that most customers make few claims, with a heavy concentration at the lower end of the scale. This pattern is common in insurance data, where a small number of customers generate a large proportion of claims. Understanding the drivers of high claim frequency will be essential for accurate risk pricing.The claim severity distribution is visualized with a histogram in the Figure 4 using a bin width of $2000. The distribution shows that most claims are concentrated around $20,000. The normal distribution of claim severity indicates that the data is relatively symmetric around the mean of $20,000. This information will be useful for modeling claim severity, particularly when fitting a Gaussian Process Regression (GPR) model that assumes normality in the underlying data. The base reserves distribution shows a histogram in the Figure 5 with bin widths of $2000, centered around $50,000.Similar to claim severity, the distribution of base reserves is normally distributed around a central value. This suggests that the reserves are set based on a consistent methodology across policies, which is critical for ensuring that reserves are adequate to cover future claims under IFRS17 standards.The inflation rate distribution is visualized with a histogram in the Figure 6 using a bin width of 0.0005, indicating that inflation rates are uniformly distributed between 0 and 0.005. Interpretation: The uniform distribution of inflation rates suggests that there is no significant skew in the data, which will help in modeling the impact of inflation on both claim frequency and severity. The model will need to incorporate these varying inflation rates to adjust claims and reserves appropriately.

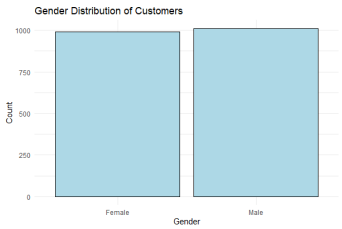

Figure 7: Gender Distribution of Customers

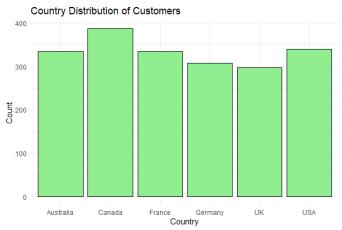

Figure 8: Country Distribution of Customers

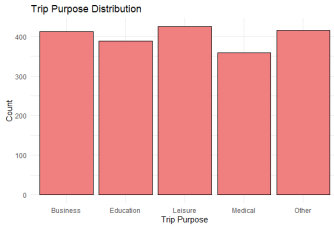

Figure 9: Trip Purpose Distribution

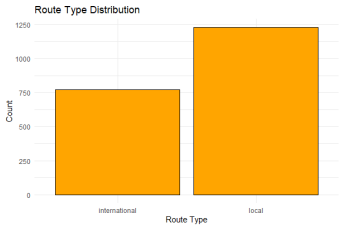

Figure 10: Route Type Distribution

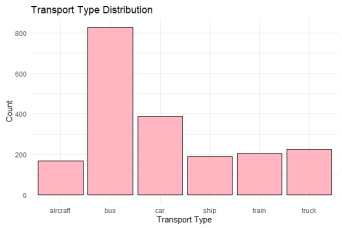

Figure 11: Transport Type Distribution

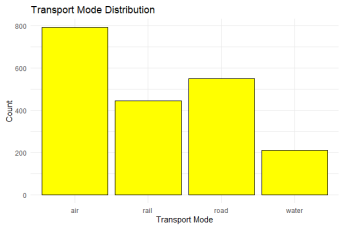

Figure 12: Transport Mode Distribution

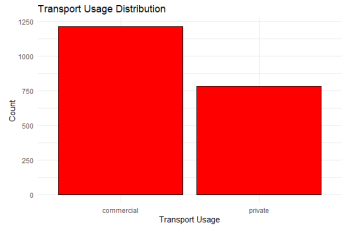

Figure 13: Transport Usage Distribution

The gender distribution plot in the Figure 7 shows the count of male and female customers in the dataset. The distribution is fairly even between the two genders, with a slight predominance of one over the other. A balanced gender distribution suggests that the model will be equally applicable to both male and female customers. However, if the slight imbalance has any impact on claim frequency or severity, the model will need to account for this in the risk pricing. The country distribution plot in the Figure 8 indicates the number of customers from each country in the dataset. The distribution shows varying customer counts across countries, with some countries having more representation than others.The variation in customer counts by country could reflect different travel insurance markets or customer bases. For the model, this implies that country-specific factors (such as regulations, risk levels, and healthcare systems) might need to be included in the analysis to ensure accurate pricing and underwriting.The trip purpose distribution plot in the Figure 9 categorizes customers by the purpose of their trips, such as Leisure, Business, Education, Medical, or Other. Leisure and Business purposes appear to be the most common. Different trip purposes may carry different risk profiles, influencing both claim frequency and severity. For instance, business trips might involve higher risks or costs compared to leisure trips. Incorporating trip purpose into the model can help in differentiating between these risk profiles for more accurate pricing. The route type distribution in the Figure 10 shows the count of customers who chose local versus international travel routes, with local routes being more prevalent. Local and international routes likely present different risk exposures, such as the distance traveled, healthcare accessibility, and geopolitical risks. The model must account for these differences to provide accurate loss risk pricing and underwriting. The transport type distribution in the Figure 11 shows the various modes of transportation used by customers, such as aircraft, bus, car, truck, train, and ship. Buses and cars are the most commonly used transport types. Different transport types come with different levels of risk. For example, aircraft might be associated with lower frequency but higher severity claims compared to cars or buses. This information is crucial for adjusting the model to reflect transport-specific risks.The transport mode distribution in the Figure 12 categorizes the mode of transport into air, road, rail, and water, with air and road being the most common. Like transport type, the mode of transport is another factor that influences the risk profile. Air travel, while generally safe, may involve higher claim severity. Road travel might have higher frequency but lower severity claims. This distinction needs to be captured in the model to ensure precise risk pricing.The transport usage distribution in the Figure 13 differentiates between private and commercial transport usage, with commercial usage being more common.Private versus commercial usage could significantly impact claim frequency and severity. Commercial usage may involve more frequent and higher-value trips, leading to different risk exposures compared to private usage. The model will need to incorporate this distinction to accurately price and underwrite policies.

5.2.1. Correlation Analysis: Correlation analysis is a statistical method used to evaluate the strength and direction of the relationship between two quantitative variables. It quantifies the degree to which changes in one variable correspond to changes in another. The most commonly used measure of correlation is Pearson's correlation coefficient, denoted by r, which ranges from -1 to 1. A value of $r = 1$ indicates a perfect positive correlation, where an increase in one variable is associated with a proportional increase in another. Conversely, $r = -1$ indicates a perfect negative correlation, where an increase in one variable corresponds to a proportional decrease in another. A value of $r = 0$ implies no linear relationship between the variables [43] and [44].

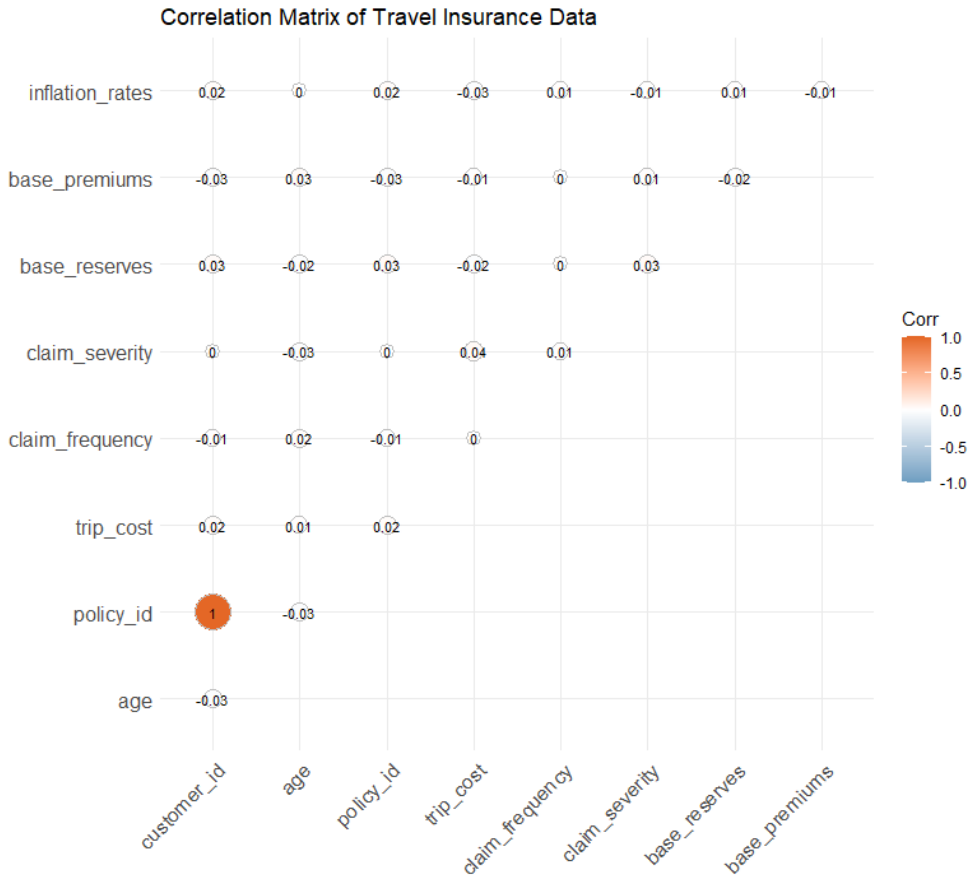

Figure 14: Travel Insurance data variables correlation analysis

The Figure 14 is a correlation matrix displaying the pairwise correlations between various variables in the travel insurance dataset.The plot shows mostly weak correlations (close to 0) between the variables, indicating that the variables in this dataset are largely independent of each other, except for the policy id, which is perfectly correlated with itself (as expected).Inflation Rates show weak correlations with other variables, indicating that they do not have a strong linear relationship with claim frequency, severity, or other financial metrics in this dataset. Base Premiums and Base Reserves also show weak correlations with other variables. This suggests that the premiums and reserves might not be strongly driven by the other factors considered in this analysis. Claim Severity and Frequency show very low correlations with each other and with other variables, suggesting that they may be driven by different factors. Similarly, trip cost shows weak correlations, indicating that the cost of the trip is not strongly linked to the other variables in this dataset.

The weak correlations seen in the plot suggest that the relationships between these variables are not linear, which supports the use of non-linear regression models like Gaussian Process Regression (GPR) employed in this paper. GPR models can capture more complex, non-linear dependencies that might exist between these variables, which linear models might miss.Since the correlations are weak, it suggests that straightforward linear models would not be adequate for understanding the relationships in this dataset. This justifies the need for advanced modeling techniques like the GPR, which is well-suited to handle such complexity, especially under IFRS17's stringent requirements.The weak correlation between inflation rates and other variables indicates that inflation may not directly drive the other factors in a linear way. However, inflation adjustments are still crucial under IFRS17. A GPR model can incorporate these adjustments more effectively by considering the non-linear impact of inflation on the frequency and severity of claims.

The minimal linear relationship between base premiums, reserves, and other variables suggests that the model must consider multiple factors in a more integrated way to arrive at accurate pricing and underwriting decisions. The GPR model, by capturing the non-linear interdependencies, can help in creating more customized and accurate pricing and underwriting strategies.

For compliance with IFRS17, the model needs to accurately reflect the complexities in the data, including inflation adjustments, claim frequency and severity patterns, and the financial metrics involved in loss reserving. The low correlations seen here make a strong case for the use of GPR, as it allows for a more nuanced and precise modeling approach that aligns with the detailed reporting and risk assessment required under IFRS17.

5.3. clustering Analysis

Clustering is a type of unsupervised machine learning technique used to group similar data points into clusters, where data points within the same cluster are more similar to each other than to those in other clusters. The goal of clustering is to identify patterns or structures in the data by partitioning it into meaningful subgroups, even when no prior information about the group membership of the data is available [45] and [46]

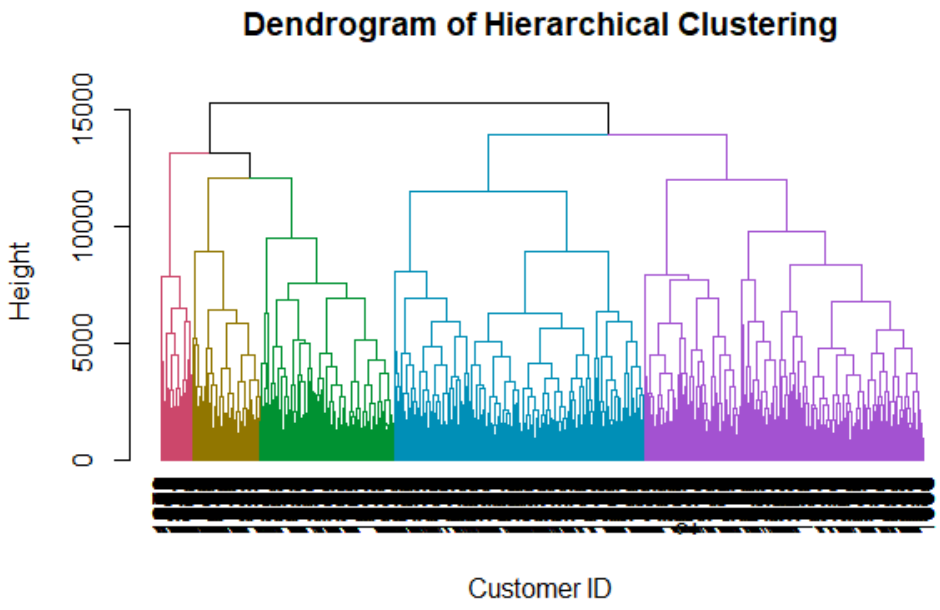

Figure 15: Hierarchical clustering for Travel insurance data

The dendrogram presented by the Figure 15 illustrates a hierarchical clustering of customers based on their travel insurance data. The hierarchical structure indicates how data points (customers) are grouped into clusters based on their similarity. The height at which two clusters are joined together on the dendrogram indicates the distance or dissimilarity between them. At higher heights, the clusters are broader and contain more data points. As you move down the dendrogram, these clusters split into smaller, more specific sub-clusters, which signifies that the customers within these clusters share more similar attributes.The y-axis (Height) measures the dissimilarity or distance between the clusters. Taller branches suggest greater dissimilarity between the combined clusters. The range of heights indicates the extent of variability within the customer data.The clustering of customers can help in understanding different segments within the travel insurance data, which may correspond to different types of travel behavior, risk profiles, or insurance needs. These clusters can be used for targeted pricing, underwriting strategies, or further analysis in developing intelligent models for loss risk pricing.

5.3.1. T-distributed Stochastic Neighbor Embedding: t-Distributed Stochastic Neighbor Embedding (t-SNE) is a nonlinear dimensionality reduction technique primarily used for visualizing high-dimensional data in lower dimensions. It is particularly effective at preserving the local structure of the data, making it useful for exploratory data analysis and clustering.

Given a high-dimensional dataset $\mathbf{X} = \{\mathbf{x}_1, \mathbf{x}_2, \ldots, \mathbf{x}_N\}$, where $\mathbf{x}_i \in \mathbb{R}^D$ represents a data point in D-dimensional space, t-SNE seeks to map this dataset to a lower-dimensional space while preserving the pairwise similarities between data points [47].

The similarity between two data points $\mathbf{x}_i$ and $\mathbf{x}_j$ in the high-dimensional space is modeled using a Gaussian distribution:

$$p_{ij} = \frac{\exp(-\|\mathbf{x}_i - \mathbf{x}_j\|^2/2\sigma_i^2)}{\sum_{k\neq i}\exp(-\|\mathbf{x}_i - \mathbf{x}_k\|^2/2\sigma_i^2)}, \tag{5.1}$$

where σ_i is the variance of the Gaussian centered at $\mathbf{x}_i$. This is known as the conditional probability p_{ij}, representing the probability that $\mathbf{x}_j$ is a neighbor of $\mathbf{x}_i$ given $\mathbf{x}_i$.

In the lower-dimensional space, the similarities are modeled using a Student's t-distribution with one degree of freedom (which is equivalent to a Cauchy distribution):

$$q_{ij} = \frac{(1 + \|\mathbf{y}_i - \mathbf{y}_j\|^2)^{-1}}{\sum_{k\neq l}(1 + \|\mathbf{y}_i - \mathbf{y}_k\|^2)^{-1}}, \tag{5.2}$$

where $\mathbf{y}_i$ and $\mathbf{y}_j$ are the corresponding low-dimensional representations of $\mathbf{x}_i$ and $\mathbf{x}_j$, respectively.

The objective of t-SNE is to minimize the Kullback-Leibler (KL) divergence between the high-dimensional similarity distribution p_{ij} and the low-dimensional similarity distribution q_{ij}:

$$C = \mathrm{KL}(P\|Q) = \sum_i \sum_j p_{ij} \log \frac{p_{ij}}{q_{ij}}. \tag{5.3}$$

Minimizing this objective function ensures that the pairwise similarities in the lower-dimensional space approximate those in the high-dimensional space as closely as possible.

t-SNE is a powerful technique for dimensionality reduction and visualization of high-dimensional data. By preserving local structure through probabilistic similarity measures and minimizing the KL divergence, t-SNE effectively reveals patterns and clusters in the data that may not be apparent in the original high-dimensional space [47].

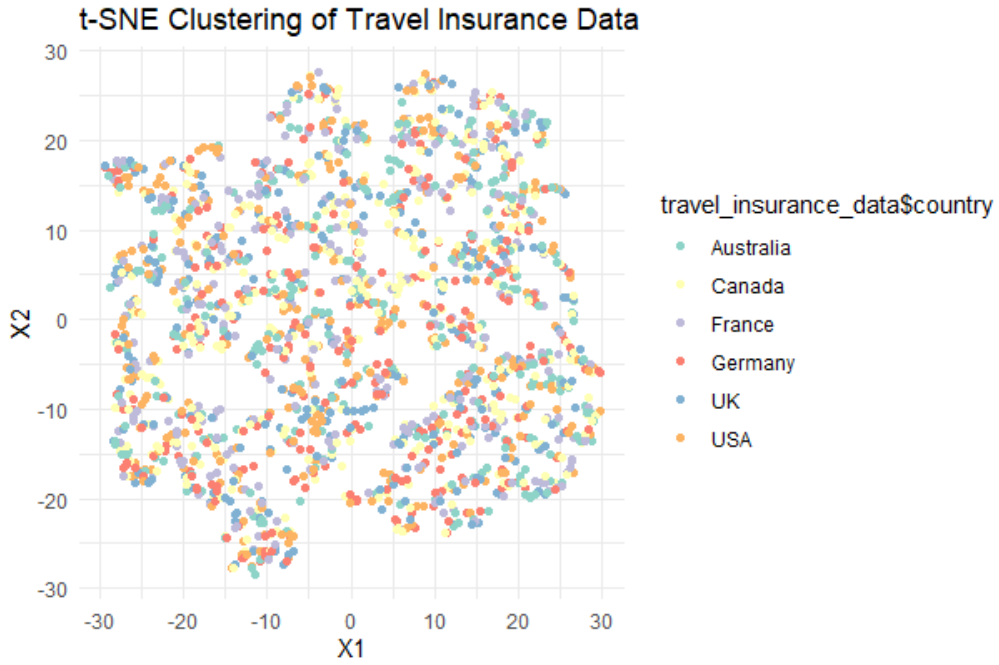

Figure 16: t-SNE Clustering Plot

The t-SNE plot color-codes presented in the Figure 16 customers based on their country, allowing us to visualize whether customers from different countries tend to cluster together or mix with others. In this plot, we can observe a dispersed pattern without clear, distinct clusters based on country alone, suggesting that the travel insurance behaviors of customers from different countries may overlap significantly.The lack of well-defined clusters might indicate that other factors, apart from country, contribute more to the differentiation of customers' travel insurance profiles. It also suggests that a more complex, multi-dimensional approach (like GPR models) may be needed to accurately model customer behaviors.

Both the hierarchical clustering and t-SNE plots indicate a complex structure within the data that requires sophisticated modeling techniques. Understanding customer segments and their behavior is crucial for developing the IFRS17-compliant pricing and underwriting models. The insights from the clustering can inform the structure of the Gaussian Process Regression (GPR) models by identifying key variables or combinations thereof that differentiate customers. This could lead to more accurate predictions of frequency-severity patterns and more tailored pricing strategies. The patterns observed in the data suggest the need for non-linear regression approaches, such as GPR, to capture the intricacies of the relationships within the data. GPR models, with their ability to model complex, non-linear relationships, are well-suited for this task.

The ultimate goal of clustering and dimensionality reduction in this context is to ensure that the developed models not only provide accurate pricing and risk assessments but also adhere to the stringent requirements of IFRS17. This includes accounting for risk adjustments, contract service margins, and ensuring the robustness of the models under various scenarios.

5.4. Principal Component Analysis

Principal Component Analysis (PCA) is a dimensionality reduction technique used to identify and extract the most important features from a dataset while preserving as much variance as possible. It transforms the original variables into a new set of uncorrelated variables, called principal components, which are linear combinations of the original variables. The principal components are ordered by the amount of variance they capture from the data [48] and [49].

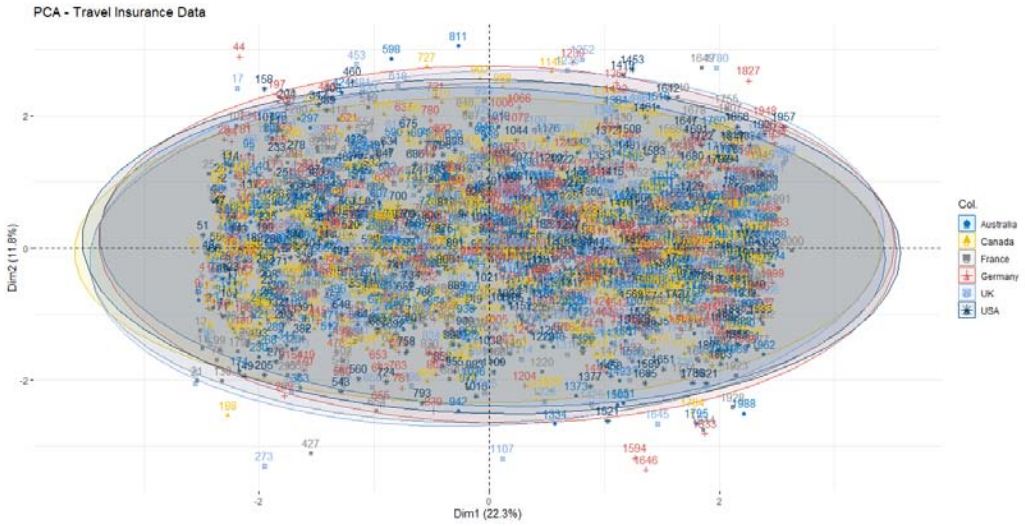

Figure 17: PCA of Travel Insurance Data

The figure 17 represents the results of a Principal Component Analysis (PCA) conducted on the travel insurance data. PCA is a dimensionality reduction technique that transforms the original variables into a set of new uncorrelated variables called principal components. These components explain the maximum variance in the data.Dim1 (22.3%) and Dim2 (11.8%) are the first two principal components, which together explain approximately 34.1% of the total variance in the data.Each point on the plot represents an observation (a data point from the dataset), and the colors correspond to different countries (Australia, Canada, France, Germany, UK, USA). The ellipses represent confidence intervals around the points for each country group, indicating how closely the points are clustered.

PCA helps in understanding the underlying structure of the data, including the relationships between different variables and the variations between different country groups. By identifying patterns or clusters within the data, PCA can highlight the presence of any latent structures or correlations that might need to be accounted for in the modeling process.The PCA can reduce the dimensionality of the data while preserving most of the variance. This reduction can help in building more efficient and robust GPR models by focusing on the most important components (Dim1 and Dim2). Dimensionality reduction is especially relevant when dealing with complex models like GPR, as it can lead to faster convergence and improved model performance.The clusters observed in the PCA plot can indicate potential differences in the behavior of insurance claims across different countries. These differences should be captured in the GPR models to ensure that the inflation-adjusted frequency-severity models are accurately predicting risks across various regions.

5.5. Model building

The Table 2 represents the performance and validation results for the Automated Inflation Adjusted Frequency Severity Risk Premium Pricing Model. The model utilizes the Gaussian Process Regression (GPR) method via the `kernlab` R package, specifically employing the `gausspr` class with an RBF kernel (`rbfdot`).

The general framework for Gaussian Process Regression (GPR) is grounded in the following function:

$$f(x) \sim GP(m(x), k(x, x')) \tag{5.4}$$

Where:

$$m(x) = E[f(x)] = 0 \tag{5.5}$$

is the mean function, often assumed to be zero for simplicity.

$$k(x, x') = \exp \quad -\frac{\|x - x'\|^2}{2\sigma^2}\Bigg) \tag{5.6}$$

is the covariance function, also known as the kernel function, which defines the similarity between any two points x and x'.

For this model, the RBF (Radial Basis Function) Kernel is defined as:

$$k(x, x') = \exp \quad -\frac{\|x - x'\|^2}{2\sigma^2}\Bigg) \tag{5.7}$$

Where:
σ^2 is the kernel width parameter, controlling the smoothness of the function.

Table 2: Automated Actuarial Loss Reserving Risk Pricing Model

Automated Inflation Adjusted Frequency Severity Risk Premium Pricing Model					
	Frequency	Severity	Reserves	Premiums	Inflation
Processing time (seconds)	4.32	4.61	4.12	4.66	4.00
Hyper parameters					
R package:kernlab Regression					
no. of training instances	1600	1600	1600	1600	1600
kernel	rbfdot	rbfdot	rbfdot	rbfdot	rbfdot
class	gausspr	gausspr	gausspr	gausspr	gausspr
kpar	automatic	automatic	automatic	automatic	automatic
sigma	0.0489964	0.0483452	0.0487040	0.0496039	0.0487709
Train error	0.7648351	0.7746887	0.7668367	0.7588382	0.7632399
Model Validation Metrics:					
MAE	1.1802790	1,645.6170000	1,637.3590000	11.7240800	0.0013627
MSE	2.2290740	4,267,010.0000000	4,036,250.0000000	227.7271000	0.0000025
RMSE	1.4930080	2,065.6740000	2,009.0420000	15.0906300	0.0015930

From the Table 2, the processing time for each model component (Frequency, Severity, Reserves, Premiums, and Inflation) was consistent, all around 4.00-4.66 seconds. This consistency in processing time indicates efficient computation, particularly with the selected kernel (`rbfdot`) and hyperparameters.

The key hyperparameters used in the GPR model are as follows:

- **Number of Training Instances:** 1600 across all components.
- **Kernel:** `rbfdot`, which is the Radial Basis Function kernel as defined in Equation (5.7).
- **Class:** `gausspr`, indicating the use of Gaussian Process Regression.
- **Kernel Parameter (sigma):** The values range around 0.0487, indicating slight variations in the smoothness of the regression functions across the different components.

The Training Error values range between 0.7588 and 0.7747. This metric provides insight into how well the model fits the training data, with lower values generally indicating a better fit. The slight variations reflect different complexities in modeling the frequency, severity, reserves, premiums, and inflation.

The validation metrics include Mean Absolute Error (MAE), Mean Squared Error (MSE), and Root Mean Squared Error (RMSE), which are key indicators of model performance:

$$\text{MAE} = \frac{1}{n}\sum_{i=1}^{n}|\hat{y}_i - y_i| \tag{5.8}$$

$$\text{MSE} = \frac{1}{n}\sum_{i=1}^{n}(\hat{y}_i - y_i)^2 \tag{5.9}$$

$$\text{RMSE} = \sqrt{\frac{1}{n}\sum_{i=1}^{n}(\hat{y}_i - y_i)^2} = \sqrt{\text{MSE}} \tag{5.10}$$

MAE for the frequency model is 1.1803, which is relatively low, indicating a small average error between the predicted and actual values.

MSE values, particularly for severity and reserves, are high, indicating that large errors are somewhat more common for these components.

RMSE values, calculated from the MSE, provide an understanding of how these errors would propagate and influence the pricing and reserving calculations. Higher values suggest greater deviation from actual values.

The Table2 summarizes the implementation of a sophisticated GPR-based model for estimating automated loss reserves and risk premiums. The selected RBF kernel and hyperparameters demonstrate good performance, particularly in the frequency and inflation components, which are critical for IFRS17-compliant pricing and underwriting.This mathematical and computational exploration illustrates the strength and adaptability of GPR in insurance risk modeling, ensuring that the developed model can align with the IFRS17 regulations for accurate loss reserving and risk pricing.

5.6. Visualizing the models

The Figures below generated from the Gaussian Process Regression (GPR) models are crucial for interpreting the relationships between the input features and the respective output variables (claim frequency, claim severity, base reserves, risk premiums, and inflation rates) in the context of travel insurance. These relationships are key to understanding and developing the IFRS17 Regulated Travel Insurance Intelligent Non-Linear Regression Based Inflation Adjusted Frequency-Severity Automated Loss Risk Pricing and Underwriting Model.

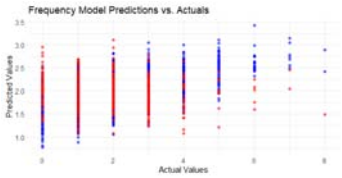

Figure 18: Frequency quency Model Plot

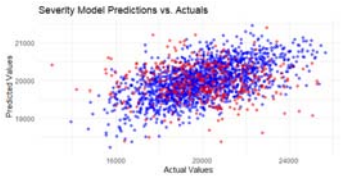

Figure 19: Severity Model Plot

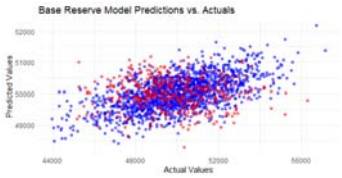

Figure 20: Base Reserve Model Plot

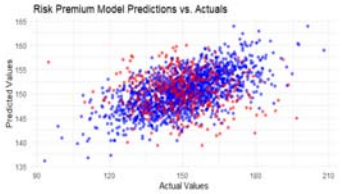

Figure 21: Risk Premium Model Plot

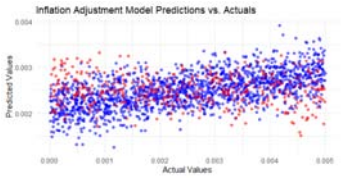

Figure 23: Iflation Adjustment Model Plot

The Figure 18 shows how well the GPR model predicts claim frequency compared to the actual values. The blue points represent the training data, and the red points represent the testing data. Accurate prediction of claim frequency is essential for calculating the base reserves and understanding the expected frequency of claims under IFRS17. This model contributes to estimating future liabilities and helps in risk adjustment.The Figure 19 compares the predicted claim severity with the actual values. Claim severity is a critical component in calculating total losses and reserves. Accurate severity predictions are necessary for determining the adequacy of reserves, pricing, and premium calculations under IFRS17, ensuring that the reserves are sufficient to cover expected claim costs.The Figure 20 shows the relationship between predicted and actual base reserves. Base reserves are directly linked to the insurer's liability estimation under IFRS17. An accurate reserve model ensures that the company maintains adequate reserves to meet future obligations, aligning with the stringent requirements of IFRS17 regarding the measurement of insurance contracts.The Figure 21 plot illustrates how well the GPR model predicts risk premiums compared to the actual values.Risk premium accuracy is crucial for pricing insurance products. Under IFRS17, insurers must ensure that premiums are sufficient to cover expected losses while also being competitive. The model helps in determining appropriate premium levels that reflect the underlying risks, which is a key requirement under IFRS17.The Figure 22 displays the accuracy of the inflation adjustment model. A strong correlation between predicted and actual inflation rates suggests the model effectively captures inflation trends. Inflation adjustments are vital for ensuring that reserves and premiums remain adequate over time, especially in environments with varying inflation rates. This model ensures that the reserves and pricing strategies reflect current economic conditions, aligning with IFRS17's requirement to consider inflation in loss reserving and pricing.

The Figures presented above provide a visual representation of the model's ability to accurately predict key metrics essential for IFRS17 compliance. By confirming the accuracy and robustness of these models through visual inspection and performance metrics, the insurer can confidently rely on the predictions for pricing, reserving, and underwriting decisions.

5.7. Estimation of Automated Actuarial Loss Reserves

The estimation of AALR involves predicting several components: claim frequency (f), claim severity (s), base reserves (R_b), and inflation rates (i). The AALR is then computed as follows:

$$\text{AALR} = R_b + (f \times s \times i) \tag{5.11}$$

where:

- R_b represents the base reserves,
- f denotes the predicted claim frequency,
- s denotes the predicted claim severity,
- i represents the predicted inflation rates.

Equation 5.15 captures the multiplicative interaction between the predicted frequency, severity, and inflation rates, added to the base reserves. This formulation reflects the actuarial principle that reserves should account for not only the current estimates but also for future uncertainties in claim development and economic factors such as inflation.

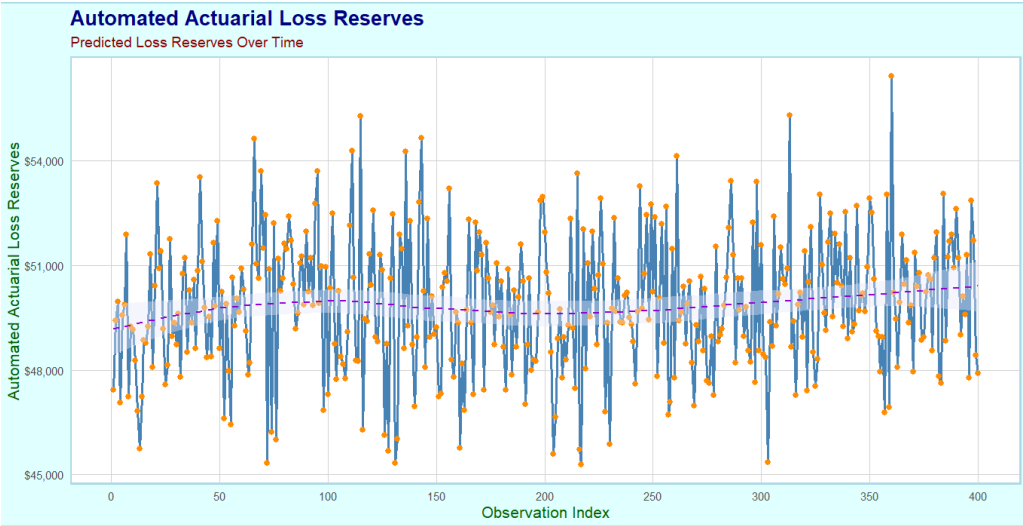

Figure 23: Automated Actuarial Loss Reserves

The Figure 23, illustrates the predicted Automated Actuarial Loss Reserves over time. The plot provides valuable insights into the stability and variability of the AALR across different observations.

- **Trend Analysis:** The solid blue line represents the AALR over time, indicating the general trend in reserves. The presence of the LOESS curve (dashed violet line) suggests a smooth, non-linear trend, capturing any potential shifts in the reserve levels.
- **Volatility:** The orange points highlight individual observations, offering a visual cue for any volatility in the reserves. Periods with closely clustered points indicate stability, while wider gaps suggest higher variability.
- **Financial Interpretation:** The AALR values are presented in monetary terms, which allow actuaries to interpret these reserves directly in the context of financial planning and risk management.

The plot, augmented with the LOESS smoothing, serves as a powerful tool for visualizing and interpreting the AALR. It enables actuaries to detect trends, assess the adequacy of reserves, and identify periods of potential financial risk.

5.8. Estimation of Automated Actuarial Risk Premiums

Automated Actuarial Risk Premium (AARP) is a crucial element in determining the appropriate pricing of insurance policies. This section outlines the methodology used to estimate AARP by leveraging Gaussian Process Regression (GPR) models to predict key actuarial factors, including claim frequency, claim severity, base reserves, and inflation rates.The AARP is calculated by adjusting the base premiums with the product of predicted values for claim frequency, claim severity, and inflation rates. The mathematical formulation is given by:

$$\text{AARP}_i = P_i + \left(\hat{F}_i \times \hat{S}_i \times \hat{I}_i\right), \tag{5.12}$$

where:

- P_i: Base premium for the i-th policy.
- $\hat{F}_i$: Predicted claim frequency for the i-th policy.
- $\hat{S}_i$: Predicted claim severity for the i-th policy.
- $\hat{I}_i$: Predicted inflation rate for the i-th policy.

The estimation of the Automated Actuarial Risk Premiums is carried out by employing the following GPR models for each component:

- **Claim Frequency:** A GPR model $\hat{F}$ is trained on historical data to predict the frequency of claims.
- **Claim Severity:** A separate GPR model $\hat{S}$ is used to estimate the severity of claims.
- **Inflation Adjustment:** The inflation rate $\hat{I}$ is predicted using a GPR model, incorporating macroeconomic factors.

The GPR models are based on the Radial Basis Function (RBF) kernel, which is represented as:

$$k(\mathbf{x}_i, \mathbf{x}_j) = \exp\left(-\frac{||\mathbf{x}_i - \mathbf{x}_j||^2}{2\sigma^2}\right), \tag{5.13}$$

where σ represents the kernel width, and $||\mathbf{x}_i - \mathbf{x}_j||^2$ is the squared Euclidean distance between data points $\mathbf{x}_i$ and $\mathbf{x}_j$.

The GPR model for claim frequency $\hat{F}$ can be expressed as:

$$\hat{F}(\mathbf{x}) = \mathbf{k}(\mathbf{x}, \mathbf{X})^\top \mathbf{K}^{-1}\mathbf{y}, \tag{5.14}$$

where:

- $\mathbf{k}(\mathbf{x}, \mathbf{X})$: Vector of kernel evaluations between test point $\mathbf{x}$ and training data $\mathbf{X}$.
- $\mathbf{K}$: Covariance matrix for the training data.
- $\mathbf{y}$: Vector of training labels (claim frequencies).

Similarly, the GPR models for claim severity $\hat{S}$ and inflation adjustment $\hat{I}$ are defined using the same kernel, with different target variables.The actual implementation involves the following steps:

(1) Train the GPR models for claim frequency $\hat{F}$, claim severity $\hat{S}$, and inflation adjustment $\hat{I}$ using historical data.
(2) Use the trained models to predict the respective values on the test data.
(3) Substitute the predicted values into Equation 5.16 to estimate the Automated Actuarial Risk Premiums.

The GPR-based estimation of AARP integrates complex interactions between claim frequency, severity, and inflation rates, providing a robust and dynamic approach to actuarial

risk premium pricing. This methodology adheres to the principles of IFRS17, ensuring compliance and actuarial soundness.

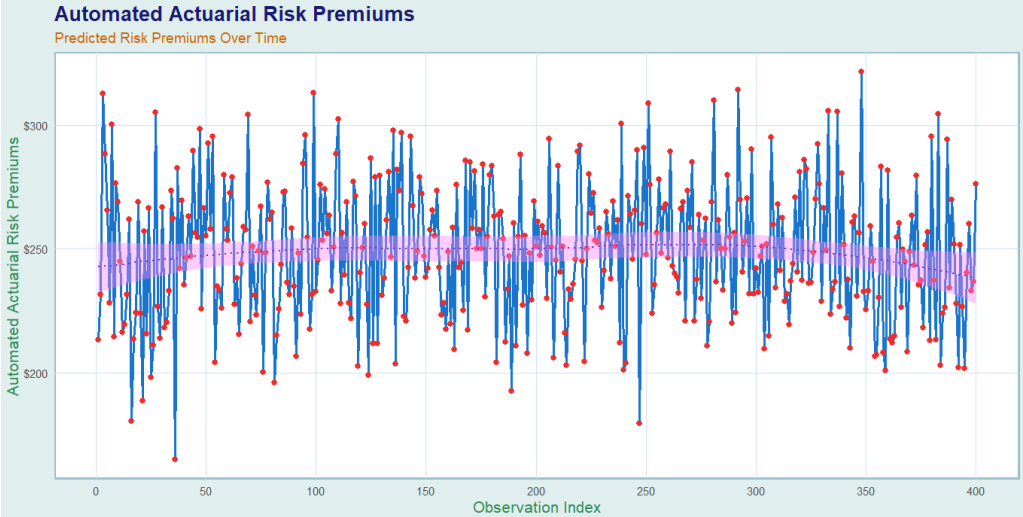

Figure 24: Automated Actuarial Risk Premiums

The Figure 24 visualizes the Automated Actuarial Risk Premiums over time or across observation indices. The fluctuations in the line suggest variability in the risk premiums, possibly reflecting changes in the underlying risk factors or adjustments in the predictive model.The purple LOESS line provides a smoothed view of the trend, making it easier to see the overall direction of the Automated Actuarial Risk Premiums without being distracted by short-term variations.

5.9. Estimation of Automated Actuarial Loss Reserve Risk Premiums

The estimation of Automated Actuarial Loss Reserves Risk Premiums (AALRRPs) is a critical component in actuarial science, particularly in the context of IFRS17-compliant travel insurance models. The AALRRPs are derived by combining the Automated Actuarial Loss Reserves (AALR) with the Automated Actuarial Risk Premiums (AARP). The following sections provide a detailed mathematical formulation of the estimation process.

The Automated Actuarial Loss Reserves (AALR) are calculated using the predicted values for claim frequency ($\hat{f}$), claim severity ($\hat{s}$), and inflation adjustment factor ($\hat{i}$) applied to the base reserves (R_{base}). The relationship is given by:

$$\text{AALR} = R_{\text{base}} + \hat{f} \times \hat{s} \times \hat{i} \tag{5.15}$$

where:

- $\hat{f}$ is the predicted claim frequency from the GPR model.
- $\hat{s}$ is the predicted claim severity from the GPR model.
- $\hat{i}$ is the predicted inflation adjustment factor from the GPR model.
- R_{base} is the base reserves.

Similarly, the Automated Actuarial Risk Premiums (AARP) are derived using the predicted values for claim frequency, claim severity, and inflation adjustment factor applied to the base premiums (P_{base}):

$$\text{AARP} = P_{\text{base}} + \hat{f} \times \hat{s} \times \hat{i} \tag{5.16}$$

where:

- P_{base} is the base premiums.
- $\hat{f}$, $\hat{s}$, and $\hat{i}$ are as defined in Equation (5.15).

The final estimation of the Automated Actuarial Loss Reserves Risk Premiums (AALRRPs) combines the AALR and AARP as follows:

$$\text{AALRRPs} = \text{AALR} + \text{AARP} \tag{5.17}$$

Substituting Equations (5.15) and (5.16) into (5.17) gives:

$$\text{AALRRPs} = (R_{\text{base}} + \hat{f} \times \hat{s} \times \hat{i}) + (P_{\text{base}} + \hat{f} \times \hat{s} \times \hat{i}) \tag{5.18}$$

Simplifying, we get:

$$\text{AALRRPs} = (R_{\text{base}} + P_{\text{base}}) + 2 \times \hat{f} \times \hat{s} \times \hat{i} \tag{5.19}$$

Equation (5.19) elegantly encapsulates the relationship between the base reserves, base premiums, and the predicted values from the GPR models. The factor of 2 reflects the dual application of the predicted values to both the reserves and premiums.The estimation of AALRRPs, as detailed above, leverages sophisticated regression techniques to combine multiple actuarial components into a cohesive metric. The resultant formula, encapsulated in Equation (5.19), provides a robust framework for evaluating actuarial loss reserves in compliance with IFRS17 standards.

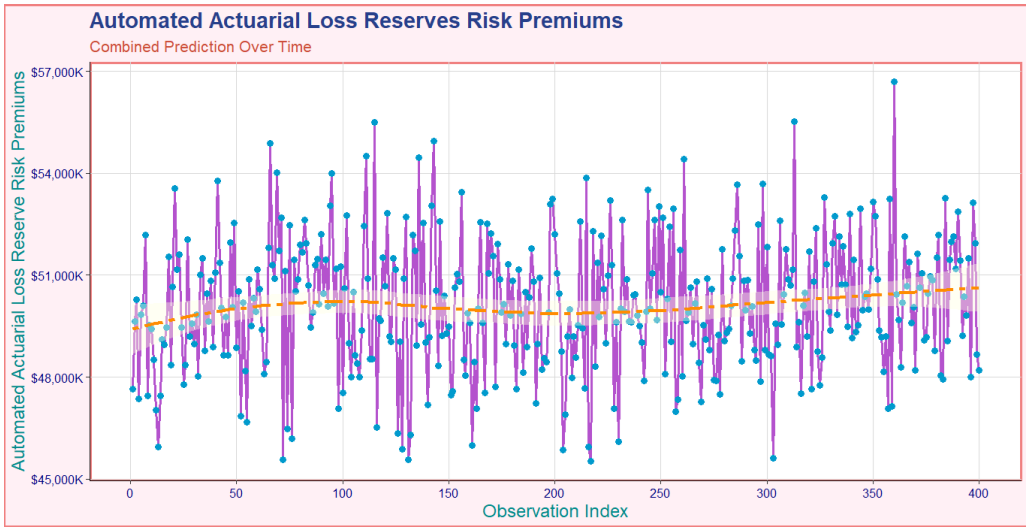

Figure 25: Automated Actuarial Loss Reserve Risk Premiums

The Figure 25 provides a visualization of the Automated Actuarial Loss Reserves Risk Premiums (AALRRPs) over time or across observation indices.There is a trend of the Automated Actuarial Loss Reserves Risk Premiums over the observation indices. The line shows how the combined values of the Automated Actuarial Loss Reserves and the Automated Actuarial Risk Premiums vary across time or indices. The LOESS (Locally Estimated Scatter plot Smoothing) line provides a smoothed approximation of the AALRRPs trend. The darkorange two dash line with a light yellow fill represents the smoothed trend and the confidence interval around it. This line helps to identify the overall trend without being influenced by short-term fluctuations, providing a clearer view of the underlying pattern in the data.

5.10. Comparison of Automated Actuarial Estimates with Test Data

The Figure 26 compares various actuarial metrics and test data related to Automated Actuarial Loss Reserves, Risk Premiums, and Base Metrics.

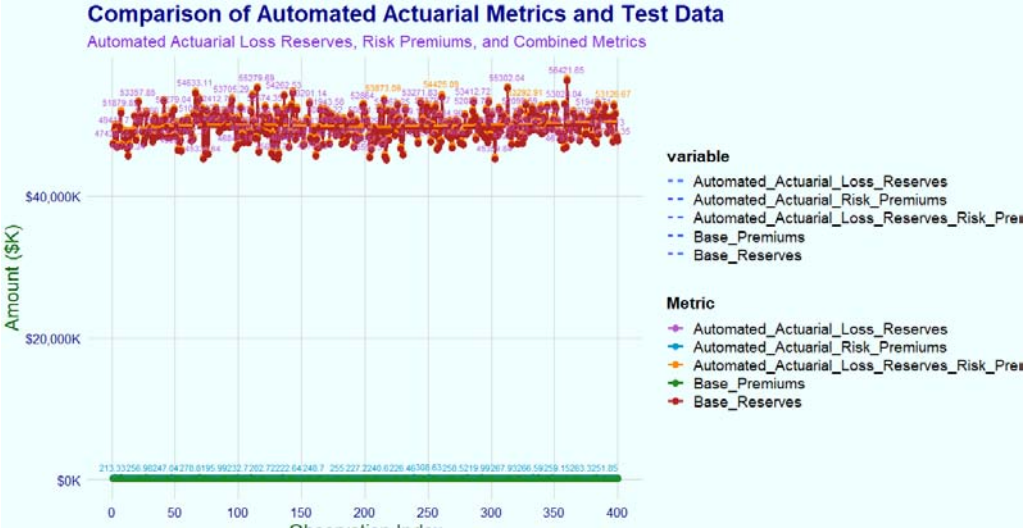

Figure 26. Comparison of Automated Actuarial Estimates with Test Data

The x-axis represents different observations. The range of the index is from 0 to 400, showing that there are 400 observations plotted.The y-axis shows the amount in thousands of dollars, ranging from \$0K to around \$40K. This suggests that the values for the different metrics are being compared in terms of monetary amounts. The Automated Actuarial Loss Reserves metric is plotted in purple, shows the calculated loss reserves using automated actuarial methods. The Automated Actuarial Risk Premiums metric is plotted in blue, this metric represents the risk premiums calculated automatically. The Automated Actuarial Loss Reserves Risk Premiums metric is plotted with an orange line combines the loss reserves and risk premiums. Base Premiums plotted in green, are the base premiums calculated from the test data.Base Reserves presented by a red line represents the base reserves from the test data.

The Automated Actuarial Loss Reserves and Risk Premiums show some variance around the \$50K mark, with minor fluctuations that might reflect changes in the underlying risk or reserve calculations across observations. The Automated Actuarial Metrics (especially Automated Actuarial Loss Reserves and Automated Actuarial Risk Premiums) tend to be higher than the base metrics, indicating that the automated methods might be incorporating additional factors or adjustments not accounted for in the base calculations. There seems to be clustering around certain values, particularly in the range of \$45K to \$55K, which could indicate a high level of confidence or a narrow range of variation in the automated models.

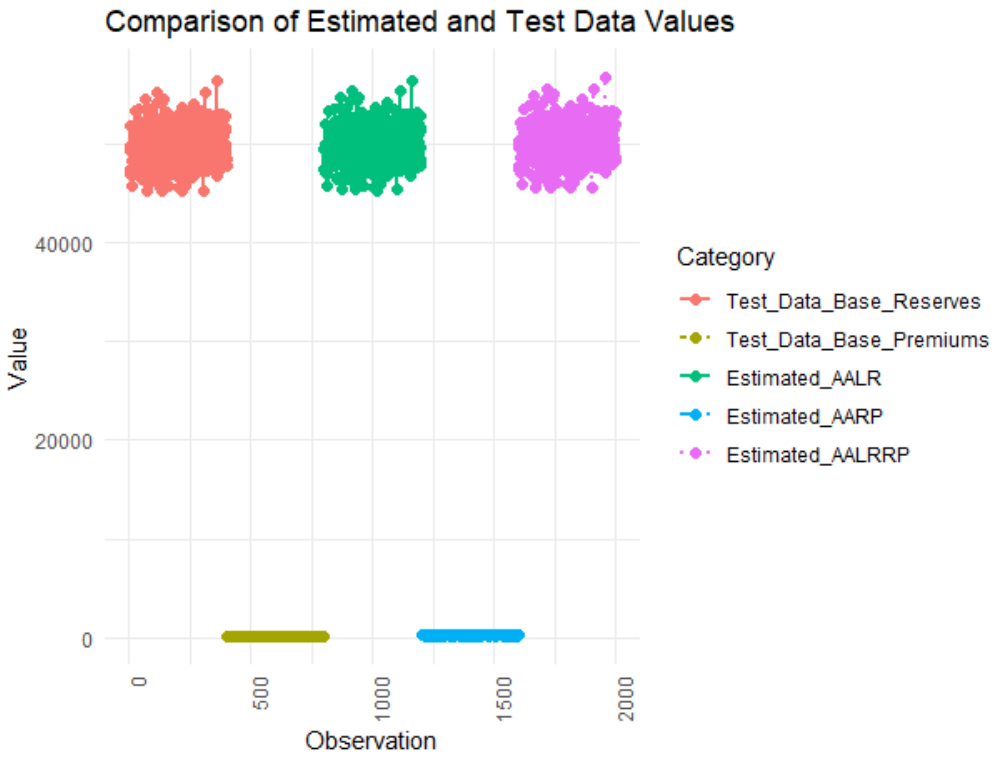

Figure 27: Comparison for Automated Actuarial Insurance metrics

The Figure 27 is a scatter plot comparing different estimated and test data values across various categories. The x-axis represents the observation number or index, with each dot corresponding to a specific observation in the dataset and on the same note, the y-axis shows the value corresponding to each observation for different categories. The scale is from 0 to over 40,000. The dots for each category are tightly clustered together, indicating that the values within each category are similar across different observations. The Base Reserves and Base Premiums have relatively lower values (around 0 to 40,000). Estimated AALRRP, Estimated AALR, and Estimated AARP values are clustered around higher ranges, with the highest density of values below 20,000.The values for Estimated AALR, Estimated AARP, and Estimated AALRRP appear consistent, as indicated by the tight clustering of data points for these categories. However, these estimates show distinct ranges, with some overlap.The plot allows for a visual comparison between actual test data values (reserves and premiums) and the estimated values for AALR, AARP, and AALRRP.

Table 3: Summary of Metrics

Metric	Value
Mean Base Reserves	49776.9389
Mean Base Premiums	149.4249
Mean Estimated AALR	49876.1805
Mean Estimated AARP	248.6665
Mean Estimated AALRRP	50124.8470

The Table 5.10 presents the mean values for several key metrics related to Automated Actuarial Loss Reserves (AALR), Automated Actuarial Risk Premiums (AARP), and Automated Actuarial Loss Reserves Risk Premiums (AALRRP). Each of these metrics is

crucial in assessing the financial health and pricing adequacy under the IFRS 17 framework.

The Mean Base Reserves (49,776.9389) represents the average amount set aside as base reserves, which are the initial estimates of the reserves needed to cover future claims. The value suggests a significant level of reserves, ensuring the insurer can meet expected liabilities.The Mean Base Premiums (149.4249) is the average base premium collected from policyholders. It represents the fundamental pricing before any adjustments for inflation or other factors. The value indicates that the base premiums are relatively modest compared to the reserves.The Mean Estimated AALR (49,876.1805) is the average estimated Automated Actuarial Loss Reserves, which includes adjustments and refinements over the base reserves. The AALR is slightly higher than the mean base reserves, indicating that the insurer has adjusted its reserves to reflect a more accurate estimate of future liabilities.The Mean Estimated AARP (248.6665)represents the average Automated Actuarial Risk Premiums, which are the adjusted premiums after considering various factors such as inflation, risk adjustments, and other actuarial considerations. The mean AARP is significantly higher than the base premiums, indicating that the insurer has adjusted its premium pricing to better reflect the underlying risks.The Mean Estimated AALRRP (50,124.8470)is the average Automated Actuarial Loss Reserves Risk Premiums, which reflect the final adjustment to both reserves and premiums to meet the regulatory and actuarial standards under IFRS 17. The mean AALRRP is slightly higher than the estimated AALR, indicating a cautious and prudent approach to reserving.

The Table 5.10 illustrates a well-calibrated actuarial process where reserves are adjusted slightly above the base estimates to account for potential risks, ensuring financial stability. The premiums have been significantly adjusted (as shown by the AARP), reflecting the insurer's understanding of the risk landscape, resulting in a more substantial buffer against potential losses. The overall alignment of AALR and AALRRP with the base reserves suggests that the insurer is taking a conservative approach to ensure that reserves are more than adequate to meet future liabilities, adhering to IFRS 17 standards. This Table 5.10 highlights the insurer's diligent approach to financial management, ensuring that both reserves and premiums are sufficient to cover potential risks, thereby protecting the financial health of the insurance portfolio.

5.11. Mathematical Development of IFRS 17 Metrics

The Loss Ratio is calculated as the ratio of the mean of the Automated Actuarial Loss Reserves (AALR) to the mean of the Automated Actuarial Loss Reserves Risk Premiums (AALRRP). Mathematically, this can be expressed as:

$$\text{Loss Ratio} = \frac{\mathbb{E}[\text{AALR}]}{\mathbb{E}[\text{AALRRP}]} \tag{5.20}$$

Where:

- $\mathbb{E}[\text{AALR}]$ is the expected value (mean) of the Automated Actuarial Loss Reserves.
- $\mathbb{E}[\text{AALRRP}]$ is the expected value (mean) of the Automated Actuarial Loss Reserves Risk Premiums.

The Reserve Ratio is defined as the ratio of the mean of the Automated Actuarial Loss Reserves (AALR) to the mean of the Base Reserves. This can be represented mathematically as:

$$\text{Reserve Ratio} = \frac{\mathbb{E}[\text{AALR}]}{\mathbb{E}[\text{Base Reserves}]} \tag{5.21}$$

Where:

- $\mathbb{E}$[AALR] is the expected value (mean) of the Automated Actuarial Loss Reserves.
- $\mathbb{E}$[Base Reserves] is the expected value (mean) of the Base Reserves.

The Premium Adequacy Ratio is computed as the ratio of the mean of the Automated Actuarial Risk Premiums (AARP) to the mean of the Base Premiums. The equation is:

$$\text{Premium Adequacy Ratio} = \frac{\mathbb{E}[\text{AARP}]}{\mathbb{E}[\text{Base Premiums}]} \tag{5.22}$$

Where:

- $\mathbb{E}$[AARP] is the expected value (mean) of the Automated Actuarial Risk Premiums.
- $\mathbb{E}$[Base Premiums] is the expected value (mean) of the Base Premiums.

The metrics developed above are key indicators under IFRS 17 for assessing the adequacy and sustainability of actuarial reserves and premiums. These ratios provide insight into the financial health and risk management practices within the insurance portfolio.

Table 4: IFRS 17 Metrics

Metric	Value
Loss Ratio	0.9950391
Reserve Ratio	1.0019937
Premium Adequacy Ratio	1.6641571

The Table 4 provides the exact values for each of these metrics:Loss Ratio (0.9950) which is very close to 1, indicating that the reserves are almost exactly in line with the risk premiums.The Reserve Ratio (1.0020) is slightly above 1, indicating that the Automated Actuarial Loss Reserves are very slightly higher than the Base Reserves, which suggests prudent reserving.Premium Adequacy Ratio (1.6642) is notably above 1, reinforcing the figure's suggestion that the premiums collected are more than adequate to cover the expected liabilities.

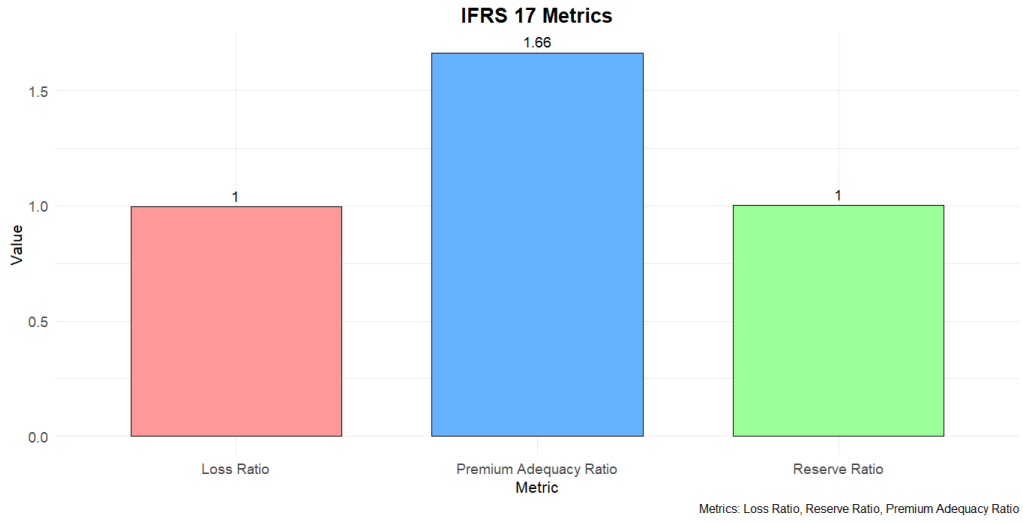

Figure 28: IFRS17 Insurance metrics

From the Figure 28 the bar for the Loss Ratio is colored red and has a value of approximately 1. This ratio indicates that the Automated Actuarial Loss Reserves (AALR) closely match the Automated Actuarial Loss Reserves Risk Premiums (AALRRP), implying that the reserves are sufficient to cover expected losses. The green bar for the Reserve Ratio also shows a value of approximately 1. This suggests that the Automated Actuarial Loss

Reserves (AALR) are very close to the Base Reserves, indicating that the reserves set aside are in line with what was initially estimated.The blue bar for the Premium Adequacy Ratio is significantly higher, with a value of 1.66. This suggests that the Automated Actuarial Risk Premiums (AARP) are significantly higher than the Base Premiums. It indicates a strong premium adequacy, meaning the premiums collected are more than sufficient to cover expected losses and expenses.

The IFRS 17 metrics presented in both the figure and table suggest a well-capitalized and adequately priced insurance portfolio. The close-to-1 ratios for the Loss and Reserve Ratios indicate that reserves are appropriate and align closely with expectations. The high Premium Adequacy Ratio reflects a conservative pricing strategy, ensuring that premiums are more than sufficient to cover potential liabilities, which is a positive sign of financial health and robustness under the IFRS 17 framework.

5.12. Actuarial Science based IFRS17 Profitability Analysis

Let n denote the number of observations. The Discounted Cash Flows (DCF) for inflows and outflows can be computed as follows:

$$\text{Discounted Inflows}_t = \frac{\text{Automated Actuarial Loss Reserves} + \text{Automated Actuarial Risk Premiums}}{(1+r)^t} \tag{5.23}$$

$$\text{Discounted Outflows}_t = \frac{\text{Automated Actuarial Loss Reserves}}{(1+r)^t} \tag{5.24}$$

where r is the discount rate (in this case, $r = 0.03$) and t denotes the time period.

The Fulfillment Cash Flows (FCF) can be calculated as the difference between Discounted Inflows and Discounted Outflows:

$$\text{FCF}_t = \text{Discounted Inflows}_t - \text{Discounted Outflows}_t \tag{5.25}$$

The Contract Service Margin (CSM) represents the unearned profit of an insurance contract and is calculated as:

$$\text{CSM} = \text{Automated Actuarial Loss Reserves} + \text{Automated Actuarial Risk Premiums} - \text{FCF} \tag{5.26}$$

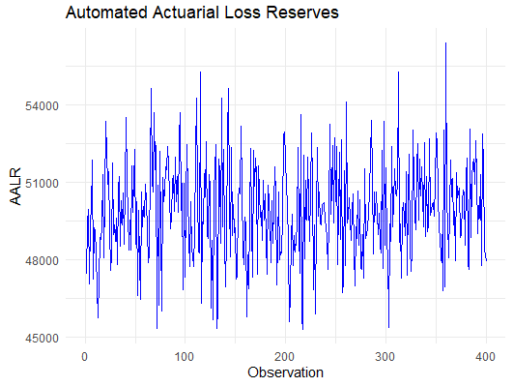

Figure 29: Automated Actuarial Loss Reserves plot

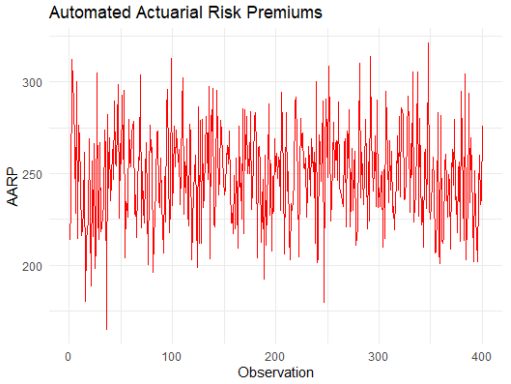

Figure 30: Automated Actuarial Risk Premiums plot

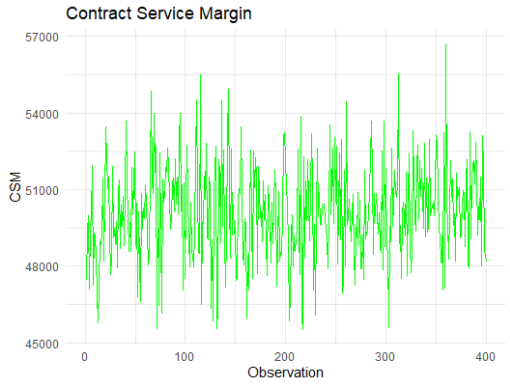

Figure 31: Contract Service Margin plot

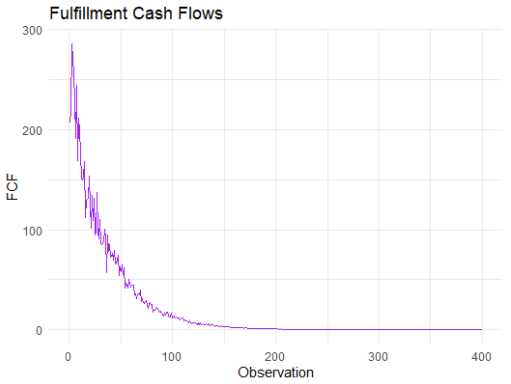

Figure 32: Fulfillment Flows plot Flows plot

The Figure 29 visualizes the reserves required to cover estimated losses. A steady or increasing trend in reserves could indicate rising expected claims, possibly due to increased risk or higher claim frequency/severity.The Figure 30 shows the premiums set aside to cover future risk. Variations might reflect changes in risk assessments or adjustments in pricing strategies. If premiums increase, it could suggest higher anticipated risk.The Figure 31 reveals the unearned profit of the insurance contracts over time. Positive values indicate profit, while negative values may signal potential losses. An increasing CSM suggests that the profitability of the contracts is improving.The Figure 32 displays the net cash flows required to fulfill insurance contracts, taking into account discounted inflows and outflows. Positive FCF indicates that the expected inflows surpass the outflows, which could be a sign of financial health and contract profitability.

5.13. IFRS17 Loss ratio analysis

Let n denote the number of observations.The Loss Ratio is calculated as the ratio of Automated Actuarial Loss Reserves and Risk Premiums to Earned Premiums:

$$\text{Loss Ratio}_t = \frac{\text{Automated Actuarial Loss Reserves} + \text{Automated Actuarial Risk Premiums}}{\text{Earned Premiums}_t} \tag{5.27}$$

The Expense Ratio is computed as the ratio of expenses to Earned Premiums:

$$\text{Expense Ratio}_t = \frac{\text{Expenses}_t}{\text{Earned Premiums}_t} \tag{5.28}$$

The Combined Ratio is the sum of the Loss Ratio and the Expense Ratio:

$$\text{Combined Ratio}_t = \text{Loss Ratio}_t + \text{Expense Ratio}_t \tag{5.29}$$

The Profit Margin represents the proportion of the earned premiums remaining after accounting for the Automated Actuarial Loss Reserves and Risk Premiums, minus expenses:

$$\text{Profit Margin}_t = \frac{\text{Automated Actuarial Loss Reserves} + \text{Automated Actuarial Risk Premiums} - \text{Expenses}_t}{\text{Earned Premiums}_t} \tag{5.30}$$

The Cost of Capital is calculated as the product of Automated Actuarial Loss Reserves and Risk Premiums and the cost of capital rate:

$$\text{Cost of Capital}_t = (\text{Automated Actuarial Loss Reserves} + \text{Automated Actuarial Risk Premiums}) \times \text{Cost of Capital Rate} \tag{5.31}$$

where the Cost of Capital Rate is assumed to be 5% (0.05).

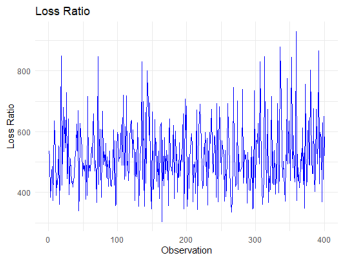

Figure 33: Loss Ratio Plot

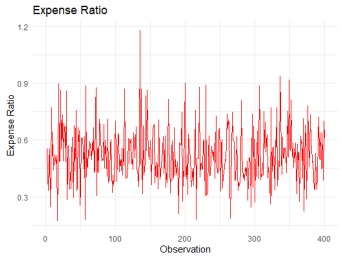

Figure 34: Expense Ratio Plot

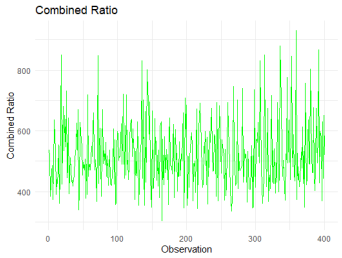

Figure 35: Combined Ratio Plot

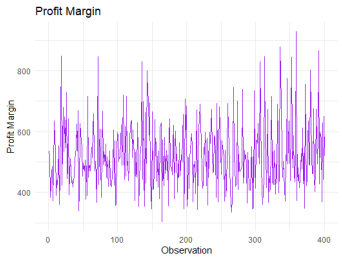

Figure 36: Profit Margin Plot

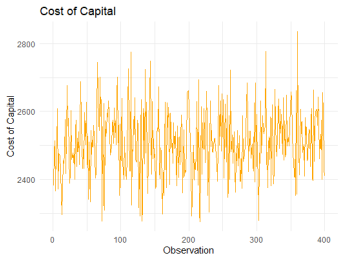

Figure 37: Cost of Capital Plot

The Figure 33 shows how much of the earned premiums is being used to cover the Automated Actuarial Loss Reserves and Risk Premiums. A high or increasing Loss Ratio indicates that a significant portion of the premiums is being allocated to cover losses, which may suggest potential issues in underwriting or risk assessment. Conversely, a decreasing trend can indicate improved loss control and risk management.The Figure 34 depicts the proportion of earned premiums that goes towards covering expenses. A high Expense Ratio may suggest inefficiencies or increasing operational costs. A decreasing trend might indicate better cost management or improved operational efficiency.The Combined Ratio Plot denoted by the Figure 35 combines the Loss Ratio and Expense Ratio to provide

an overall picture of underwriting performance. A ratio greater than 100% means the insurance company is spending more on claims and expenses than it earns in premiums, indicating an underwriting loss. A ratio below 100% indicates underwriting profitability.The Figure 36 represents the profitability of the insurance contracts after accounting for losses and expenses. Positive values reflect a profit, while negative values suggest a loss. Observing trends in this plot helps gauge the overall financial performance and profitability of the insurance operations.The Figure 37 shows the cost associated with maintaining the reserves and risk premiums. It is an important metric for assessing whether the returns on insurance contracts justify the cost of capital. Rising costs of capital might indicate increasing financial burden or changes in capital costs, which could impact the profitability of the insurance contracts.

5.14. Adherence of the GRP Regression model to IFRS17 Regulations

Figure 38: Discounted Automated Actuarial Loss Reserves Risk Premiums vs Actual Base Reserves

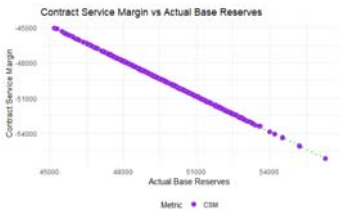

Figure 39: Contract Service Margin (CSM) vs Actual Base Reserves

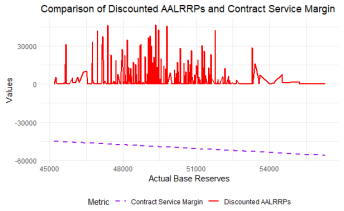

Figure 40: Comparison of Discounted AALRRPs and Contract Service Margin

From the Figure 38 the majority of points are ideally scattered around a line that reflects a relationship between actual base reserves and discounted AALRRPs.The dashed blue line from the linear model helps to visualize the general trend or relationship between the actual base reserves and the discounted AALRRPs. Under IFRS 17, discounted reserves are important for accurately reflecting the time value of money. If the discounted AALRRPs closely follow the actual base reserves, it indicates that the GPR model is reasonably estimating reserves and capturing the time value of money correctly.A good fit of the line would suggest that the model's estimates align well with actual values, reflecting accurate reserve estimations in accordance with IFRS 17.The Figure 39 shows that there is a consistent relationship between the base reserves and the CSM.The dotted green line should show the general trend of the CSM relative to the actual base reserves. IFRS 17 requires that the CSM reflects the unearned profit in the insurance contract. If the CSM calculated from your model aligns well with actual base reserves, it implies that your model is effectively capturing the margin of unearned profit. A clear and consistent trend or pattern in the CSM relative to base reserves suggest adherence to IFRS 17 principles, as it reflects the profitability and expected margins in insurance contracts.The Figure 40 compares the trends of the Discounted AALRRPs and CSM. Ideally, both lines shows a coherent pattern that matches with your expectations based on the actual base reserves.

5.15. Automated Actuarial Underwriting Model

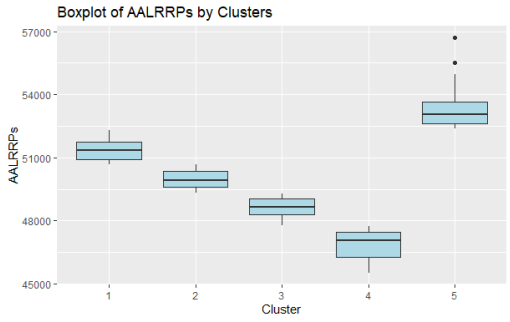

Figure 41:

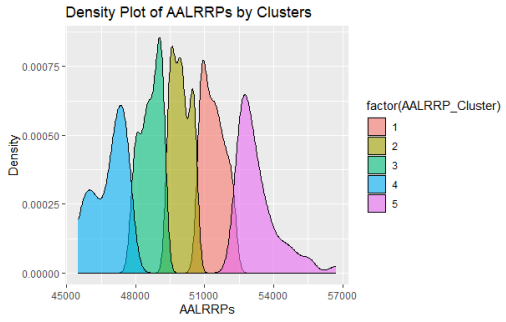

Figure 42:

Each boxplot from the Figure 41 represents the distribution of AALRRPs within a specific cluster. It shows the median (central line), interquartile range (box), and potential outliers (points beyond the whiskers).If the clusters have significantly different AALRRPs, it indicates that there are distinct risk segments within the data. This can guide how underwriting criteria might be adjusted based on the risk profile. Understanding the distribution within each cluster helps in tailoring underwriting policies to better match the risk characteristics of each segment. For example, clusters with higher AALRRPs might represent higher-risk profiles, which could require different underwriting approaches.The Figure 42 shows the distribution of AALRRPs within each cluster. Each shaded area corresponds to a different cluster and indicates how concentrated or spread out the AALRRPs are within that cluster. Different clusters may have different shapes in their density plots. For example, some may have a single peak (unimodal), while others might be bimodal or have multiple peaks. Overlapping densities between clusters can indicate areas where clusters share similar risk profiles, while distinct peaks suggest clear differentiation between clusters.

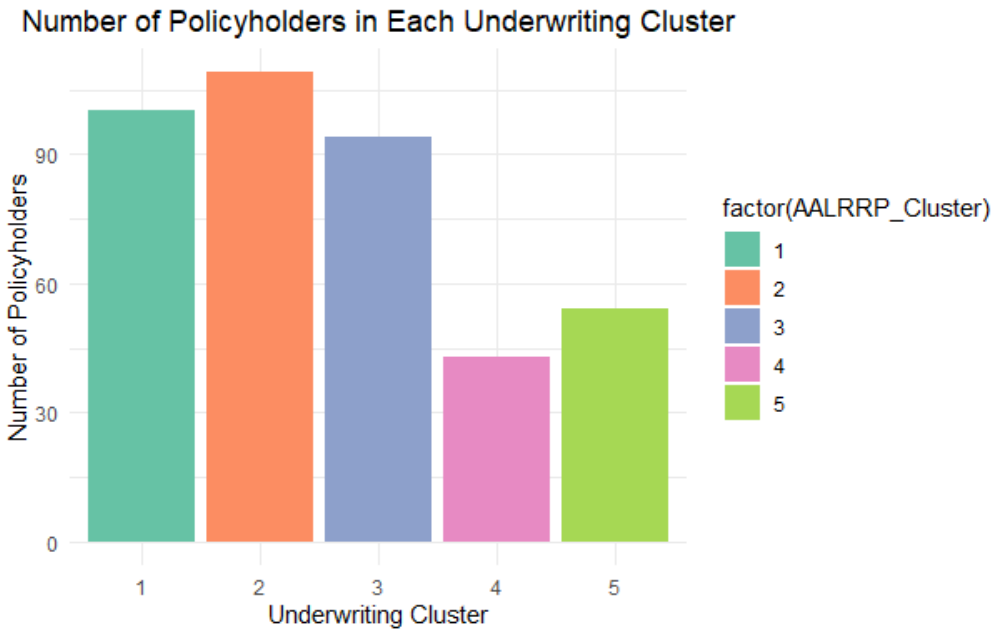

Figure 43: Number of Policyholders in Each Underwriting Cluster

Figure 43 observes how policyholders are distributed across different clusters. A higher bar indicates a cluster with more policyholders, while a lower bar shows fewer policyholders.Clusters with a large number of policyholders might represent common risk profiles. These clusters might require more attention to refine underwriting criteria to manage risks effectively. Clusters with fewer policyholders might represent niche or less common risk profiles. These may still need appropriate underwriting strategies but could be less of a priority if they are small.The first two clusters have a large number of policyholders, it might be necessary to allocate more resources towards managing these clusters, including tailored underwriting policies and more detailed risk assessments. Understanding which clusters are larger can help in developing underwriting policies that address the most common risk profiles, ensuring that they are well-suited to the majority of policyholders.

5.15.1. Further IFRS17 Based Actuarial Underwriting evaluation: The Contractual Service Margin (CSM) is given by:

$$\text{CSM} = \max(\text{Premium} - \text{Reserve}, 0)$$

This metric reflects the unearned profit that will be recognized as insurance services are provided.

The Risk Adjustment (RA) accounts for the uncertainty in the future cash flows:

$$\text{RA} = 0.05 \times (\text{Premium} + \text{Reserve})$$

Here, a 5% risk adjustment is applied to the sum of premiums and reserves.

The Loss Component (LC) measures the expected loss:

$$\text{LC} = \max(\text{Reserve} - \text{Premium}, 0)$$

This metric indicates if the reserve exceeds the premium received, which is a key factor in evaluating the financial health of insurance contracts.

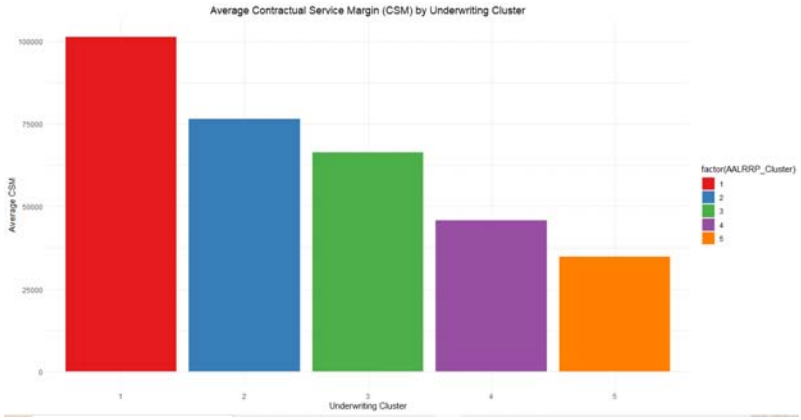

Figure 44: Average Contractual Service Margin (CSM) by Underwriting Cluster

The Figure 44 for Average CSM by Underwriting Cluster shows how the unearned profit varies across different clusters. Higher CSM values indicate more profit retained in the underwriting process, which could be attributed to lower reserves or higher premiums.

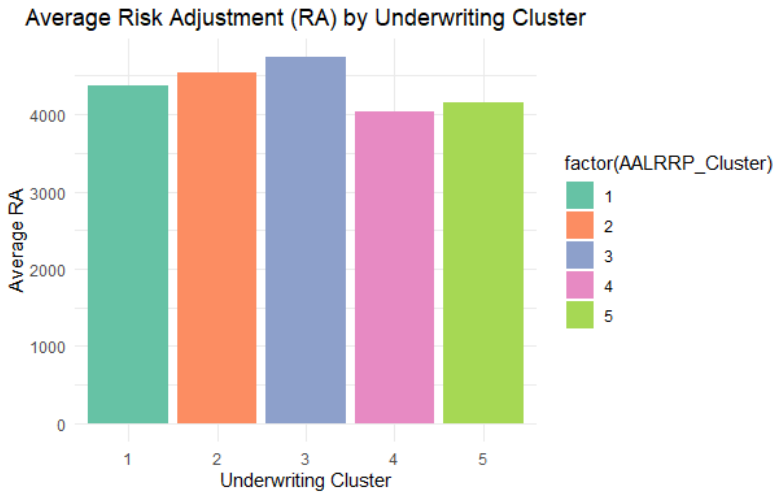

Figure 45: Average Risk Adjustment (RA) by Underwriting Cluster

The Figure 45 for Average Risk Adjustment by Underwriting Cluster provides insights into the risk associated with each cluster. Variations in RA across clusters help in understanding the relative riskiness and profitability of the clusters.

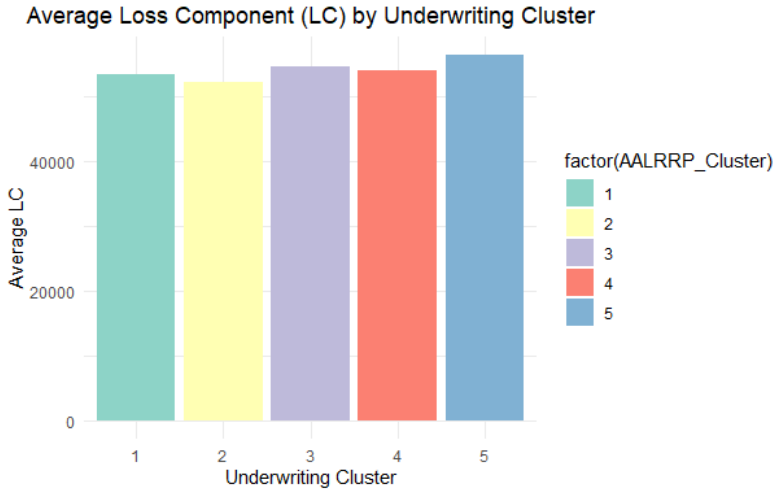

Figure 46: Average Loss Component (LC) by Underwriting Cluster

The Figure 46 for Average Loss Component highlights the loss component across clusters. A higher LC suggests that the reserves are significantly exceeding the premiums, indicating potential underwriting losses.

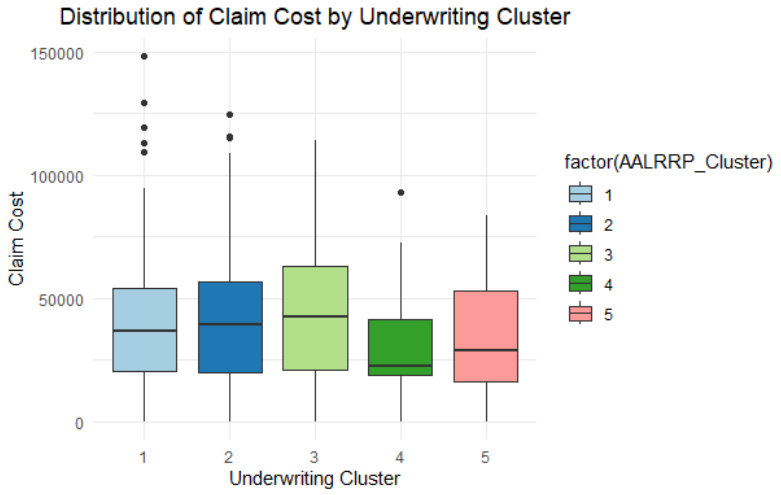

Figure 47: Distribution of Claim Cost by Underwriting Cluster

The box plot of claim costs across clusters in the Figure 47 shows the spread and central tendency of claim costs. Clusters with higher median costs or greater spread may indicate higher risk or claims complexity.

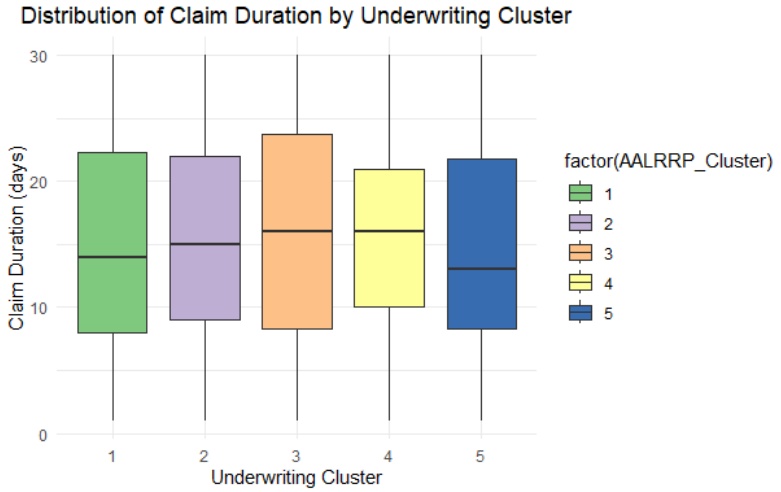

Figure 48: Distribution of Claim Duration by Underwriting Cluster

The Figure 48 for Claim Duration shows the variability in the length of claims across clusters. Longer durations may indicate more complex or severe claims, affecting the overall financial stability of the insurance product.

5.15.2. IFRS17 Based Actuarial Underwriting evaluation with inclusion of expenses:

The Contractual Service Margin (CSM) is calculated as follows:

$$\text{CSM} = \max\left(P_{\text{premium}} - R_{\text{reserve}} - E_{\text{expense}}, 0\right)$$

where:

- P_{premium} is the total premium.
- R_{reserve} is the reserve.
- E_{expense} is the expense.

The Risk Adjustment (RA) is calculated using a percentage of the sum of premiums, reserves, and expenses:

$$\text{RA} = 0.05 \times (P_{\text{premium}} + R_{\text{reserve}} + E_{\text{expense}})$$

where 0.05 (5%) is the assumed risk adjustment factor.

The Loss Component (LC) is calculated as:

$$\text{LC} = \max(R_{\text{reserve}} + E_{\text{expense}} - P_{\text{premium}}, 0)$$

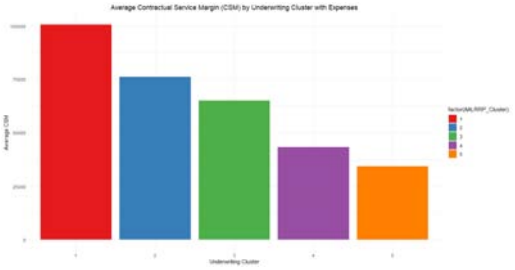

Figure 48: Average Contractual Service Margin (CSM) by Underwriting Cluster

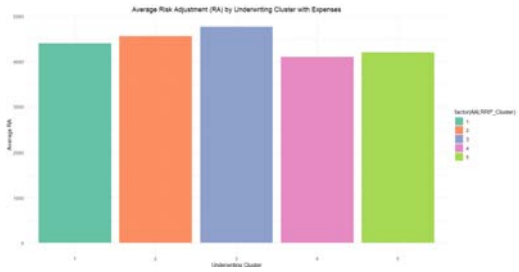

Figure 50: Average Risk Adjustment (RA) by Underwriting Cluster

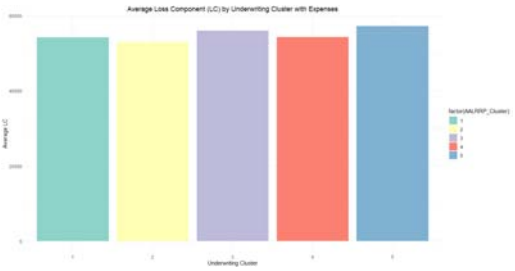

Figure 51: Average Loss Component (LC) by Underwriting Cluster

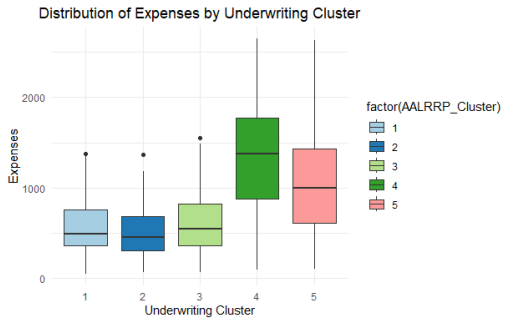

Figure 52: Distribution of Expenses by Underwriting Cluster

The Figure 49 shows the average Contractual Service Margin (CSM) for each underwriting cluster. Clusters with high average CSM values are in a favorable position, as they have a higher margin left after accounting for reserves and expenses. This suggests these clusters are more profitable.Clusters with low or zero CSM indicate that the premiums collected are barely enough to cover the reserves and expenses, potentially signaling less favorable performance or higher risk.The Figure 50 presents the average Risk Adjustment (RA) for each underwriting cluster. Clusters with higher RA values might be perceived as riskier, as more adjustment is needed to cover the perceived risks. This is expected if the clusters have higher premiums, reserves, and expenses.Clusters with lower RA values are considered less risky or more stable. These clusters might have more predictable performance, leading to lower required risk adjustments.The Figure 51 illustrates the average Loss Component (LC) across different underwriting clusters. A high LC indicates that the combination of reserves and expenses exceeds the premiums collected. This could be a sign of potential financial distress or inefficiencies in these clusters.Lower LC values suggest that the premiums collected are adequate to cover reserves and expenses, indicating a healthier financial state for these clusters.The Figure 52 shows the distribution of expenses

for each underwriting cluster.Clusters with wider boxes and higher ranges indicate greater variability in expenses. This variability could be due to diverse risk profiles or differing operational efficiencies within the cluster.Clusters with lower median expenses (the central line in the box) are performing better in terms of expense management compared to clusters with higher median expenses.

These visualizations provide insights into how each underwriting cluster performs in terms of CSM, RA, and LC, as well as how expenses are distributed across clusters. This analysis helps in understanding the financial health and risk profiles associated with different clusters.

5.16. Model Evaluation

Model evaluation in the context of robust testing, stress testing, and scenario testing involves assessing a model's performance and reliability under various conditions and challenges. These techniques are essential in ensuring that models not only perform well under normal conditions but also remain accurate and stable when subjected to unusual or extreme scenarios.Model evaluation through robust testing, stress testing, and scenario testing is essential for ensuring the reliability and stability of models under various conditions. These techniques help to identify weaknesses, validate performance, and provide confidence that the model can handle real-world challenges [37],[40] and [41].

5.16.1. Robust Testing: Robust testing refers to the process of evaluating a model's performance under different conditions to ensure its reliability and stability. This type of testing ensures that the model remains accurate and effective even when faced with small changes or variations in the input data or assumptions [34],[35] and [36].

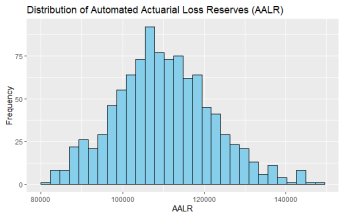

Figure 53: Distribution of Automated Actuarial Loss Reserves (AALR)

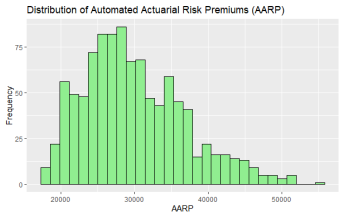

Figure 54: Distribution of Automated Actuarial Risk Premiums (AARP)

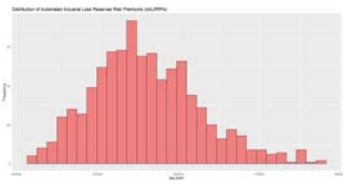

Figure 55: Distribution of Automated Actuarial Loss Reserves Risk Premiums (AALRRPs)

The Figure 53 displays the distribution of Automated Actuarial Loss Reserves (AALR) estimated by the GPR model. The histogram shows a continuous distribution of AALR values, which reflects the variability in the loss reserves predicted by the model. A well-behaved distribution (e.g., near normal) with no extreme skewness or kurtosis suggests that the model is effectively capturing the underlying patterns in the data.The distribution appears reasonable and thus it indicates that the GPR model is robust and not overfitting. The GPR model has learned the relationship between the predictors and the loss reserves well, leading to a realistic and reliable estimation of AALR.The Figure 54 shows the distribution of Automated Actuarial Risk Premiums (AARP) estimated by the GPR model. Similar to the AALR distribution, the histogram of AARP reveals how risk premiums are distributed across the dataset. A smooth and centered distribution implies that the model's estimates are balanced and reflect the variability in the risk premiums accurately.

A well-distributed AARP indicates that the GPR model has effectively estimated the risk premiums without bias. If the distribution is consistent with expected results (e.g., no extreme values or skewness), this supports the robustness of the GPR model in predicting risk premiums.The Figure 55 displays the distribution of Automated Actuarial Loss Reserves Risk Premiums (AALRRPs), which combines AALR and AARP. This histogram shows the combined distribution of loss reserves and risk premiums. A well-distributed AALRRP indicates that the combination of these components reflects realistic overall financial metrics. The shape of the distribution provides insight into the balance between loss reserves and risk premiums.The AALRRPs distribution is smooth and free from extreme skewness or anomalies, it suggests that the GPR model is robust. The combined estimates of AALR and AARP are reasonable and consistent, demonstrating that the model captures the joint behavior of these metrics accurately.

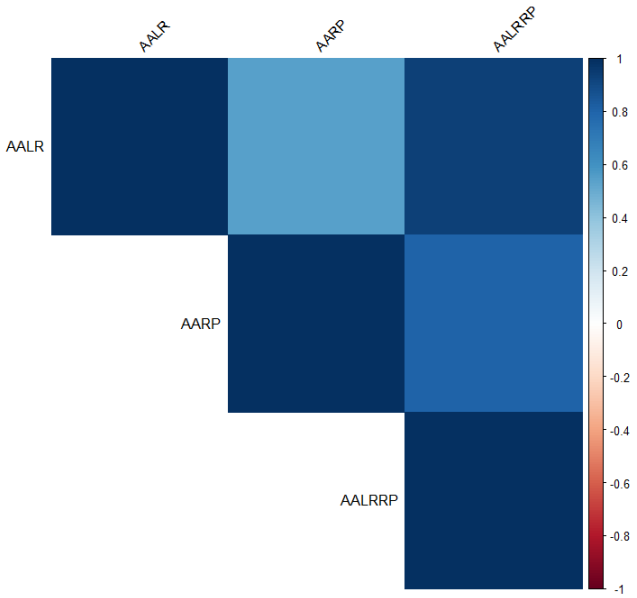

Figure 56: Correlation matrix plot

The correlation matrix presented by the Figure 56 shows the pairwise correlation coefficients between the variables: Automated Actuarial Loss Reserves (AALR), Automated Actuarial Risk Premiums (AARP), and Automated Actuarial Loss Reserves Risk Premiums (AALRRPs). The corrplot function visualizes these correlations with color coding.There is a strong positive correlation between AALR vs. AALRRP since AALR is a component of AALRRPs. A high correlation here confirms that the GPR model's predictions for loss reserves and their combination with risk premiums are consistent.There is also expected to show a high positive correlation between AARP vs. AALRRP, as AARP is another component of AALRRPs. A high correlation indicates that the GPR model is effectively capturing the relationship between risk premiums and the overall combined metric.While AALR and AARP are be related through the model's estimation process, their correlation is moderate compared to their relationships with AALRRPs. This indicates that the GPR model differentiates between the loss reserves and risk premiums in a meaningful way.

The high correlations between AALR and AALRRPs, and AARP and AALRRPs, support the idea that the GPR model is robust. It suggests that the model effectively captures how changes in loss reserves and risk premiums affect the combined metric (AALRRPs). Moderate or low correlation between AALR and AARP suggests that the model correctly estimates these components separately without overemphasizing their relationship, reflecting robustness in how it handles individual variables.

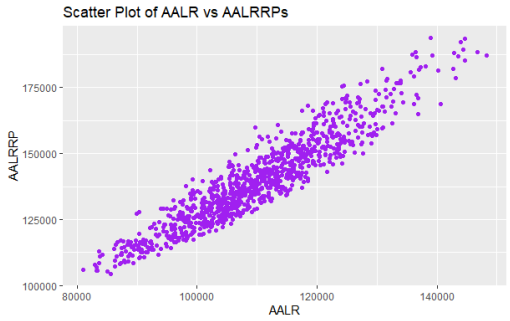

Figure 57: Scatter Plot of AALR vs AALRRPs

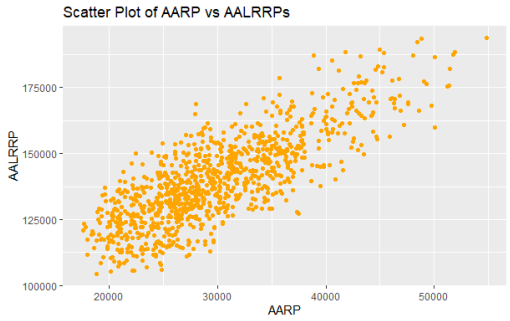

Figure 58: Scatter Plot of AARP vs AALRRPs

The Figure 57 visualizes the relationship between Automated Actuarial Loss Reserves (AALR) and Automated Actuarial Loss Reserves Risk Premiums (AALRRPs).A positive trend in this scatter plot would indicate that as AALR increases, AALRRPs also increase, which is expected since AALR is part of the calculation for AALRRPs. The points generally align along a line or show a clear positive trend, it confirms that the GPR model's predictions for AALR are consistent with its predictions for AALRRPs. This linearity suggests the model's reliability in estimating AALRRPs based on AALR.There are no extreme outliers or clusters of points that deviate significantly, it indicates that the GPR model is stable and does not produce erratic or unrealistic predictions.

The Figure 58 visualizes the relationship between Automated Actuarial Risk Premiums (AARP) and Automated Actuarial Loss Reserves Risk Premiums (AALRRPs). A positive trend here indicates that as AARP increases, AALRRPs also increase. This is expected since AARP is another component of AALRRPs.A clear positive trend would support that the GPR model is robust, as it shows that changes in AARP are consistently reflected in changes in AALRRPs. Similar to the previous scatter plot, the absence of significant outliers suggests that the model produces stable and realistic predictions for risk premiums and their combination with loss reserves.

5.16.2. Stress Testing: Stress testing involves evaluating a model by subjecting it to extreme or adverse conditions to determine its breaking point or how it performs under significant pressure. This method is particularly important in fields like finance and insurance, where models must be resilient to extreme market conditions or catastrophic events [37],[38] and [39].

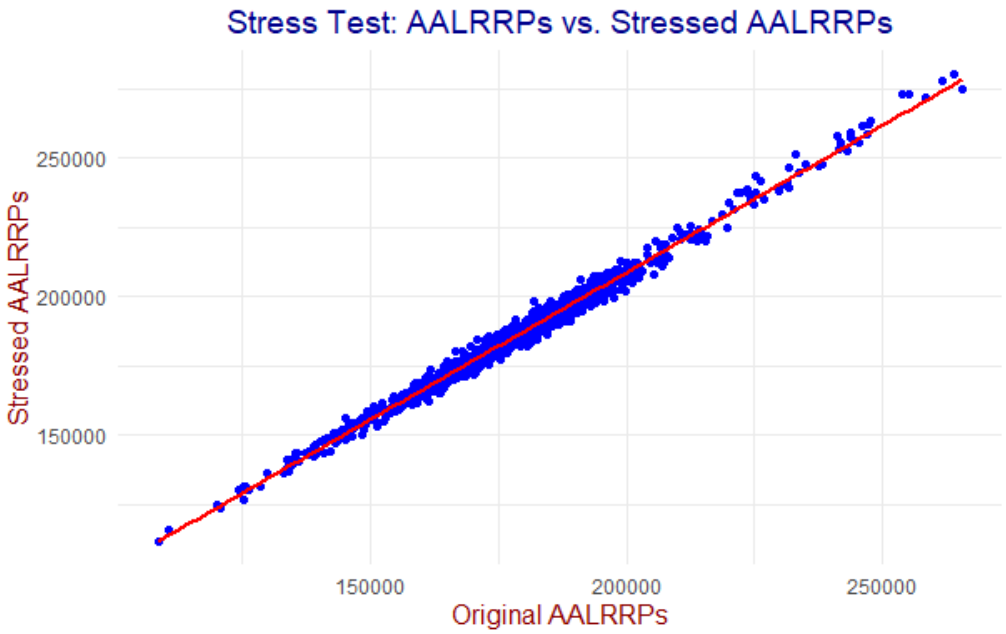

Figure 59: Stress Testing Plot

The Figure 59 displays a scatter plot of Automated Actuarial Loss Reserves Risk Premiums (AALRRPs) before and after applying a stress test where inflation is increased by 10%. The plot includes a linear regression line to show the relationship between the original and stressed AALRRPs.The scatter plot shows a strong positive trend (points generally aligning with the diagonal line where Original AALRRPs equals Stressed AALRRPs), it indicates that the GPR model's estimates are consistent under the stress scenario. This positive relationship suggests that while the absolute values of AALRRPs have increased, the model's behavior is predictable and aligns well with the expected effect of the inflation increase.The red line represents the linear regression fit of the data points and a close alignment of this line with the diagonal suggests that the GPR model is robust, as the inflation stress test leads to a proportional increase in AALRRPs without introducing significant distortions.

In short, the stress test plot shows that the GPR model is robust because it provides consistent and reliable predictions even under stress scenarios. The proportional increase in AALRRPs with increased inflation and the absence of significant deviations or outliers indicate that the model effectively captures the relationships between the variables and responds predictably to changes

5.16.3. Scenario Testing: Scenario testing involves assessing a model's performance by simulating various hypothetical situations, each based on a different set of assumptions or conditions. Unlike stress testing, which focuses on extreme events, scenario testing considers a range of possible outcomes, including both positive and negative scenarios. This approach is often used to explore the potential impact of different future events or decisions on the model's outputs [40],[41] and [42].

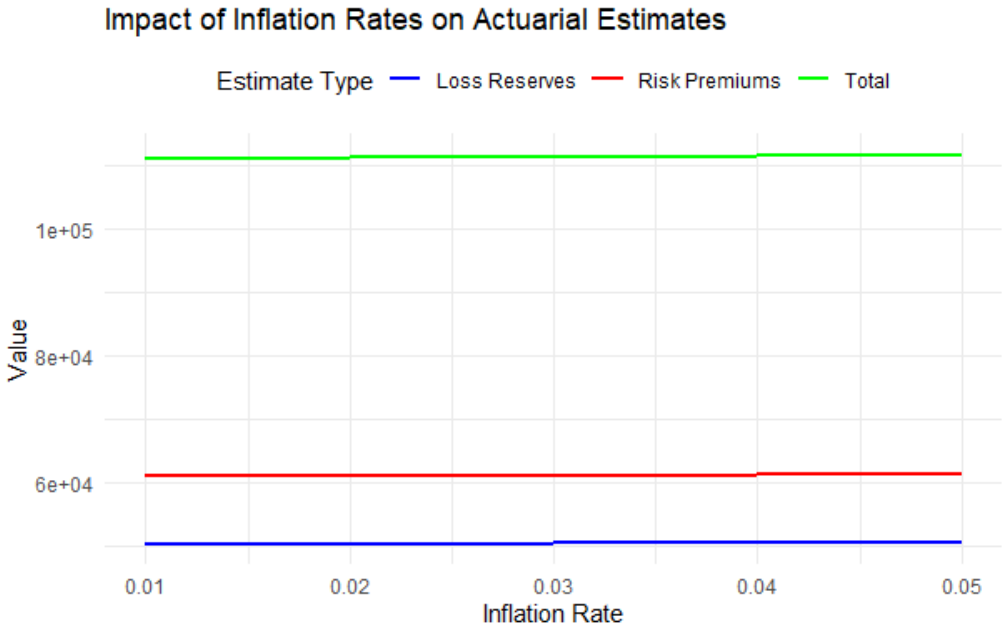

Figure 60: Scenario Testing plot

The Figure 60 produced from the scenario testing displays how changes in inflation rates impact the Automated Actuarial Loss Reserves, Risk Premiums, and the combined Loss Reserves Risk Premiums. The x-axis represents the inflation rate scenarios, ranging from 0.01 to 0.05 in increments of 0.01 and the y-axis represents the values of the actuarial estimates (Loss Reserves, Risk Premiums, and Total).The consistent horizontal trends in the Loss Reserves, Risk Premiums, and Total with increasing inflation rates demonstrate that the model responds logically and predictably to changes in inflation. This indicates that the model captures the impact of inflation effectively and provides a robust response to different inflation scenarios.

VI. DISCUSSION

The methodology proposed in this study introduces several key advancements in actuarial modeling for travel insurance. By leveraging Gaussian Process Regression (GPR), our approach captures complex non-linear relationships in claim data, leading to more precise predictions of claim frequency and severity compared to traditional parametric models. This non-parametric approach is particularly beneficial in handling the inherent variability and uncertainty in insurance data.The integration of an inflation adjustment model within the GPR framework enhances the model's ability to respond dynamically to economic changes, providing more accurate estimates of reserves and premiums. This is crucial for maintaining financial stability and regulatory compliance under IFRS 17.The application of advanced data visualization techniques, including clustering and dimensionality reduction, allows for a more granular analysis of policyholder data. The k-means clustering approach segments policyholders into distinct groups based on their actuarial profiles, facilitating targeted underwriting and risk management strategies. Visualization tools such as boxplots and density plots further enhance the understanding of data distributions and relationships, providing valuable insights for decision-making.Our robustness and stress testing procedures demonstrate the model's resilience to variations in inflation rates and other economic factors. The scenario analysis highlights the sensitivity of actuarial estimates to different inflation scenarios, offering a forward-looking perspective on potential risks and impacts.The inclusion of simulated actuarial features and expenses enriches the

dataset, providing a more comprehensive evaluation of financial health. The recalculated IFRS 17 metrics, reflecting the impact of simulated expenses, offer a detailed assessment of financial performance and adherence to regulatory standards.In short, the proposed methodology represents a significant advancement in actuarial modeling for travel insurance. It combines sophisticated statistical techniques with a thorough understanding of regulatory requirements, offering a robust framework for pricing, underwriting, and financial reporting

VII. CONCLUSION

In conclusion, this study presents a comprehensive and innovative methodology for actuarial modeling and risk pricing in the travel insurance sector under IFRS 17. The use of Gaussian Process Regression (GPR) for predicting claim frequencies and severities, coupled with an inflation adjustment model, significantly enhances the accuracy and responsiveness of actuarial estimates. The integration of advanced clustering and visualization techniques provides valuable insights into policyholder data and supports more informed underwriting decisions.Our approach also includes rigorous testing and scenario analysis, which demonstrates the model's robustness and its ability to handle economic uncertainties. The simulated actuarial features and updated IFRS 17 metrics offer a detailed evaluation of financial health, contributing to improved regulatory compliance and financial reporting.The methodology introduced in this paper not only advances the field of actuarial science but also provides practical tools for better managing travel insurance risks. Future work could explore the application of these techniques to other lines of insurance or further refine the models based on real-world data. The continued development of such methodologies will be crucial for adapting to evolving regulatory standards and economic conditions in the insurance industry

7.1. Funding

The research was not supported by any funding.

7.2. Data availability

The data was simulated in R and kept for ethical reasons.

7.3. Declaration

There were no any conflicts of interest.

ACKNOWLEDGMENT

Special thanks goes to members of staff at University of Zimbabwe through the department of Mathematics & Computational sciences for both academic,social and moral support.

REFERENCES

1. International Financial Reporting Standards Foundation, 2017. IFRS 17: Insurance Contracts. IFRS Foundation, London.
2. Rasmussen, C.E. and Williams, C.K.I., 2006. Gaussian Processes for Machine Learning. MIT Press, Cambridge.
3. Boucher, J.P. & Inoussa, M., 2014. A Hierarchical Model for Claims Reserving. Scandinavian Actuarial Journal, 2014(3), pp.189-211.
4. EIOPA, 2018. Consultation Paper on the Draft Opinion on the Supervision of the Use of Climate Change Risk Scenarios in ORSA. EIOPA-BoS-18/251.

5. Henckaerts, R., Beirlant, J., & Antonio, K., 2021. Local Gaussian Process Regression Models for Non-Life Insurance Pricing. Insurance: Mathematics and Economics, 101, pp.126-138.
6. Kaas, R., Goovaerts, M. & Dhaene, J., 2008. Modern Actuarial Risk Theory: Using R. 2nd ed. New York: Springer.
7. Noll, A., Salzmann, R. & Wüthrich, M.V., 2018. Case Study on Using Machine Learning in Claims Reserving. ASTIN Bulletin: The Journal of the IAA, 48(1), pp.331-359.
8. Ohlsson, E. & Johansson, B., 2010. Non-Life Insurance Pricing with Generalized Linear Models. New York: Springer.
9. Mahohoho, B., 2024. Automated Actuarial Data Analytics-Based Inflation Adjusted Frequency Severity Loss Reserving Model. Open Journal of Statistics, 14(3), pp.341393.
10. Ravi Kumar, P., Thenmozhi, M. & Ramya, R., 2020. Artificial Neural Network Applications in Insurance: A Review. International Journal of Recent Technology and Engineering, 8(6), pp.1022-1026.
11. Wüthrich, M.V., 2021. Statistical Foundations of Actuarial Learning and its Applications. Cham: Springer.
12. Wüthrich, M.V. & Merz, M., 2015. Stochastic Claims Reserving Methods in Insurance. 2nd ed. New York: Wiley.
13. Mack, T., 1993. Distribution-free calculation of the standard error of chain-ladder reserve estimates. *ASTIN Bulletin*, 23(2), pp.213-225.
14. Bornhuetter, R.L. & Ferguson, R.E., 1972. The actuary and IBNR. *Proceedings of the Casualty Actuarial Society*, 59, pp.181-195.
15. IASB. (2021). *IFRS 17 Insurance Contracts*. International Accounting Standards Board. Available at: https://www.ifrs.org/standards/ifrs-17/.
16. IFRS Foundation. (2020). *IFRS 17 Insurance Contracts: Overview*. IFRS Foundation. Available at: https://www.ifrs.org/issued-standards/list-of-standards/ifrs-17-insurance-contracts/.
17. Swiss Re. (2021). *Understanding IFRS 17: An Introduction*. Swiss Re Institute. Available at: https://www.swissre.com/institute/research/topics/ifrs-17.html.
18. Deloitte. (2021). IFRS 17: Insurance Contracts – A Guide to Implementation. Deloitte.
19. EY. (2020). IFRS 17 – Insurance Contracts: Financial Impact and Implementation Considerations. EY.
20. International Accounting Standards Board. (2020). IFRS 17 Insurance Contracts. IFRS Foundation.
21. KPMG. (2021). Understanding IFRS 17: Key Impacts on the Insurance Industry. KPMG.
22. Milliman. (2020). Actuarial Challenges Under IFRS 17. Milliman.
23. PwC. (2020). IFRS 17: What It Means for Insurers. PwC.
24. Willis Towers Watson. (2020). Navigating the Financial Impact of IFRS 17. Willis Towers Watson.
25. Bryman, A. (2016). Social Research Methods (5th ed.). Oxford University Press.
26. Creswell, J. W. (2014). Research Design: Qualitative, Quantitative, and Mixed Methods Approaches (4th ed.). Sage Publications.
27. Kothari, C. R. (2004). Research Methodology: Methods and Techniques (2nd ed.). New Age International Publishers.

28. Box, G. E. P., Hunter, J. S., & Hunter, W. G. (2005). Statistics for Experimenters: Design, Innovation, and Discovery (2nd ed.). Wiley-Interscience.
29. Wickham, H. (2019). R for Data Science: Import, Tidy, Transform, Visualize, and Model Data. O'Reilly Media.
30. Morris, T. P. (2012). Using Simulation Studies to Evaluate Statistical Methods. University College London.
31. Behrens, J. T. (1997). Principles and Procedures of Exploratory Data Analysis. Psychological Methods, 2(2), 131-160.
32. Jolliffe, I. T. (2002). Principal Component Analysis (2nd ed.). Springer.
33. Tukey, J. W. (1977). Exploratory Data Analysis. Addison-Wesley.
34. Huber, P. J. (2011). Robust Statistics (2nd ed.). Wiley.
35. Anderson, R. (2006). Stress Testing: Risks and Mitigations. Journal of Financial Risk, 7(2), 45-57.
36. Basel Committee on Banking Supervision. (2009). Principles for Sound Stress Testing Practices and Supervision. Bank for International Settlements.
37. Embrechts, P., Resnick, S. I., & Samorodnitsky, G. (1999). Extreme Value Theory as a Risk Management Tool. North American Actuarial Journal, 3(2), 30-41.
38. Jorion, P. (2007). Value at Risk: The New Benchmark for Managing Financial Risk (3rd ed.). McGraw-Hill.
39. Kahneman, D., & Tversky, A. (1979). Prospect Theory: An Analysis of Decision under Risk. Econometrica, 47(2), 263-292.
40. McNeil, A. J., Frey, R., & Embrechts, P. (2015). Quantitative Risk Management: Concepts, Techniques, and Tools (Revised ed.). Princeton University Press.
41. Morgan, M. G., & Henrion, M. (1990). Uncertainty: A Guide to Dealing with Uncertainty in Quantitative Risk and Policy Analysis. Cambridge University Press.
42. Saltelli, A., Chan, K., & Scott, E. M. (2004). Sensitivity Analysis. Wiley.
43. Cohen, J., Cohen, P., West, S.G. and Aiken, L.S., 2013. *Applied multiple regression/correlation analysis for the behavioral sciences*. 3rd ed. New York: Routledge.
44. Field, A., 2018. *Discovering statistics using IBM SPSS statistics*. 5th ed. London: SAGE Publications Ltd.
45. Jain, A.K., 2010. Data clustering: 50 years beyond K-means. Pattern Recognition Letters, 31(8), pp.651-666.
46. Xu, R. and Wunsch, D., 2005. Survey of clustering algorithms. IEEE Transactions on Neural Networks, 16(3), pp.645-678.
47. van der Maaten, L.J.P. and Hinton, G.E., 2008. Visualizing data using t-SNE. *Journal of Machine Learning Research*, 9, pp.2579-2605.
48. Jolliffe, I.T., 2011. *Principal Component Analysis*. 2nd ed. New York: Springer.
49. Shlens, J., 2014. A tutorial on principal component analysis. *arXiv preprint arXiv:1404.1100*.